ABSTRACT

Title of Document: SOLVATION, STRUCTURE AND ORGANIZATION AT LIQUID SURFACES

Michael Ross Brindza, Ph.D., 2009

Directed By: Professor Robert A. Walker
Department of Chemistry and Biochemistry

This dissertation presents the results of nonlinear spectroscopic studies whose goal is to understand how the asymmetric nature of interfaces and intermolecular interactions give rise to interfacial solvation properties and solvent structure. The first part of this thesis uses resonance enhanced second harmonic generation to examine the polarity and hydrogen bonding opportunities at interfaces formed between hydrophilic silica and both weakly and strongly associating organic liquids. Measuring interfacial electronic spectra of probe molecules that exhibit solvatochromic sensitivity to polarity and hydrogen bonding, we saw that small changes in solvent structure affect interfacial polarity, and strongly associating alcohols solvents create a region of heterogeneous polarity at the interface. Silica appears to donate hydrogen bonds to adsorbates no matter what solvent (protic or aprotic) was chosen.

The second part of this dissertation uses another nonlinear spectroscopic technique, vibrational sum frequency generation, to determine the structure and orientation of solvent molecules adsorbed to silica/vapor, silica/liquid, and neat liquid/vapor interfaces. By comparing spectral features appearing under different experimental polarization conditions, we have determined average solvent orientations and degree of organization. Our initial studies of alkanes adsorbed to the silica/vapor interface show that despite strong substrate-adsorbate interactions, molecules at the interface show some degree of long range order and organization.

In order to examine how the strength of intermolecular forces between adsorbates and either the substrate or neighboring molecules affect interfacial organization, we measured vibrational spectra of octanol isomers as well as different functional group containing *n*-alkyl molecules at silica/vapor and silica/liquid interfaces. The octanol studies show that strongly associating molecules form ordered monolayers at the silica/vapor interface, but that strength of lateral interactions is important for preserving that order when the liquid is brought into contact. Branched isomers appeared very disordered at solid/liquid interfaces.

Further examining this change in order between solvents at silica/vapor and silica/liquid interfaces using equal length but different functional group containing solvents, we see that the energetics of adsorption and solvation are likely to be responsible for the degree of order both at the solid/vapor surface (adsorption) and solid/liquid interface (both adsorption and solvation).

SOLVATION, STRUCTURE AND ORGANIZATION AT LIQUID SURFACES

By

Michael Ross Brindza

Dissertation submitted to the Faculty of the Graduate School of the
University of Maryland, College Park, in partial fulfillment
of the requirements for the degree of
Doctor of Philosophy
2009

Advisory Committee:
Professor Robert A. Walker, Chair
Professor Michael Coplan
Professor Jeffery Davis
Professor Philip DeShong
Professor John Weeks

Dedication

To Mom and Dad.

Acknowledgements

There are many people who must be thanked for their support, guidance, and friendship during the course of these studies, but first and foremost is my advisor, Professor Robert A. Walker. Without his teachings, advice, and patience this work would never have been completed. One could only hope to follow his example of academic leadership.

I also acknowledge past and present members of the Walker Research Group for both contributing to work presented in this thesis as well as offering their friendship. I am grateful to have worked with Dr. Carmen Huffman, Dr. Michael Pomfret, Dr. Suleyman Can, Dr. Wendy Heiserman, Anthony Dylla, Debjani Roy, Bryan Eigenbrodt and Renee Siler. Having such a wonderful group both in and outside of the lab has made my time at the University of Maryland an exceptional experience. Dr. Carmen Huffman and Dr. Suleyman Can must be additionally thanked for teaching me experimental techniques. They gave their time and experience freely, guaranteeing an easy transition into new fields. I also thank Dr. Okan Esenturk for valuable discussions and experimental advice.

Some of the work presented in this thesis is a result of collaboration, and for this I am grateful to additional members of the department. I thank Professor John Fourkas, Dr. Terry Ding, and Dr. Qin Zhong for welcoming me into their lab for our successful collaboration, and greatly contributing to this thesis.

I thank Dr. Kimberly Briggman for experimental discussions and help with preliminary measurements. I also thank Dr. Daniel Kosov and Dr. James Foresman for help and guidance in performing calculations. They have all played a vital role

toward the success of these studies, and have shown how generous the scientific community can be.

Finally, I am grateful to several friends outside of the Walker Group. Dr. Neil Campbell, William Harrell, and Brian Borak have been friends I could always count on over the last five years.

Table of Contents

List of Tables

List of Figures

List of Abbreviations

ACN	acetonitrile
AFM	atomic force microscopy
DMOA	N,N-dimethyloctylamine
DMSO	dimethyl sulfoxide
H20	water
HBA	hydrogen bond accepting
HBD	hydrogen bond donating
IEFPCM	integral equation formalism polarizable continuum model
MD	molecular dynamics
MP2	second order Møller-Plesset correlation energy correction
NHB	non hydrogen bonding
NLO	nonlinear optical
P	vertical light polarization
pNAs	*para*-nitroanisole
PPP	experimental beam geometry using vertically polarized SF, visible and IR light
S	horizontal light polarization
SF	sum frequency
SFA	surface force apparatus
SH	second harmonic
SHG	second harmonic generation
SPS	experimental beam geometry using horizontally polarized SF and IR, and vertically polarized visible light
SSP	experimental beam geometry using horizontally polarized SF and visible, and vertically polarized IR light
TDDFT	time dependent density functional theory
TGA	thermogravimetric analysis
VSFG	vibrational sum frequency generation
λ_{max}	maximum absorption wavelength
λ_{SHG}	maximum second harmonic wavelength

Chapter 1: Introduction

1.1 Liquid Interfaces

1.1.1 Importance of Studying Liquid Interfaces

To motivate the study of liquid interfaces, one need only look around at the naturally occurring boundaries formed between two separate phases. In fact, almost everything that we *do* see *is* an interface. One of the most common visible surfaces is that between water and a vapor phase. These surfaces, in the form of lakes, oceans, and even raindrops are often covered with a thin film comprised of many different types of organic molecules, whose composition affects properties such as aerosol formation and evaporation.[1] Soil found in the earth's crust forms interfaces with water, air, hydrocarbons, and a host of other materials.[2-4] Properties such as pollutant migration will depend on how analytes adsorb to these boundaries.[5-7] Everyday we rely upon interfaces that we cannot see, such as in biology where cell membranes represent interfaces that separate the cell interior from the extracellular environment. Cell membranes are composed of lipids and these lipids have different shapes, sizes and compositions.[8-10] The organization of these lipids correlates with cell function.[11-16] In addition to these examples, scientists rely on liquid surfaces or the formation of thin films at solid surfaces for many industrial uses, including separation science, in which the relative strengths of solvent and solute interactions with silica particles can result in mixture purification due to differential mobility.[17,18] Whether one is attempting to understand a naturally occuring phenomenon or design a new material,

one of the first considerations must be how the system interacts with its environment. Answering this question requires understanding interfacial properties.

The properties of a molecular interface will be determined by interfacial structure and organization of surface species. Interfacial molecular organization is driven by the system's need to minimize its overall free energy. Molecules at liquid surfaces necessarily have higher free energy than molecules in bulk solution. To minimize this value, a neat liquid drop will adopt a spherical shape. In binary liquid systems, interfaces are preferentially rich with species that have the lower surface tension.[19-21] The best example of how surfaces minimize free energy by any means necessary is the behavior of surfactants at aqueous interfaces. Water has high surface tension because water molecules at surfaces cannot have a full complement of hydrogen bonding partners. As a result hydroxyl groups are not solvated and are exposed to the gas phase.[22-24] Surfactants are amphiphilic molecules, meaning one end strongly associates with water and one is hydrophobic. These amphiphiles spontaneously adsorb to water surfaces, forming molecularly thin layers with alkyl chains structured between the water and an adjacent less polar phase.[25-27] By forming monolayers, surfactants minimize hydrophobic repulsive forces, maximize interaction between surfactants, and allow interfacial water to satisfy hydrogen bonding needs.[28,29] Conceptually, these driving forces are easy to understand. However, due to the asymmetric nature of the interface and the variety of forces at work, interfacial structure is not always easy to *predict*. Work presented in this thesis uses nonlinear optical spectroscopy and thermodynamic methods to investigate the properties, structure and organization of different solvent molecules adsorbed to solid/vapor,

solid/liquid, and liquid/vapor interfaces. The solvents themselves are chosen to represent a broad array of chemical functionalities and structures. The overall goal of this thesis is to begin to identify how molecules at surfaces adopt unique conformations and organizations to achieve equilibrium.

Given the asymmetry and wide array of interactions at surfaces, anticipating interfacial structure can be complicated. To simplify considerations, experiments are often designed to probe properties at solid/vapor interfaces because adsorbed molecules will only experience interactions with the immobile solid surface and with neighboring adsorbates. Because of its natural abundance and environmental and technological relevance, silica is often chosen as a substrate for such experiments. Much of the work described in this thesis considers the effect that silica surfaces have on interfacial solvent organization and interfacial solvation. In addition to being the most abundant mineral in the earth's crust, silica's practical uses in chemistry include applications in separation science and moisture absorption.

Silica is a naturally found metal oxide whose surface is composed of two different types of bound oxygen. In the bulk material oxygen and silicon are tetrahedrally bound. This Si-O-Si siloxane bond also occurs at the interface, but due to defects a large number of interfacial oxygen atoms remain bound to only one silicon. The presence of even trace amounts of water at the interface enables these free oxygen to complete their bonding and form silanol groups with surface densities of ~2-4 OH/nm^2.[30] These free hydroxyl groups are not unlike "dangling" OH bonds found at the aqueous/vapor interface, and both surfaces have similar interfacial

energies.[30] Furthermore, silica has been shown to be very polar, and has the ability to both donate and accept hydrogen bonds with adsorbed species.

Because of silica's high surface energy, individual vapor phase molecules will tend to adsorb to the silica surface and interact through a combination of hydrogen bonding, dipole, or simple van der Waals forces. Isolated molecules adsorbed to silica will tend to lie flat if possible so as to maximize adsorbate-substrate interactions even if different parts of the adsorbate interact with the substrate through a variety of forces. For example, strongly bound alkanethiol monolayers at gold and silica interfaces are disordered and lie flat at low surface coverage.[31,32] When an ensemble of molecules adsorbs to the surface, one must consider not only adsorbate and substrate interactions, but also lateral interactions between adsorbed monomers. The relative strengths of adsorbate-substrate interactions and lateral, in-plane interactions between adsorbates will combine to determine molecular organization within the film. Many naturally occurring molecules have complicated, asymmetric structures, thus the adsorption energetics of branched isomers will differ from linear chain organic surfactants due to size and steric constraints. This difference in lateral interactions between adsorbed surfactants will affect significantly the degree of ordering within the interfacial region.

Considerations become even more involved when one begins to think about structure and organization at solid/liquid interfaces. Interphase interactions and interfacial ordering at these buried interfaces play important roles in a host of technologically important processes. For example, chromatography relies on the preferential adsorption of more polar species at the silica/liquid interface to separate

chemical mixtures. The properties sampled by either a solvent or solute molecule at the solid/liquid interface will necessarily be different than in the adjacent bulk liquid, due to the asymmetric nature of the interface. The local solvation environment of solutes at the silica surface may differ from the bulk due to both solute interactions with the substrate, as well as changes in local solvent properties. Because of the increased mobility and decreased barrier to desorption, predicting the structure and organization of molecules at the solid/liquid interface becomes much more difficult than at the solid/vapor interface. Interfacial solvent molecules at the solid/liquid interface are subject to the same substrate-adsorbate and lateral surface solvent interactions, but also to favorable solvation interactions in the bulk liquid.

Complementing studies of solvation and solvent structure at silica/liquid interfaces are corresponding experiments that probe structure and organization of neat liquid/vapor interfaces and aqueous/vapor interfaces having monolayers of surface active species. As noted above, aqueous/vapor interfaces share many similarities with silanol terminated silica/vapor interfaces. The primary difference is that surface silanols and the resulting hydrogen bonding opportunities at silica interfaces are immobile. The solid surface has less conformational freedom than the aqueous/vapor interface, so adsorbates that may be solvated and induce water rearrangement at aqueous surfaces lose that ability at the silica/vapor interface. Consequently, adsorption energetics at solid/vapor interfaces will be impacted by steric restrictions not found at aqueous/vapor interfaces.

A final type of interface that can help identify how intermolecular shape and forces lead to anisotropic organization is the interface formed at the neat liquid/vapor

interface. Like the solid/liquid interface, structure across the liquid/vapor interface must necessarily transition from that of the isotropic bulk to isotropic vapor. Again, interfacial free energy must be minimized, but at these surfaces the driving force for organization will be a competition between solvation of interfacial species, and self assembling tendencies of the interfacial molecules. Many studies have shown that long range order and monolayer solvent organization exists at the liquid/vapor interface arising from interactions solely between liquid molecules themselves. In some instances such as with strong hydrogen bonding liquids (i.e. water and methanol) the origin of such structure is easy to understand. For weakly interacting liquids such as alkanes, the origin of interfacial organization is not as clear. While the work presented in this thesis focuses on molecular structure at solid surfaces, examining the balance of forces leading to changes in interfacial organization in these other systems provides insight about molecular structure at the solid interface.

1.2 Methods to Determine Interfacial Structure and Organization

Many different experimental techniques are available to probe the properties, structure, and organization of molecules at interfaces. Thermodynamic techniques such as surface tension measurements, thermogravimetric analysis (TGA), and contact angle measurements can determine the strength of macroscopic or ensemble averaged interactions between adsorbed species and solid substrates. Thermodynamic measurements are often relatively easy (and inexpensive) to perform. Furthermore, results can provide insightful guidance when interpreting data from spectroscopic experiments. TGA is used to measure the amount of adsorbate on solid samples and strength and the reversibility of adsorbate-substrate interactions.

Goniometers measure solid/liquid contact angles and can report on the affinity that a liquid has for itself versus an adjacent solid surface. Results presented in this thesis measure the surface tension of pure liquids using a modified analytical balance.

The surface tension of a liquid or solution quantifies the strength of attractive forces between adjacent molecules at the interface, manifested as the excess interfacial free energy. Liquids that associate very strongly with each other, such as water, tend to have higher surface tensions. Because the aqueous/vapor interface consists of water molecules that do not experience a complete hydrogen bond network, water's surface tension is very large at ~72 mN/m. Alkanes, on the other hand only interact through weak van der Waals forces and are on the other end of the energetic spectrum, with surface tensions of 20-25 mN/m (depending on chain length).

Thermogravimetric analysis (TGA) is a technique that can measure solid-adsorbate interactions. In these experiments, the mass lost from a sample of small, high surface area particles is recorded as the sample temperature is increased. Both the total amount of adsorbate lost and the temperature at which the loss occurs indicate interaction strength between adsorbates and the substrate. TGA experiments relevant to this thesis use the method to examine the relative amounts of various octanol isomers physisorbed and chemisorbed water on silica samples to determine relative surface coverages. More quantitative measurements should be able to differentiate the heats of adsorption for different isomers. As an example of this technique's potential, previous studies have shown that the heat of adsorption of water on alumina depends sensitively on surface hydroxyl group concentration, and

rises from less than 50 to greater than 250 kJ/mol as surface silanol concentration increases.[33]

A final measure of interfacial energetics quantifies the contact angle formed between a liquid drop and a solid surface is related to the magnitude of interaction between the two phases by solving Young's equation.[34] A good example showing difference in contact angles due to solid/liquid interaction are the water/Teflon and water/silica interfaces. Water completely wets hydrophilic silica, indicating a strong affinity for the silanol terminated surface, but has contact angles with Teflon in excess of 115 degrees.[35]

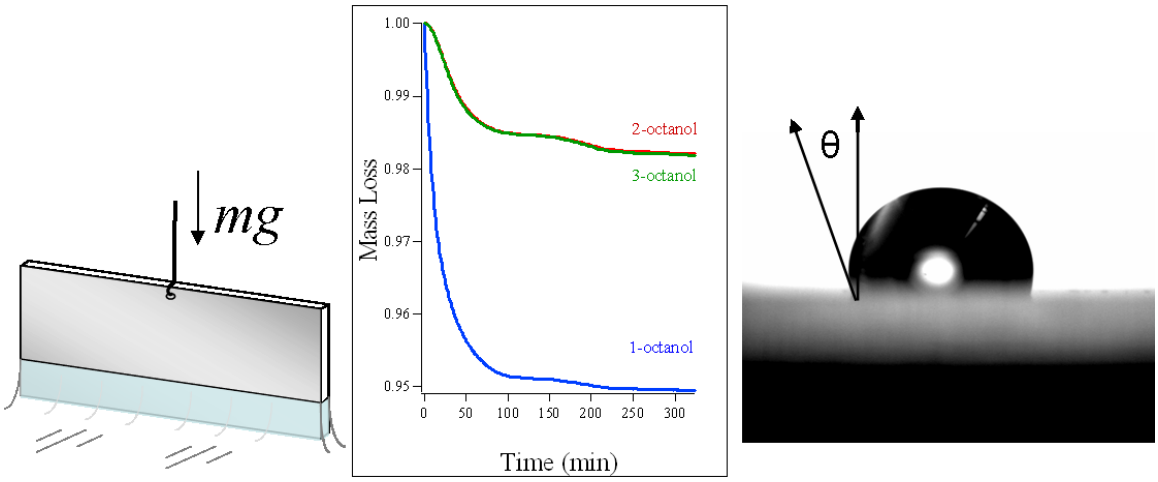

Figure 1.1. Three different thermodynamic techniques are used in this thesis to quantify macroscopic surface energetics. Surface tension measurements, which use the Wilhelmy Plate method (left), TGA measurements (middle) which show mass of adsorbates lost with increasing time or temperature, and contact angle measurements (right), where the angle formed at the interface between a solid (hydrophobic glass) and liquid (water) corresponds to the interaction strength.

Additional techniques can measure other aspects of thin film structure. Here "thin film" is taken to mean either a full monolayer adsorbed to a solid substrate or aqueous interface or the asymmetric region created in a liquid by an adjacent surface. One common method used to characterize thin films is ellipsometry. Ellipsometry

measurements of adsorbed film thickness at solid/vapor interfaces can help one infer molecular structure within the film itself.[27,36,37] For example, a film of long chain molecules with a measured thickness on the order of a few atoms is likely to lie flat at the surface, but if the film measures more than 1 nm in width, the adsorbed molecules is likely to be standing upright. Data from neutron and x-ray scattering experiments are used to infer interfacial structure through electron or atomic density, but again, these measurements do not directly probe the strength and directionality of the intermolecular interactions responsible for organization within the film.[38-41]

These various experimental measurements of solvent structure, organization, and energetics at different interfaces all report different interfacial properties arising from a competition between many forces. To help understand the relative magnitude and importance of these forces on interfacial structure and organization, molecular dynamics (MD) simulations provide valuable complementary information. Though MD simulations are generally not definitive as stand-alone studies, when one compares experimental results with simulations that vary interaction parameters, one often gains valuable insight into the microscopic origins responsible for experimental observations. Furthermore, spurred by the dramatic increase in experimental studies of interfacial organization, MD simulations have evolved to explore a broad range of topics.

Examples of experimental results which can be modeled and explained by MD simulations include simulations of interfacial width and polarity across liquid interfaces.[42,43] Simulations have been performed to show that interfacial structure and disorder affect macroscopic properties such as friction between surfaces with

adsorbed thin films.[44-46] Additional studies have examined ion distributions across aqueous interfaces in order to compare results with spectroscopic and scattering data.[47-49]

Information from MD simulations can also lead to predictions that can be tested using optical spectroscopy. Spectroscopic experiments have the ability to investigate local environment through changes in molecular electronic or vibrational structure. Furthermore, coherent spectroscopic measurements using polarized light can be used to measure a molecule's average orientation making optical spectroscopy an ideal tool for probing intermolecular forces and their directionality at interfaces. To study interfaces optical methods must have a degree of surface specificity, meaning that measurements must be able to discriminate the response from molecules at surfaces from those in bulk. A primary reason that traditional spectroscopic techniques are not effective for studying surfaces is that linear spectroscopic methods such as absorption or emission lack surface specificity. When one considers the difference in molecule populations between the bulk and interface, one quickly realizes that any spectroscopic signal arising from an interface will likely be masked by signal from the bulk that is orders of magnitude larger. Second order nonlinear (NLO) spectroscopy solves this dilemma, due to the technique's inherent surface specificity.

Described in this work are experiments that use 2^{nd} order nonlinear optical spectroscopy to measure directly the solvation environment, structure and organization of molecules adsorbed to solid and liquid surfaces. Signals that arise from resonance-enhanced, Second Harmonic Generation (SHG) or Vibrational Sum

Frequency Generation (VSFG) spectroscopy are only nonzero in a non-centrosymmetric medium, thus making these techniques ideal for studying molecules adsorbed to interfaces.

SHG relies on a second order polarization induced at the surface by an incident light field. The molecular specificity arises from the increased interfacial response and signal when the sum of the energies of those two photons is resonant with an allowed electronic transition in the molecule.[50-54] In practice, a tunable, short (~150 femtosecond) visible wavelength laser pulse is directed toward the surface of a silica prism in contact with the sample solution. Because selection rules require the SH signal to vanish in isotropic media, any SH light scattered coherently forward must arise from solutes at the surface. The origin of the generated signal field is described in detail in Chapter 2 of this work. Choosing solvatochromic sensitive solutes allowed examination of the local solvation environment. SHG has been used for a variety of studies examining properties of liquid interfaces such as interfacial width, molecular orientation and interfacial acid-base equilibria.[55-60]

Experimental considerations for VSFG are also determined by the same selection rules, however in a VSFG experiment only one of the two incident fields is resonant with an allowed infrared transition in the molecule.[51,61-63] By coupling knowledge of molecular transition dipole moment orientations with experimental polarization analysies of VSFG signals, one can determine average molecular orientation and the strength of interactions within the interfacial region.[29,31,64-66] A detailed explanation of VSFG theory and its application to quantifying molecular orientation appears in Chapter 3.

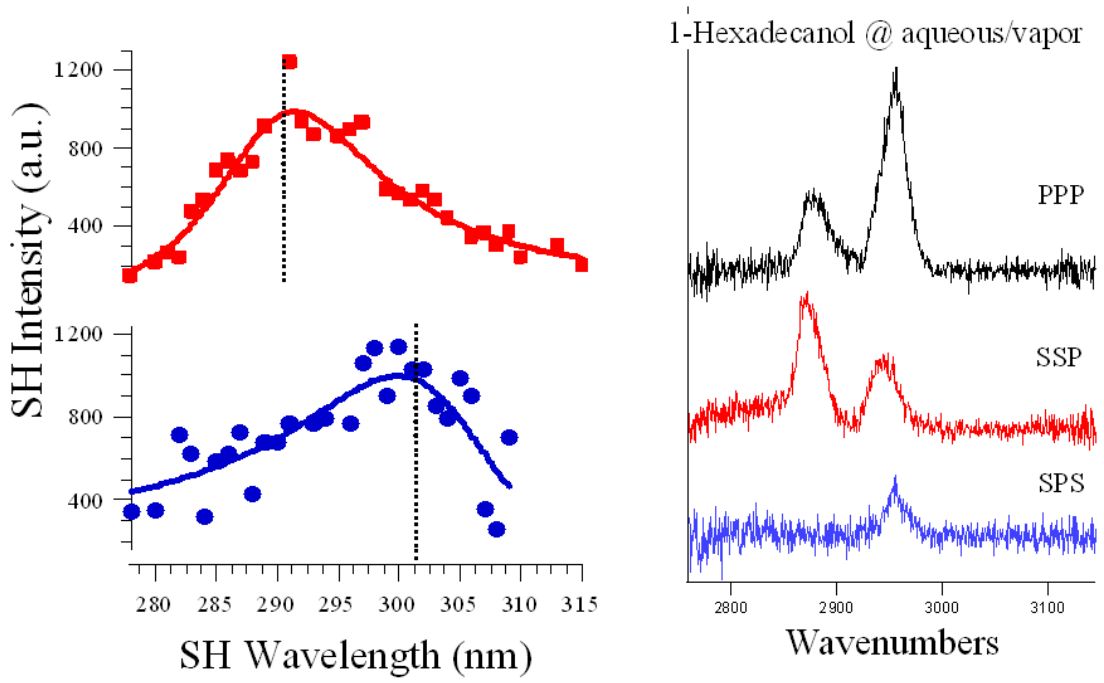

Figure 1.2 Representative SHG (left) and VSFG (right) spectra. On the left are the spectra of indoline adsorbed to the hydrophilic (red) and hydrophobic (blue) silica/cyclohexane interfaces. The differences in peak wavelengths represent hydrogen bonding opportunities at hydrophilic (top) and hydrophobic (bottom) silica surfaces. Indoline's electronic transition shifts to higher energy in a hydrogen bond donating environment. The right panel shows SFG spectra acquired under PPP, SSP, and SPS polarization conditions of 1-hexadecanol adsorbed to the aqueous/vapor interface.

1.3 Systems Studied

1.3.1 Interfacial Solvation Studies

Experiments presented in this work employ several techniques to study interactions responsible for the properties, structure and organization of molecules at liquid interfaces. Motivated by experiments that probed interfacial polarity as a function of interphase forces and solvent molecular structure, experiments described in Chapter 2 use SHG spectroscopy in addition to bulk UV-Vis absorbance spectroscopy and computer simulations to differentiate specific from nonspecific solvation forces at interfaces. These studies examine the role of solvent structure and

solvent identity on both local polarity and hydrogen bonding at interfaces formed between silica and different classes of organic solvents. Two probe molecules, *para*-nitroanisole (pNAs) and indoline, are sensitive to different types of solvation forces. The electronic structure of pNAs depends solely on polarity, but indoline is sensitive to hydrogen bond donating and accepting opportunities regardless of the local dipolar environment. These solutes were used to measure the interfacial nonspecific and specific solvation environment at the silica/liquid interface, where the liquid in question is an alkane, or different length *n*-alcohol solvents.

Solutes adsorbed to or near the silica substrate may interact directly with the polar, hydrogen bonding solid, or may experience an interfacial solvation environment different from the bulk due to silica enforcing a net order or density difference on the adjacent solvent. Any changes to local solvent density will change the polarity experienced by an adsorbed solute and this effect should be sensitive to solvent packing efficiencies. In contrast, if a solute is sensitive only to interacting with the substrate, surface induced changes to solvent structure should have minimal effect on interfacial solvation. Nonlinear spectroscopic results of para-nitroanisole (pNAs) and indoline adsorbed to the silica/cyclohexane, silica/methylcyclohexane, silica/1-octanol, and silica/1-propanol are presented in Chapter 2. Spectra of solutes at the two silica/alkane interfaces show that while solvent structure impacts the local polarity at the interface, hydrogen bonding opportunities remain unchanged. In addition, spectra acquired at silica/alcohol interfaces show heterogeneous polarity and imply Langmuir film-like monolayer solvent structure within the first solvent layer at the solid/liquid interface. Again, hydrogen bonding remains unchanged. Only by

removing the substrate's ability to donate hydrogen bonds can indoline's electronic structure (and solvation) be significantly altered.

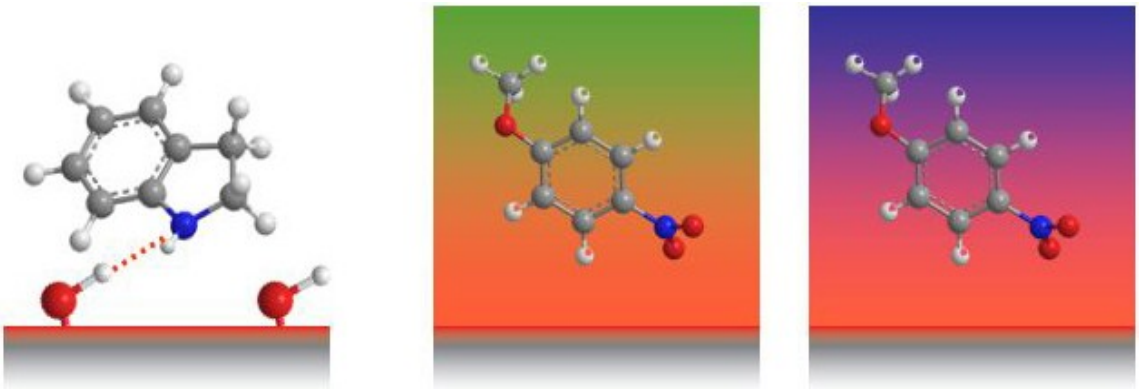

Figure 1.3 *p*-nitroanisole (middle and right) adsorbed to silica surfaces is sensitive to local polarity and this nonspecific solvation property varies with solvent identity. Indoline, however, is sensitive solely to specific solvation interactions with the silica substrate. (left) In particular, indoline adsorbed to silica surfaces from a variety of solvents appears to be sensitive solely to the hydrogen bond donating properties of the hydrophilic silica substrate.

Assisting in the interpretation of second harmonic spectra presented in Chapter 2 are the results of *ab initio* electronic structure calculations. Experimental results show solvatochromic shifts based on bulk solvent properties, and calculations performed serve to clarify the origin of the intermolecular interactions responsible for observed spectra. Since indoline, silica and the alcohols used in experiments can all accept *and* donate hydrogen bonds, calculated electronic transition moments of indoline directly hydrogen bonded to H-bond accepting or donating solvents (water and DMSO) are essential for identifying the strength and affinity of individual contributions.

1.3.2 Interfacial Solvent Structure and Organization Studies

Chapters 3 through 5 of this thesis describe experiments intended to quantify relative strengths and directionality of forces responsible for interfacial structure and organization at liquid interfaces. By comparing how experimental spectroscopic results change with small differences in solvent structure (molecule size, isomer conformation, and functional group identity) results can systematically isolate how intermolecular forces between the solvent and substrate and between interfacial solvent molecules themselves conspire to create highly varied, anisotropic structures intrinsic to interfaces.

Chapter 3 of this work details experiments performed using VSFG to investigate the interfacial structure of films formed at the silica/vapor interface by medium length (C_8-C_{11}) alkanes adsorbed from the vapor. By comparing the spectral features present under different experimental polarization conditions, as well as the intensity of selected features from one solvent system to the next, results in this chapter present directly measured information on the structure and orientation of adsorbed monolayers. Despite the relatively simple bulk spectroscopies of these linear alkanes, relative differences between transition dipole moments of methyl groups on either end of the molecule lead to significantly different spectra as the chain length increases.

Films of adsorbed alkanes at the silica/vapor interface are relatively simple model systems. Predicting structure and organization of functional group containing organic molecules at interfaces is more complex. Previous results from our group used VSFG to study octanol isomer monolayers adsorbed to the aqueous/vapor interface also sought to examine which intermolecular interactions give rise to

changes in interfacial order. VSFG spectra of 1-octanol at the aqueous/vapor interface have the characteristic spectral features of well-ordered, upright monolayers. Furthermore, surface tension measurements of these interfaces confirm surface areas per monomer consistent with an upright molecule. The isomers 2- and 3-octanol, however, sample both a larger surface area, and have spectra consistent with increased disorder and gauche defects within the monolayer that minimize aqueous-alkane interactions.[64] At all of these interfaces, the assumed strongest interaction is hydrogen bonding or solvation of the octanol hydroxyl group. Monolayers of octanol isomers at the silica/vapor interface will also be able to form strong hydrogen bonds. At the solid/vapor or solid/liquid interface, however, the alcohol cannot be solvated, thus the methyl- (ethyl-) group of the 2- (3-)octanol isomers must necessarily adopt a conformational defects in order to allow hydrogen bonding. While a number of studies have shown the thickness and density of 1-octanol adsorbed to the silica/vapor interface to be consistent with an upright orientation of alkyl chains, much less is known about how other isomers are organized at interfaces.

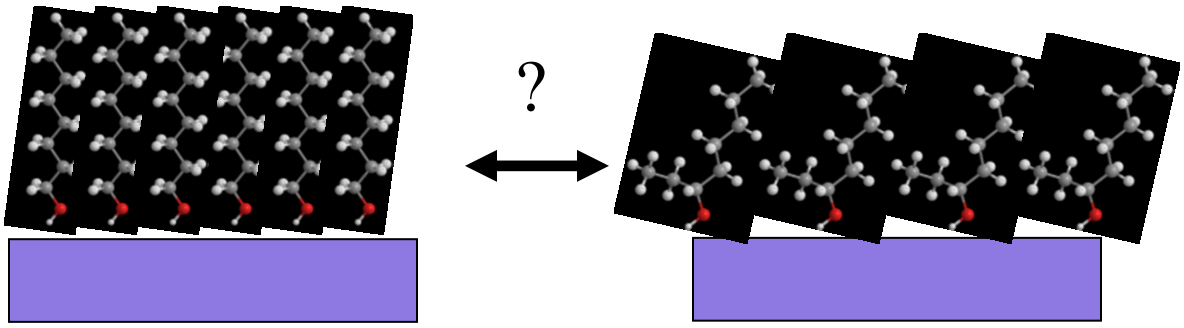

Figure 1.4 Schematic representation of octanol isomer monolayer formation at the silica/vapor interface. Experiments described in Chapter 4 show that all isomers appear to form well ordered, upright molecular monolayers at this interface, consistent with hydrogen bonding being the strongest molecular interaction with the substrate.

Experiments presented in Chapter 4 of this work describe both thermodynamic and spectroscopic studies that examine the structure and organization of octanol isomers adsorbed to the silica/vapor and silica/liquid interfaces. Properties of solid/liquid interfaces examined in Chapter 2 of this work can be used to infer the local structure and organization of 1-octanol in contact with silica. Results from the VSFG experiments that probe isomer structure directly suggest that like the aqueous/vapor interface, 1-, 2-, and 3-octanol at silica/vapor interfaces all form well ordered monolayers with molecules sampling an upright average orientation. Despite the strong hydrogen bonding interactions between octanol isomers and the substrate, interfacial structure changes dramatically when the substrate is brought into contact with the bulk liquid. Notably, 2- and 3-octanol at the silica/liquid interface lose all long range order present when these solvent molecules adsorb to the silica/vapor interface. Even 1-octanol loses some interfacial order, though the loss is less pronounced. Results presented here also show changes in interfacial structure when the solid/vapor interface is brought into contact with the liquid.

Many of the naturally occurring or technologically relevant examples of molecules organized at interfaces involve surfaces comprised of different types of molecules, or combinations or molecules. Order and organization there will depend on molecular identity, which in turn governs type and strength of interactions present between phases or molecules. Chapter 5 describe experiments and presents results showing how strength of substrate-solvent interactions impacts order at both the solid/vapor and solid/liquid interface by comparing VSFG spectra of equal size, but different functional group organic molecules adsorbed to these two interfaces. This

work compares measured surface organization to systematically varied possibilities available for interaction. These interactions include van der Waals (silica/octane), dipole or weak hydrogen bonding (silica/octyl cyanide), hydrogen bond donation from the substrate (silica/dimethyloctylamine), hydrogen bond donation and accepting (silica/1-octanol), and multiple hydrogen bond opportunities (silica/octylamine).

Chapter 2 of this thesis was published as a journal article. Results presented in Chapters 3-5 are also in preparation as separate journal articles. As a result, these chapters may contain some redundant material.

1.4 References

(1) Seidl, W. *Atmos. Environ.* **2000**, *34*, 4917-32.

(2) Laha, S.; Tansel, B.; Ussawarujikulchai, A. *J. Environ. Manage.* **2008**, *90*, 95-100.

(3) Cousins, I. T.; Beck, A. J.; Jones, K. C. *Sci. Total Environ.* **1999**, *228*, 5-24.

(4) Scheidegger, A. M.; Sparks, D. L. *Soil Sci.* **1996**, *161*, 813-31.

(5) Parikh, S. J.; Lafferty, B. J.; Sparks, D. L. *J. Coll. Int. Sci.*, *320*, 177-85.

(6) Kanti Sen, T.; Khilar Kartic, C. *Adv. Coll. Int. Sci.* , *119*, 71-96.

(7) Berka, M.; Pla Sandrine, P.; Rice James, A. *Langmuir*, *22*, 687-92.

(8) Honerkamp-Smith, A. R.; Veatch, S. L.; Keller, S. L. *Biochim. Biophys. Acta, Biomembr.* **2009**, *1788*, 53-63.

(9) van Meer, G.; Voelker, D. R.; Feigenson, G. W. *Nat. Rev. Mol. Cell Biol.* **2008**, *9*, 112-24.

(10) Wolf, C.; Quinn, P. J. *Prog. Lipid Res.* **2008**, *47*, 15-36.

(11) Hamon, Y.; Bernard, A.-M.; Salles, A.; Hawchar, O.; Marguet, D.; He, H.-T.; Guo, X.-J. *Immunol., Endocr. Metab. Agents Med. Chem.* **2008**, *8*, 358-65.

(12) Levi, V.; Villamil Giraldo, A. M.; Castello, P. R.; Rossi, J. P. F. C.; Gonzalez Flecha, F. L. *Biochem. J.* **2008**, *416*, 145-52.

(13) Kalipatnapu, S.; Chattopadhyay, A. *Cell. Mol. Neurobiol.* **2007**, *27*, 1097-116.

(14) Sengupta, P.; Hammond, A.; Holowka, D.; Baird, B. *Biochim. Biophys. Acta, Biomembr.* **2008**, *1778*, 20-32.

(15) Danielsen, E. M.; Hansen, G. *Mol. Membr. Biol.* **2006**, *23*, 71-79.

(16) Gombos, I.; Kiss, E.; Detre, C.; Laszlo, G.; Matko, J. *Immunol. Lett.* **2006**, *104*, 59-69.

(17) Ikegami, T.; Tomomatsu, K.; Takubo, H.; Horie, K.; Tanaka, N. *J. Chromatogr., A* **2008**, *1184*, 474-503.

(18) Scott, R. P. W. *Adv. Chromatogr.* **1982**, *20*, 167-215.

(19) Nath, S. *J. Coll. Int. Sci.* **1999**, *209*, 116-22.

(20) Hey, M. J.; Kippax, P. G. *Coll. Surf., A* **2005**, *262*, 198-203.

(21) Tahery, R.; Modarress, H.; Satherley, J. *Chem. Eng. Sci.* **2005**, *60*, 4935-52.

(22) Henn, A. R. *Biophys. Chem.* **2003**, *105*, 533-43.

(23) Garfias, F. J. *J. Phys. Chem.* **1980**, *84*, 2297-300.

(24) Perry, A.; Ahlborn, H.; Space, B.; Moore, P. B. *J. Chem. Phys.* **2003**, *118*, 8411-19.

(25) Lu, J. R.; Thomas, R. K.; Penfold, J. *Adv. Coll. Int. Sci.* **2000**, *84*, 143-304.

(26) Lu, J. R.; Thomas, R. K. *Appl. Neutron Scattering Soft Condens. Matter* **2000**, 205-25.

(27) Reiter, R.; Motschmann, H.; Orendi, H.; Nemetz, A.; Knoll, W. *Langmuir* **1992**, *8*, 1784-8.

(28) Chanda, J.; Bandyopadhyay, S. *J. Phys. Chem. B* **2006**, *110*, 23443-49.

(29) Benderskii, A. V.; Eisenthal, K. B. *J. Phys. Chem. B.* **2000**, *104*, 11723-28.

(30) Papirer, E.; Editor *Adsorption on Silica Surfaces.* ; Marcel Dekker, Inc.: New York, 2000.

(31) Liu, Y.; Wolf, L. K.; Messmer, M. C. *Langmuir* **2001**, *17*, 4329-35.

(32) Kawasaki, M.; Imazeki, S.; Oh-e, M.; Ando, M. *Jpn. J. Appl. Phys.* **2008**, *47*, 6247-50.

(33) McHale, J. M.; Auroux, A.; Perrotta, A. J.; Navrotsky, A. *Science* **1997**, *277*, 788-91.

(34) Searcy, A. W.; Beruto, D. T.; Barberis, F. *J. Chem. Phys.* **2009**, *130*, 184713/1-13/10.

(35) Van Oss, C. J.; Good, R. J.; Chaudhury, M. K. *Langmuir* **1988**, *4*, 884-91.

(36) Langevin, D. *Adv. Coll. Int. Sci.* **2001**, *89-90*, 467-84.

(37) Bain, C. D. *Curr. Opin. Coll. Int. Sci.* **1998**, *3*, 287-92.

(38) Inaba, A. *Pure Appl. Chem.* **2006**, *78*, 1025-37.

(39) Schlossman, M. L. *Curr. Opin. Coll. Int. Sci.* **2002**, *7*, 235-43.

(40) Magid, L.; Penfold, J.; Schurtenberger, P.; Wagner, N. *Curr. Opin. Coll. Int. Sci.* **2002**, *7*, 193-95.

(41) Fragneto-Cusani, G. *J. Phys.: Condens. Matter* **2001**, *13*, 4973-89.

(42) Benjamin, I. *Ann. Rev Phys. Chem.* **1997**, *48*, 407-51.

(43) Benjamin, I. *Chem. Phys. Lett.* **2004**, *393*, 453-56.

(44) Chandross, M.; Lorenz, C. D.; Stevens, M. J.; Grest, G. S. *Langmuir* **2008**, *24*, 1240-46.

(45) Chandross, M.; Webb, E. B., III; Stevens, M. J.; Grest, G. S.; Garofalini, S. H. *Phys. Rev. Lett.* **2004**, *93*, 166103/1-03/4.

(46) Schmitt, J.; Danner, B.; Bayerl, T. M. *Langmuir* **2001**, *17*, 244-46.

(47) Chang, T.-M.; Dang, L. X. *Chem. Rev.* **2006**, *106*, 1305-22.

(48) Ishiyama, T.; Morita, A. *J. Phys. Chem. A* **2007**, *111*, 9277-85.

(49) Sun, X.; Dang, L. X. *J. Chem. Phys.* **2009**, *130*, 124709/1-09/4.

(50) Corn, R. M.; Higgins, D. A. *Chem. Rev.* **1994**, *94*, 107-25.

(51) Eisenthal, K. B. *Chem. Rev.* **1996**, *96*, 1343-60.

(52) Shen, Y. R. *Nature.* **1989**, *337*, 519-25.

(53) Shen, Y. R. *Solid State Communications* **1992**, *84*, 171-2.

(54) Tamburello Luca, A. A.; Hebert, P.; Brevet, P. F.; Girault, H. H. *J. Chem. Soc., Faraday Trans.* **1995**, *91*, 1763-8.

(55) Corn, R. M. *Proceedings of SPIE-The International Society for Optical Engineering* **1992**, *1636*, 117-24.

(56) Ong, S.; Zhao, X.; Eisenthal, K. B. *Chem. Phys. Lett.* **1992**, *191*, 327-35.

(57) Steel, W. H.; Beildeck, C. L.; Walker, R. A. *J. Phys. Chem. B* **2004**, *108*, 16107-16.

(58) Steel, W. H.; Lau, Y. Y.; Beildeck, C. L.; Walker, R. A. *J. Phys. Chem. B.* **2004**, *108*, 13370-78.

(59) Wang, H.; Borguet, E.; Eisenthal, K. B. *J. Phys. Chem. A.* **1997**, *101*, 713-18.

(60) Wang, H.; Borguet, E.; Eisenthal, K. B. *J. Phys. Chem. B.* **1998**, *102*, 4927-32.

(61) Shen, Y. R. *Nonlinear Spectroscopy for Molecular Structure Determination* **1998**, 249-71.

(62) Shultz, M. J.; Baldelli, S.; Schnitzer, C.; Simonelli, D. *J. Phys. Chem. B.* **2002**, *106*, 5313-24.

(63) Zhu, X. D.; Suhr, H.; Shen, Y. R. *Phys. Rev. B: Condensed Matter and Materials Physics* **1987**, *35*, 3047-50.

(64) Can, S. Z.; Mago, D. D.; Esenturk, O.; Walker, R. A. *J. Phys. Chem. C* **2007**, *111*, 8739-48.

(65) Can, S. Z.; Mago, D. D.; Walker, R. A. *Langmuir* **2006**, *22*, 8043-49.

(66) Shultz, M. J.; Schnitzer, C.; Simonelli, D.; Baldelli, S. *Int. Rev. Phys. Chem.* **2000**, *19*, 123-53.

Chapter 2: Differentiating Solvation Mechanisms at Polar Solid/Liquid Interfaces

2.1 Abstract

This chapter describes experiments that use resonance enhanced second harmonic generation (SHG) has been used to identify solvation mechanisms at different solid/liquid interfaces. Solvation interactions are characterized as being either nonspecific and averaged over the entire solute cavity or specific, referring to localized, directional interactions between a solute and its surroundings. SHG spectra report the electronic structure of solutes adsorbed to silica/organic solvent interfaces, and different solutes are chosen to probe either interfacial polarity or interfacial hydrogen bond donating/accepting opportunities. SHG results show that interfacial polarity probed by *p*-nitroanisole depends sensitively on solvent structure whereas hydrogen bonding interactions probed by indoline are insensitive to solvent identity and instead are dominated by the hydrogen bond donating properties of the polar silica substrate. The bulk solvation interactions were modeled with a series of *ab initio* calculations that characterized solute electronic structure within a dielectric continuum and in the presence of explicit, individual solvent molecules. Collectively, these measurements and calculations create a comprehensive picture of how solvation mechanisms vary at different polar, solid surfaces.

2.2 Introduction

Solvation at solid/liquid interfaces will differ from bulk solution limits due to a solute's interactions with the substrate as well as the structural and dynamic changes induced by the substrate in the adjacent solvent. Given that surface mediated solvation will control solute concentration, structure and reactivity at interfaces, understanding the effects of a surface on solvation is essential for predicting solution-phase surface chemistry. Numerous studies have shown that different solute properties near solid/liquid interfaces can depend on solvent structure, surface composition and solute identity.[1-12] However, many of these reports vary only a limited number of parameters, and the resulting interpretation provides only a partial picture of how the chemical asymmetry found at surfaces leads to unique interfacial environments. Experiments described below examine how solvation mechanisms vary at interfaces formed between organic liquids and polar silica surfaces. Specifically, solutes are chosen to probe independently interfacial polarity and hydrogen bonding. Results show that solvent polarity depends sensitively on solvent structure, whereas, hydrogen bonding opportunities remain largely independent of solvent identity, even when the solvent itself can form strong hydrogen bonds.

In this study, we characterize solvation as being either nonspecific or specific.[13-15] Nonspecific solvation refers to solvent-solute interactions that are averaged over the entire solute cavity. Solvent polarity stands out as an example of this type of solvation. When considering polarity, one treats the solvent as an effective polarizable continuum around an overall solute dipole. Polarity itself lacks a rigorous, quantitative definition and includes a sum over all noncovalent

interactions experienced between a solute and its surroundings. Nevertheless, numerous theoretical and empirical scales have emerged to characterize this property, and in recent years simulations have attempted to isolate contributions made by solvent dipolar and dispersion forces to a solute's electronic structure.[16-19] In contrast to solvent polarity, specific solvation describes solvent-solute interactions that are localized and directional. Examples of this type of solvation include dipole-dipole, charge-dipole and hydrogen bonding interactions. Again, many studies have proposed empirical scales to treat the effects of specific solvation interactions on solute chemistry, but only a few of these efforts have resulted in models that are sufficiently general to cover a variety of solutes solvated by many different classes of solvents.[13,20-22]

At solid/liquid interfaces one expects both nonspecific and specific solvation interactions to be different than in bulk solution. First, depending on the magnitudes and types of interactions, interfacial solute concentrations may be enhanced through adsorption or depleted by unfavorable energetics (such as Coulomb repulsions or hydrophobic effects).[23-26] Second, the surface itself will alter a solvent's density, local dielectric constant and viscosity, thereby changing solvent-solute interactions across the anisotropic, interfacial region.[6,8,27-31] These effects – direct substrate/solute interactions and substrate induced changes in solvent properties – can have consequences for a multitude of technologically and biophysically relevant phenomena. For example, attractive substrate-solute interactions can be tailored to drive the assembly of well-ordered arrays of adsorbates at the solid/liquid interface. Such systems can include functionalized

electrodes and thin films constructed specifically to serve as sensors. [32,33] Creation of an organized assembly requires that the overall change in system free energy be favorable but often necessitates overcoming specific individual interactions (such as arrays of parallel aligned dipoles or like-charges) that are energetically (or entropically) destabilizing. If, however, the surface also enhances interfacial solvation interactions, effectively screening adsorbed solutes from each other, then such self assembled species can enjoy greater structural and organizational uniformity.

A second example of how different types of solvation can impact interfacial processes comes from the general area of chromatography. Adsorption to silica surfaces has been investigated intensively for decades.[34-37] These studies have led to a detailed understanding of how chemisorbed solutes aggregate on silica surfaces as well as empirical procedures designed to functionalize these surfaces and minimize the chromatographic tailing. In reverse phase chromatography columns, the silica is treated with an alkylating agent to reduce the number of surface silanol groups.[37] Large scale industrial applications motivate manufacturers to go to great lengths to "cap" these hydrogen bonding sites with small alkyl silanes. Still, researchers propose that uncapped, acidic silanol groups and topographical inhomogeneities bear responsibility for retaining more basic analytes through hydrogen bond donation *from* the silanol to the adsorbed solute.[36,38-41]

In the experiments described below, resonance enhanced second harmonic generation (SHG) is employed to examine specific and nonspecific solvation

properties at solid/liquid interfaces formed between hydrophilic silica and different organic liquids. Complementing these measurements are a series of *ab initio* calculations intended to isolate and quantify the role played by different intermolecular interactions contributing to solvation. Experiments measure the solvatochromic behavior of both pNAs and indoline adsorbed to these boundaries, and results show that polarity varies considerably with solvent structure, but hydrogen bonding appears to be controlled primarily by solute/substrate interactions. In particular, interfaces formed between silica and alkanes are more polar than bulk solution but the quantitative change(s) in local dielectric environment correlate with solvent packing efficiencies (as inferred from bulk densities, melting points, and previously reported X-ray scattering studies).[8,30] Strongly associating solvents such as alcohols create a heterogeneous distribution of polarities across the interface implying the existence of anisotropic, ordered Langmuir film-like structures.[11,12] In contrast to the solvent-dependent polarity results, specific solvation experienced by indoline at these same interfaces is dominated by the hydrogen bond donating properties of the solid surface, regardless of solvent identity. Only by rendering the silica surface hydrophobic are specific solvation forces changed at the solid/liquid interface.

2.3 Experimental

To establish benchmark solvent-solute interactions in bulk solution, absorbance spectra of the solutes in different solvents were acquired using a Hitachi U-3010 spectrophotometer, with 1 nm resolution. Solution concentrations were adjusted

such that the maximum absorbances were between 0.1 and 1.0. Figure 1 shows the absorbance maxima corresponding to the lowest allowed electronic excitations of *p*-nitroanisole (pNAs) and indoline in a variety of solvents. The solvents are distinguished by their Onsager polarity functions f(ε)[42]

$$f(\varepsilon) = \frac{2(\varepsilon - 1)}{(2\varepsilon + 1)} \qquad (2.1)$$

where ε is a solvent's static dielectric constant. (Table 2.1) pNAs is sensitive to nonspecific solvation forces as evidenced by an excitation wavelength that increases monotonically from 293 nm to 317 nm as solvent polarity increases from that of alkanes (ε = 2.0, f(ε) = 0.40) to that of water and DMSO (ε_{H2O} = 78, $f(\varepsilon)_{H2O}$ = 0.98; ε_{DMSO} = 37, $f(\varepsilon)_{DMSO}$ = 0.96), respetively. (Figure 2.2, top) In contrast, λ_{max} of indoline is insensitive to polarity, remaining near 300 nm for a collection of solvents varying in polarity from alkanes to acetonitrile (ACN). When indoline is dissolved in DMSO, however, λ_{max} shifts to 307 nm and in H_2O (pH = 6.2), λ_{max} of indoline falls to 288 nm. (Figure 2.1, bottom) While ACN, DMSO and H_2O have similar polarities – f(ε) = 0.96 – 0.98 for the three solvents – ACN is a poor hydrogen bonding solvent, DMSO is a strong hydrogen-bond accepting solvent and H_2O can both accept *and* donate hydrogen bonds. The hydrogen bond donating ability of H_2O is responsible for the dramatic shift to shorter wavelength for λ_{max} as will be discussed in Section 2.3.

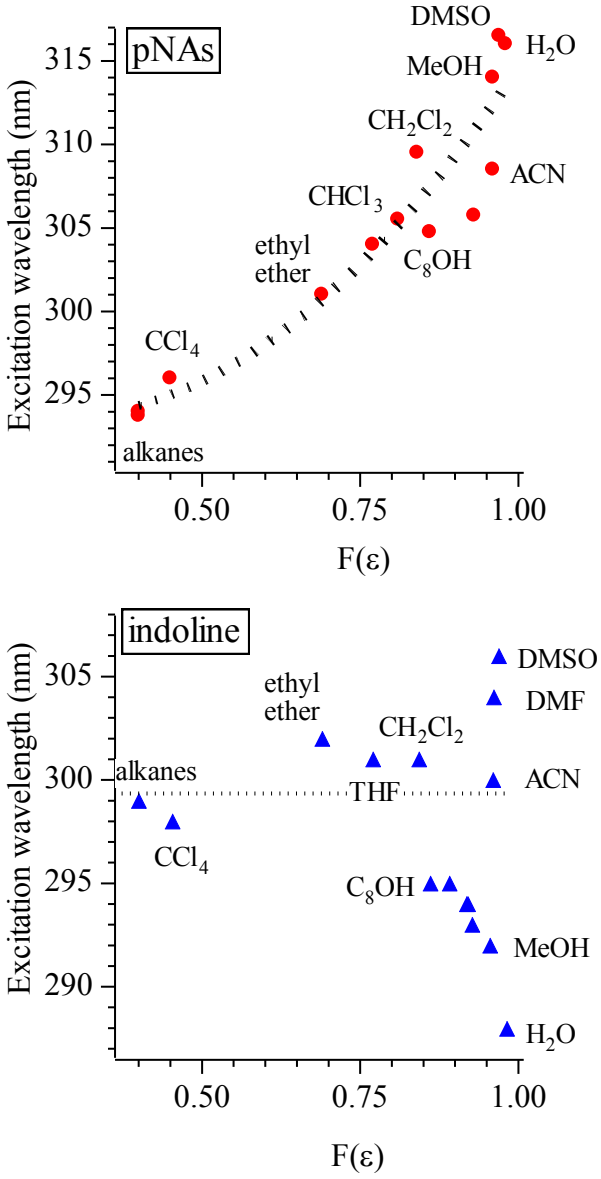

Figure 2.1. Solvatochromic activity of pNAs and indoline in various bulk solvents. Excitation wavelengths are plotted as a function of solvent's Onsager polarity function defined in Equation 1. Uncertainties in excitation maxima are ± 1 nm. Linewidths in solution vary between 30 – 40 nm. Dashed lines are included to serve as guides to the eye.

To measure solvation interactions at solid/ liquid interfaces, resonance enhanced SHG was used to acquire effective excitation spectra of adsorbed solutes. SHG is

a second order, nonlinear optical (NLO) technique that is inherently surface specific.[9,43,44] A number of studies have used SHG to report solvatochromic shifts of solutes adsorbed to liquid interfaces,[11,45-47] and Wang, *et al*. used solvatochromic activity measured by SHG to develop a generalized interfacial polarity scale.[48] SHG relies on the generation of a second order polarization by an incident oscillating electromagnetic field. The second harmonic field is proportional to the square of the incident field:

$$P^{(2)}(2\omega) = \chi^{(2)} E(\omega)^2 \qquad (2.2)$$

where $\chi^{(2)}$ is the sample's macroscopic second order susceptibility. This third ranked tensor contains all of the information related to the spatially averaged hyperpolarizability of molecules at surfaces, and, under the electric dipole approximation, is zero in isotropic media. The tensor contains both resonant and nonresonant contributions:

$$\chi^{(2)} = \chi^{(2)}_{R} + \chi^{(2)}_{NR} \qquad (2.3)$$

Typically, the resonant portion is much larger than the nonresonant term, and can be expressed as a function of real and virtual excitation energies:

$$\chi_R^{(2)} = \sum_{k,e} \frac{\mu_{gk}\mu_{ke}\mu_{eg}}{(\omega_{gk} - \omega - i\Gamma)(\omega_{eg} - 2\omega + i\Gamma)} \qquad (2.4)$$

where μ_{ij} is the transition matrix element between two states i and j. The intensity of the second harmonic field depends quadratically on the incident light intensity and the squared magnitude of the nonlinear susceptibility.

$$I_{2\omega} \propto \left|P^{(2)}\right|^2 = \left|\chi^{(2)}\right|^2 \cdot I_\omega{}^2 \qquad (2.5)$$

By scanning the incident wavelength and monitoring the intensity of the coherently scattered second harmonic signal, experiments can measure effective excitation spectra of solute molecules in the isotropic environment presented by liquid interfaces.

SHG experiments in these studies were conducted with a variety of solutions consisting of pNAs or indoline dissolved in organic solvents that were then brought into contact with a hydrophilic or hydrophobic silica prism. The solutes were purchased from Aldrich and used without further purification. (Reported purities were 99% for indoline, ≥ 97% for pNAs with major contaminants being structural isomers.) The SHG cell and detection assembly has been described previously.[11,12,31,49] For experiments requiring a hydrophilic silica surface the prism was cleaned in a 50/50 mixture (by volume) of sulfuric and nitric acids for several hours, thoroughly rinsed with deionized water (Millipore) and allowed to dry under a N_2 atmosphere. Given that all experiments were carried out with solvents that contained varying amounts of dissolved H_2O, no additional efforts were made to remove any H_2O film that likely remained adsorbed to the hydrophilic silica surface. For experiments requiring a hydrophobic surface, the prism was cleaned in a similar fashion and then exposed to dichlorodimethylsilane vapor overnight. Static contact angle measurements with water showed angles in excess of 100 degrees in agreement with literature reports.[50] All SHG spectra were collected at a temperature of 21 ± 1° C. Solution concentrations ranged from 50-100 mM for both solutes in alkanes, 200 mM in alcohols, and 200 mM for indoline in cyclohexane for measurement at the hydrophobic silica interface.

These concentrations were necessary in order to acquire measurable SHG data. Smaller concentrations led to anticipated reductions in signal intensity, but not to qualitative changes in electronic resonance wavelengths or band shapes.

The SHG apparatus uses the 1 kHz output of a Ti:sapphire regeneratively amplified, femtosecond laser (Clark-MXR CPA 2001, 130 fs pulse duration, 700 μJ). The output of the Ti:sapphire laser pumps a commercially available visible optical parametric amplifier (OPA, Clark-MXR). The visible output of the OPA is tunable from 550 – 700 nm with a bandwidth of 2.5 ± 0.5 nm. The polarization of the incident beam is controlled using a Glan-Taylor polarizer and a half wave plate. The fundamental 775 nm and any SH light generated from preceding optics are blocked with a series of filters prior to the detector. The incident light impinges on the interface at an angle of 68˚ relative to the surface normal and the second harmonic response is detected in reflection using photon counting electronics. A second polarizer selects the SH polarization, and a short pass filter and monochromator serve to separate the signal from background radiation due to scattering or fluorescence.

All reported spectra were collected using p-polarized incident light, and passing p-polarized second harmonic signal. SH signals were normalized for incident power, and care was taken to confirm quadratic behavior of $I(2\omega)$ on $I(\omega)$ at all wavelengths. Spectra shown in this work represent the average of 2-4 separate experiments acquired on separate days with new solutions and freshly cleaned cells. Each data point in a spectrum represents the average of at least three, ten-second integrations of detected SHG signal.

In addition to interfacial solvation, the average orientations of pNAs and indoline adsorbed to representative solid/liquid interfaces were determined from the polarization dependent second harmonic response. Following established protocols, the data enabled us to determine three unique, nonzero elements of $\chi^{(2)}$, χ_{XXZ}, χ_{ZXX}, and χ_{ZZZ},. These data were coupled with calculated hyperpolarizabilities to estimate averaged adsorbate orientations at both alkane/silica and alcohol/silica interfaces using well developed methods reported in the literature.[43,44,51] *Ab initio* methods (Gaussian 03[52]) were also used to calculate electronic transition energies of pNAs and indoline in a cavity surrounded by a polarizable continuum characterized by a static dielectric constant, ε. Where hydrogen bonding might be expected, explicit solvent molecules were included in the cavity itself to simulate specific solvent-solute interactions. To model the experimental results, we performed a series of calculations using time dependent density functional theory (TDDFT) to determine excitation energies in cavities created within a polarizable continuum model (IEFPCM). Solvent systems were chosen to model results from experiments, namely, pNAs in nonpolar and polar cavities, indoline in nonpolar and polar cavities, and indoline in polar cavities with explicit water and DMSO solvent molecules included to capture the effects of hydrogen bond donation and acceptance. pNAs and indoline's gas phase geometries were optimized for the lowest energy structure at the MP2 level of theory using a 6-31G(d) basis set. After geometry optimization a TDDFT calculation was performed with the BLYP functional and 6-31+G(d,p) basis set in order to determine the electronic transition

wavelengths and hyperpolarizabilities. Due to a systematic error in excitation energies, we normalized the frequencies to the gas phase calculation limit to enable comparison with experimental results. (Table 1) Determining the hyperpolarizabilities of pNAs and indoline required using a HF level of theory with a 6-31+G(d,p) basis set and the POLAR=EnOnly keyword. All calculations were performed using Gaussian 03.[52]

2.4 Results

2.4.1 Electronic structure calculations

Experimental and calculated solute transition wavelengths and solvatochromic activity are reported in Table 1. Since the electronic structure of pNAs is sensitive only to solvent polarity, calculations of this solute's electronic structure were carried out without explicit solvent molecules in the cavity. Given indoline's polarity-independent electronic structure, calculations for this solute required the presence of explicit solvent molecules to replicate solute electronic structure in hydrogen bond donating and hydrogen bond accepting environments. DMSO can only accept H-bonds. Water can both accept and donate hydrogen bonds, but reported calculations of the negative enthalpies of hydrogen bond formation show that the hydrogen bond donated by H_2O to related phenols is much stronger than the hydrogen bond formed with H_2O as the hydrogen bond acceptor.[53-55]

Figure 2 shows optimized, gas-phase structures of pNAs and indoline as well as the scaled, calculated wavelengths of both solutes in representative solvent environments. The calculated solvatochromic data are also summarized in Table 2.1.

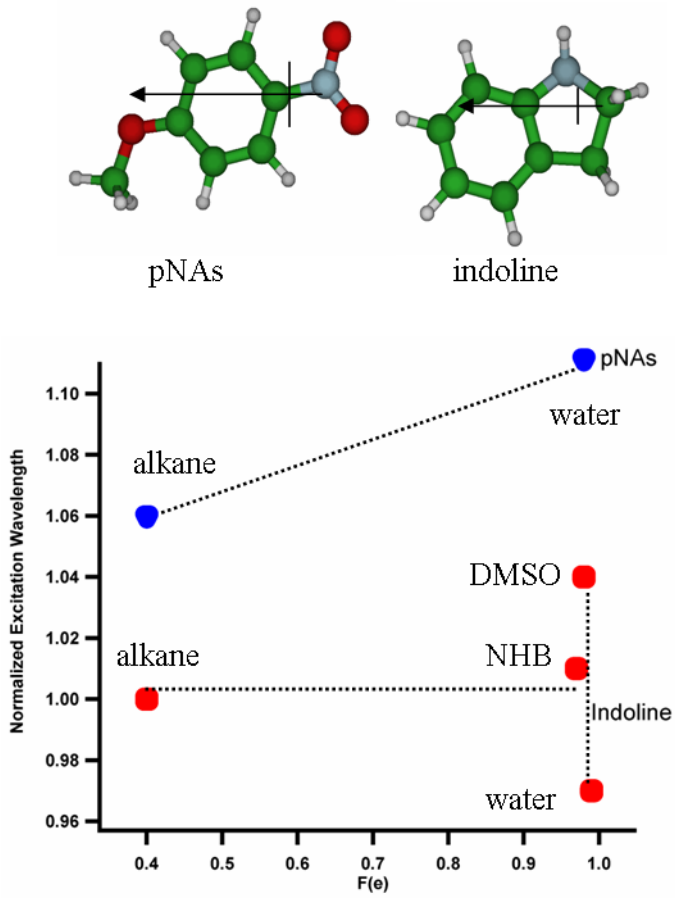

Figure 2.2. Normalized transition wavelengths for pNAs in different solvents as determined from *ab initio* calculations described in the text. NHB stands for a polarizable continuum without any explicit solvent molecules in the solute cavity capable of accepting or donating hydrogen bonds. Reported normalized wavelengths are scaled to the calculated gas phase transition wavelengths. (A normalized wavelength of 1.00 coincides with the gas phase limit.) Also shown are the molecular structures with the S_0-S_1 transition dipole vectors superimposed.

Table 2.1. Polarity data and excitation wavelengths *p*-nitroanisole (pNAs) and indoline in different solvents. Onsager polarity functions (f(ε)) were calculated according to Reference 42. Calculated wavelengths were determined using a polarizable continuum model (IEFPCM) as described in the text. In the case of indoline, the DMSO and water calculations also included an explicit solvent molecule inside of the solute cavity as described in the text.

Solvent	ε	f(ε)	λ□ (bulk, nm)		λ(calculated, nm)	
			pNAs	indoline	pNAs	indoline
cyclohexane	2.04	0.41	293	299	321.3	304.6
methylcyclohexane	2.03	0.41	294	299		
CCl_4	2.24	0.45	294	298		
ethyl ether	4.20	0.68	300	302		
chloroform	4.89	0.72	310	299		
methylene chloride	8.93	0.8	309	301		
1-octanol	10.3	0.86	304	295		
1-propanol	20.5	0.93	307	293		
methanol	32.7	0.95	313	292		295.6
acetonitrile	35.9	0.96	308	300		305.8
DMSO	46.5	0.97	317	307		313.4
water	78.4	0.98	317	288	336.9	294.7

The computational results reported in Figure 2.2 and Table 2.1 reflect clearly the trends observed experimentally and reported in Figure 2.1, namely that pNAs exhibits a pronounced red shift in excitation wavelength with increasing polarity whereas indoline electronic structure depends little on its local dielectric environment. Furthermore, the red and blue shifts of indoline's excitation wavelength in DMSO and water, respectively, can be understood by the participation of the nitrogen lone pair in the solute's electronic structure. The hydrogen-bond accepting ability of DMSO leaves the indoline nitrogen's lone pair isolated and inductively promotes lone pair delocalization into the aromatic ring following excitation. The resulting larger change in permanent dipole leads to a shift in excitation to lower energies (and longer wavelength). In contrast, the hydrogen bond donating property of water stabilizes indoline in its ground state thereby increasing the energetic gap between ground and excited electronic states leading to the experimentally observed blue shift in excitation wavelength.[21,56,57]

2.4.2 Polarity and hydrogen bonding at alkane/silica interface

The data in Figure 2.1 show pNAs to be very sensitive to its local dielectric environment while indoline samples hydrogen bonding opportunities. Figure 2.3 shows SHG spectra of pNAs and indoline adsorbed to the silica/cyclohexane and silica/ methylcyclohexane interfaces. For pNAs the dashed vertical lines represent excitation wavelengths of the solute in both polar (water) and nonpolar (alkane) limits. The solid vertical lines indicate the excitation wavelength maximum resulting from fitting the data to equations 2.2-5. Nonzero contributions from the nonresonant piece of $\chi^{(2)}$, can lead to asymmetry in the band profiles meaning that

the interfacial excitation wavelength does not always match the wavelength having maximum signal intensity in the SHG spectra.

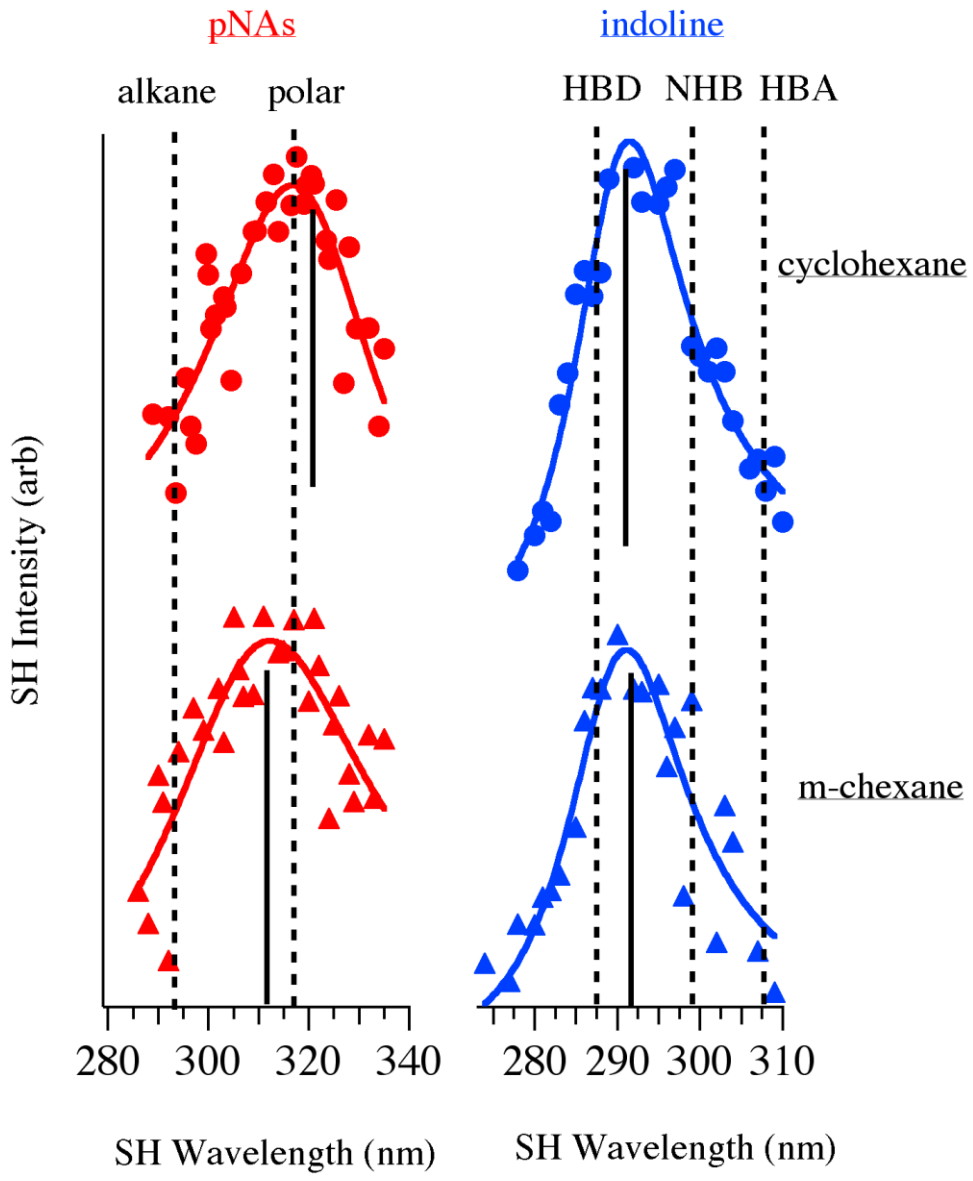

Figure 2.3. SHG data from pNAs (left) and indoline (right) adsorbed to silica/cyclohexane interfaces (top) and silica/methylcyclohexane (bottom) interfaces. The "polar" and "alkane" dashed lines in the pNAs spectra denote excitation wavelengths in bulk water and alkane solvents, respectively. "HBD", "NHB" and "HBA" labels on the dashed lines in the indoline spectra denote excitation wavelength limits in hydrogen bond donating, non-hydrogen bonding and hydrogen bond accepting solvents. The black solid lines represent excitation

wavelengths of the different solutes at solid/liquid interfaces. Note that differences between intensity maxima in the spectra and the calculated excitation wavelengths can result from a nonresonant contribution to the $\chi^{(2)}$ tensor as shown in Equation 2.3, and described in the text.

Spectra in Figure 2.3 show that pNAs samples distinctly different nonspecific solvation environments at the interface between silica and these two solvents. Based on their static dielectric constants, cyclohexane (2.04) and methylcyclohexane (2.03) have virtually identical polarities as reflected by equivalent maximum absorption wavelengths of pNAs in both solvents (293 nm). At the silica/cyclohexane interface, however, pNAs experiences a more polar environment (λ_{SHG}= 321 ± 3nm) compared to the less polar interface formed between silica and methylcyclohexane (λ_{SHG}= 312 ± 3nm). Using data in Figure 2.1 to approximate an effective interfacial polarity for both of these systems, we find that the cyclohexane/silica interface is even more polar than an aqueous environment ($f(\varepsilon) \sim 1.0$) whereas the methylcyclohexane/silica interface has a dipolar environment corresponding to a local Onsager function of 0.9. With its high density of silanol groups one might expect the interfacial polarity to be close to that of a polar, protic solvent such as water. However, the spectra of pNAs adsorbed to these different silica alkane interfaces show that nonspecific solvation at these boundaries depends on solvent structure as well as solute/substrate interactions.

Surface silanol groups can contribute to the local dipolar environment in several ways. First, surface silanol groups represent a dense collection of immobile dipoles that can polarize the interfacial solute (and solvent) creating a local

dielectric environment more polar than bulk solution. Surface silanol groups can also donate and/or accept hydrogen bonds. The collective effect of these contributions to interfacial polarity is reported by adsorbed pNAs, a solute chosen to probe nonspecific or spatially averaged interactions. Indoline's electronic structure, however, is capable of differentiating the general dielectric effects from hydrogen-bond donating and accepting interactions. The right side of Figure 2.3 shows the SHG spectra of indoline adsorbed to the silica/cyclohexane and silica/methylcyclohexane interfaces. In these spectra vertical dashed lines indicate the absorption maxima in bulk water (288 nm), non-hydrogen bonding solvents such as alkanes and acetonitrile, 299 nm), and DMSO (307 nm). These solvents are chosen to reflect limiting cases for indoline in hydrogen bond donating (HBD), non-hydrogen bonding (NHB), and hydrogen bond accepting (HBA) environments, respectively. The spectra are fit as described above with excitation maxima marked by solid vertical lines. Both spectral fits have maxima at 291 ± 2 nm, a result characteristic of a strong hydrogen bond donating environment.

We attribute these specific solvation effects to the hydrogen-bond donating properties of the surface silanol groups of the silica substrate, although we can not rule out contributions from water strongly bound to the silica substrate. Supporting our assignment are several studies that report on highly acidic properties of surface silanol groups on chromatographic silica,[58] as well as the fact that the polarity-dependent results show clear differences in the interfacial dielectric environments, even for different alkanes having equivalent bulk solvating properties. If interfacial water were responsible for the observed

hydrogen bond donating properties of the surface, we might expect the polarities of both interfaces (silica/cyclohexane and silica/methylcyclohexane) to be similar.[59,60] Regardless of the source of the strong hydrogen bond donating properties, the data in Figure 2.3 show clearly that interfacial solvation differs considerably from bulk solution limits *and* interfacial effects on solvation *are not* the same for different solutes.

To further explore the dependence of nonspecific and specific solvation on solvent structure, we examined the solvatochromic responses of pNAs and indoline at interfaces formed between hydrophilic silica and solvents capable of interacting strongly with the solid substrate. Figure 2.4 compares the SHG spectra of pNAs and indoline at interfaces formed between silica and 1-octanol and between silica and 1-propanol.

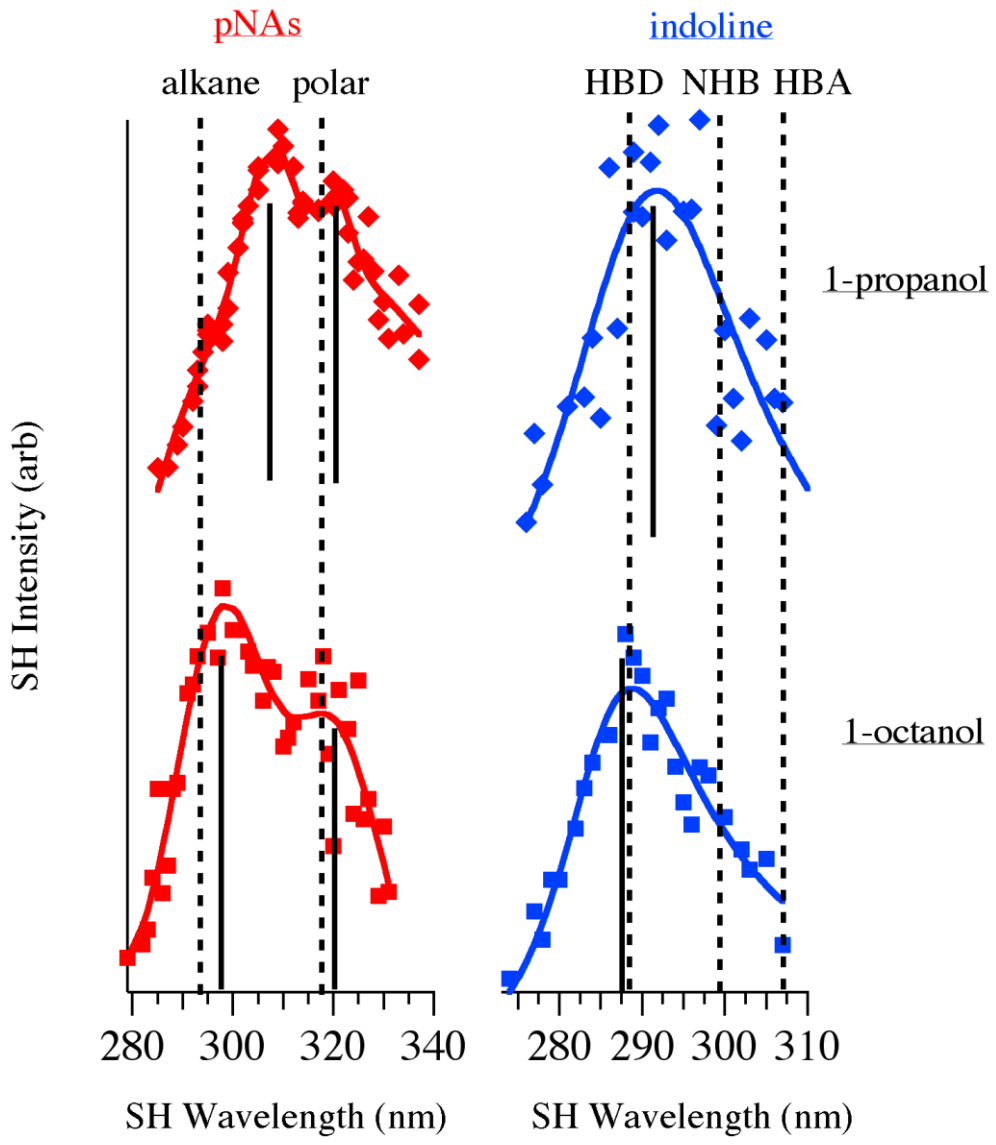

Figure 2.4. SHG data from pNAs (left) and indoline (right) adsorbed to silica/1-propanol interfaces (top) and silica/1-octanol (bottom) interfaces. Other markings as in Figure 3. Data for pNAs were fit to two distinct electronic resonances. Similar efforts to fit the indoline data to two features resulted in the second feature always having amplitudes > 10x smaller than the primary feature.

Unlike the spectrum from the silica/cyclohexane interface that shows only a single electronic resonance, the SHG spectra of pNAs at a silica/1-octanol and

silica/1-propanol interfaces can only be fit with two contributing features having the same phase. The higher intensity features show maxima centered at 297 ± 3 nm and 307 ± 3 nm for octanol and propanol, respectively, and the lower intensity peaks appear at ~320 nm for both solid/liquid systems. That there are two features in the silica/alcohol spectra is not surprising. Previous studies have reported similar heterogeneous environments at hydrophilic solid/protic solvent, solid/liquid interfaces.[11,12,31] Creation of these microscopic domains having dramatically varying properties has been ascribed to surface induced polar ordering of the interfacial solvent species.[61,62]

Based on the data in Figure 4 as well as related findings from previous reports, we conclude that pNAs adsorbed to silica/1-octanol and silica/1-propanol interfaces samples two distinct polarities – one having a high effective dielectric constant ($f(\varepsilon_{eff}) \sim 1.0$ and $\varepsilon_{eff} > 80$) and the other being distinctly nonpolar ($f(\varepsilon_{eff}) \sim 0.5$ and $\varepsilon_{eff} \sim 4$ for 1-octanol; $f(\varepsilon_{eff}) \sim 0.8$ and $\varepsilon_{eff} \sim 9$ for 1-propanol). The lack of interference between the two features implies that pNAs monomers in the two different dipolar environments share similar orientations, and orientation measurements of pNAs at the silica/1-octanol interface presented below further support this claim.

This result supports a picture of interfacial solvent structure where the –OH groups of the alcohol solvent hydrogen bond to the silica substrate, and the chains organize to form a Langmuir-like film that is responsible for the nonpolar environment sampled by the solute. The solutes then partition into the nonpolar region with some monomers continuing to interact strongly with the silica

substrate. If relative band intensities reflect approximate populations, one would conclude that for both silica/1-octanol and silica/1-propanol, more pNAs samples the nonpolar environment. Such a conclusion would be consistent with partitioning studies that show pNAs to be ~20x more soluble in alkanes than in water.[49] However, this interpretation neglects the effects of average solute orientation on SH intensity and the higher intensity may simply reflect a more upright orientation of the pNAs in the nonpolar region leading to a larger projection of it's hyperpolarizability on the surface normal. Average solute orientation results determined from polarization dependent changes in SHG intensity described below support the claim that differences in peak intensities are due to population differences and not changes in solute orientation.

The heterogeneities in polarity observed across silica/alcohol interfaces are not reflected in hydrogen bonding opportunities across these same boundaries. Figure 2.4 also shows the SH spectra of indoline adsorbed to the same silica/1-octanol and silica/1-propanol interfaces. Dashed lines indicate bulk excitation limits in hydrogen bond donating, non-hydrogen bonding and hydrogen bond accepting environments, and solid vertical lines represent excitation wavelength maxima. The distinctive environments indicating clear differences in *nonspecific* solvation at the silica/1-octanol and silica/1-propanol interfaces are absent in the data from indoline adsorbed to these same boundaries. Indoline at the silica/1-octanol interface has an single maximum at 287 ± 2 nm in its SH spectrum. This λ_{max} is shifted slightly beyond the strong hydrogen bond donating limit represented by a bulk aqueous solvent. For the case of silica/1-propanol, the SH

maximum falls at 290 ± 2 nm. This observation provides additional evidence that specific solvation forces at these polar solid/liquid interfaces depend largely on solute-substrate interactions with little contribution from the solvent itself. We propose that the small but reproducible shift of the indoline solvatochromic data beyond the strong hydrogen bonding limit at the silica/1-octanol interface arises from reduced solute mobility. Strong hydrogen bonding between the silica substrate and the interfacial octanol solvent creates a well ordered monolayer that should be subject to fewer solvent fluctuations and allow for stronger hydrogen bond formation. Based on the 1-octanol vs. 1-propanol differences, we surmise that the hydrogen bonds formed between the indoline's nitrogen lone pair and the interfacial H-bond donors are weaker at the silica/1-propanol interface, a result that stands in contrast to the specific solvation interactions observed in bulk solution. (See Figure 2.1.)

Experiments to clarify further the different types of solvation present at silica/organic solvent interfaces measured the polarization dependent SH response as a function of incident fundamental polarization. Representative data from experiments measuring P-polarized SHG signal as a function of incident fundamental polarization for pNAs and indoline at the silica/cyclohexane interface are shown in Figure 2.5. Together with the measurement of S-polarized SHG signal arising from a visible field polarized 45˚ relative to the surface normal (containing both S & P components), the individual components of the surface nonlinear susceptibility tensor can be calculated according to Equations 2.6-8:

$$\chi^{(2)}_{pss} = L_{zz}L_{xx}L_{xx}\sin\theta_{SH}\chi_{zxx} \qquad (2.6)$$

$$\chi^{(2)}_{sps} = L_{xx}L_{zz}L_{xx}\sin\theta_{SH}\chi_{xzx}$$
$$\chi^{(2)}_{ssp} = L_{xx}L_{xx}L_{zz}\sin\theta_{SH}\chi_{xxz} \qquad (2.7)$$

$$\chi^{(2)}_{ppp} = -L_{xx}L_{xx}L_{zz}\cos\theta_{SH}\cos\theta_{vis}\sin\theta_{vis}\chi_{xxz} - L_{xx}L_{zz}L_{xx}\cos\theta_{SH}\cos\theta_{vis}\sin\theta_{vis}\chi_{xzx}$$
$$+ L_{zz}L_{xx}L_{xx}\sin\theta_{SH}\cos\theta_{vis}\cos\theta_{vis}\chi_{zxx} + L_{zz}L_{zz}L_{zz}\sin\theta_{SH}\sin\theta_{vis}\sin\theta_{vis}\chi_{zzz} \qquad (2.8)$$

where L_{ii} are the nonlinear Fresnel factors for the second harmonic and incident light.[44,51,63]

Relating the elements of the macroscopic $\chi^{(2)}$ tensor to the elements of molecular hyperpolarizability, β, requires knowledge about the electronic structure of the molecule itself. With this information, the measured surface nonlinear susceptibility can be related to the molecular hyperpolarizability using a coordinate transformation involving the Euler rotation matrix:

$$\chi^{(2)}_{ijk} = N_s \sum_{i'j'k'} \left\langle R_{ii'}R_{jj'}R_{kk'} \right\rangle \beta^{(2)}_{i'j'k'} \qquad (2.9)$$

We employed *ab initio* methods described above to calculate the non-zero (gas phase) β_{ijk} elements for both pNAs and indoline. Consistent with its pseudo-C_{2v} structure, the hyperpolarizability of pNAs is dominated by two terms β_{zzz} and β_{zxx} (= β_{zyy}) where $\beta_{zzz} >> \beta_{zxx}$. In contrast, indoline has 10 non-zero β elements of significant magnitudes. Consequently, determination of indoline's orientation required a more detailed analysis as described by Simpson and coworkers. [51]

Table 2.2. The nonzero elements of pNAs and indoline are presented below (in relative atomic units[68]). Details regarding the calculations themselves can be found in the manuscript text. For pNAs, only those elements highlighted in bold had a measurable influence on the calculated orientation.

	pNAs	Indoline
β_{zzz}	**838.9**	-225.0
β_{xxx}	-33.0	31.7
β_{xxy}	0.00	3.48
β_{yyy}	-0.05	41.3
β_{xxz}	**-167.2**	4.12
β_{xyz}	-0.07	3.77
β_{yyz}	-23.3	-51.9
β_{xzz}	32.6	18.6
β_{yzz}	0.10	-8.10
β_{xyy}	-20.1	15.9

The polarization dependent intensities and resulting orientation calculations lead to an average orientation of the molecular electronic transition dipole. Results are reported in Table 2.3 and illustrated schematically in Figure 2.5.

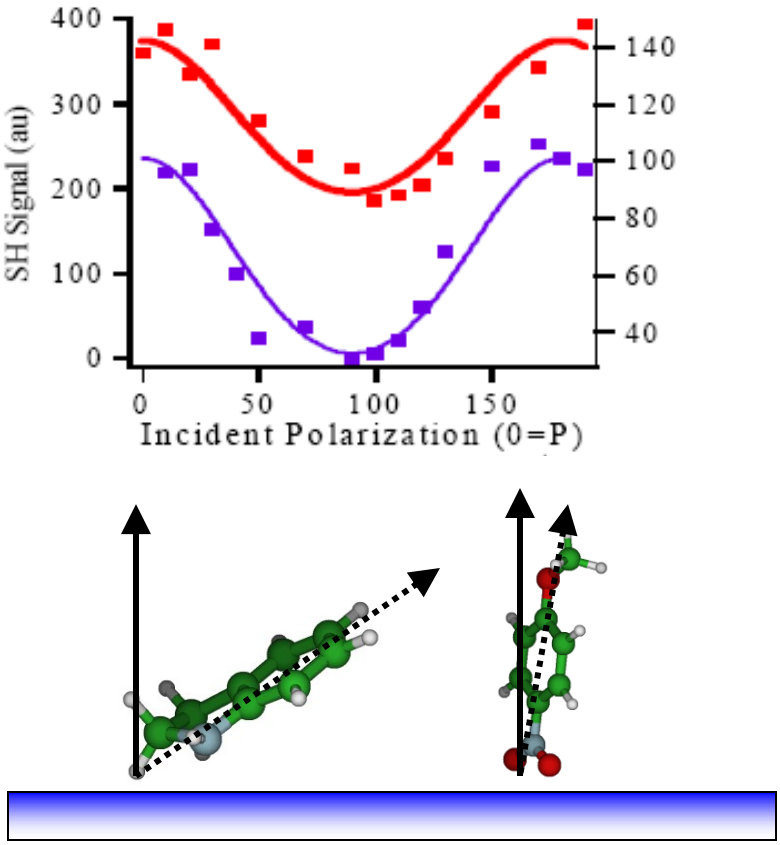

Figure 2.5. Orientation data for pNAs (top) and indoline (bottom) at the silica/cyclohexane interface. The data was collected by varying the incident light polarization angle from P (0º) to S (90º) then back to P (180º), while observing the P-polarized SH signal. (P-polarized light corresponds to light with its electric field vector in the plane defined by the surface normal and the light propagation direction.) Data are fit to Equation 8 to determine the individual contributions to the surface nonlinear susceptibility. Also shown are representative figures illustrating pNAs in a mostly upright orientation and indoline lying relatively flat to optimize hydrogen bonding opportunities.

Table 2.3. Orientation of pNAs and indoline at selected solid/liquid interfacesOrientation results for pNAs and indoline at silica/cyclohexane and silica/1-octanol interfaces using data shown in Figure 2.5 and Equations 2.6-9 in text.

Solute	Solvent	λ (nm)	orientation
pNAs	cyclohexane	321	19 ± 5
pNAs	1-octanol	297	≤ 9
	1-octanol	321	≤ 9
indoline	cyclohexane	291	150 ± 5

For all of the solid/liquid systems studied, pNAs adopts a mostly upright geometry with an average orientation of the molecular long axis relative to surface normal of 19 ± 5º at the silica/cyclohexane interface and less than 10˚ at the silica/1-octanol interface *at both wavelength maxima*. This result suggests that despite the distinctly different dielectric environments present at the silica/1-octanol interface, the average orientations for both adsorbed pNAs populations are quite similar, thus supporting the argument that observed differences in intensities arise from differences in population.

Analysis of the indoline data shows this solute to adopt a more horizontal orientation at the silica/cyclohexane interface. Orientation measurements lead to an average molecular orientation of 150 ± 5º from the surface normal. This result directs indoline's 2˚ amine towards the silica surface where it can accept hydrogen

bonds from surface silanol groups, consistent with the observed SHG data presented in Figures 2.4 and 2.5.

The last experiment conducted in this study was designed to test the contributions of the silica substrate to specific solvation forces at the solid/liquid interface. Previous reports in the literature have indicated that polarity at hydrophobic solid surfaces is much lower than bulk solution limits.[64] We eliminated the substrate's ability to donate hydrogen bonds by allowing a film of dimethyldichlorosilane to chemisorb to the silica substrate. Static contact angles formed between water and this surface measured 105°.[65]

Preparation of hydrophobic silica surfaces

The hydrophobic prisms used to measure hydrogen bonding interactions at the cyclohexane/hydrophobic interface were prepared in the following way: hemispherical fused silica prisms were first cleaned in a solution containing a 50-50 mixture (by volume) of concentrated sulfuric acid and fuming nitric acid. The prisms were then rinsed thoroughly with deionized water. The cleaned prisms were then placed flat surface down on a teflon reservoir containing a small amount of dimethyldichlorosilane. The prisms were exposed to the silane vapor overnight. This procedure resulted in a chemisorbed hydrophobic film assumed to be 1 monomolecular film thick.[65,66] Static contact angle measurements yielded a contact angle with water of $> 105^{\circ}$ consistent with previous reports in the literature.[67] (The contact angle was measured with a commercial goniometer (Rame-Hart) using vendor supplied software.) A picture of a water droplet on a hydrophobic prism is shown in Figure 2.6.

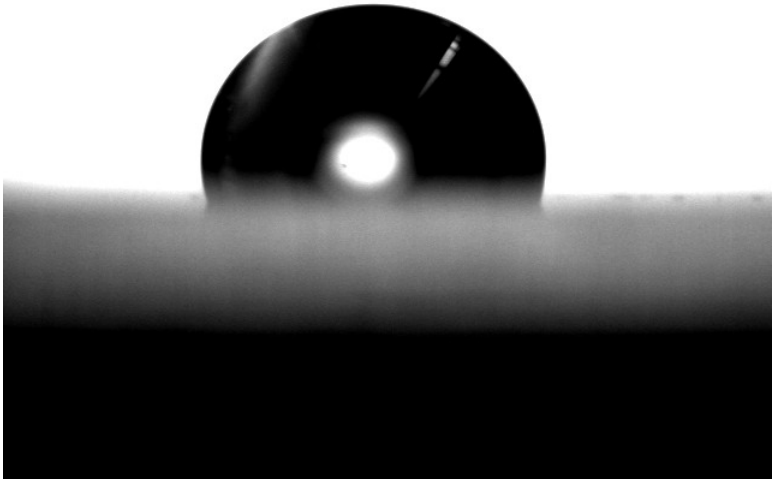

Figure 2.6. Picture of a water droplet on dimethyldichlorosilane coated silica.

Figure 2.7 shows the results of SHG spectra of indoline at both the hydrophilic silica/cyclohexane and hydrophobic silica/cyclohexane interfaces.

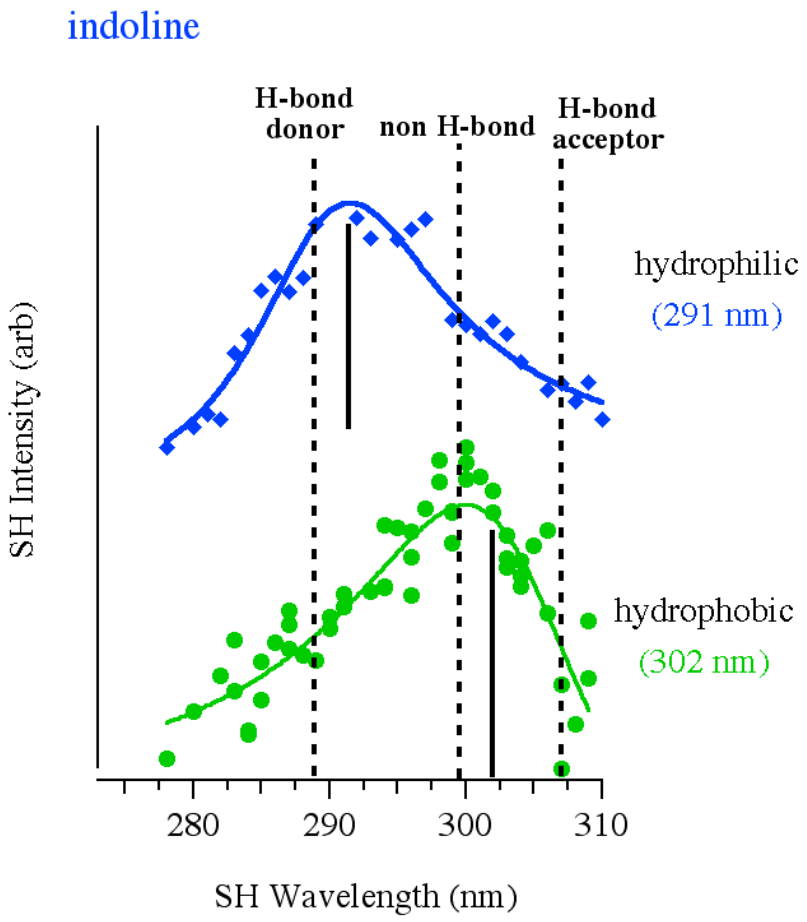

Figure 2.7. SHG data for indoline adsorbed to the hydrophilic silica/cyclohexane interface (top) and to the hydrophobic silica/cyclohexane interface. The hydrophobic surface was created by exposing overnight a hydrophilic silica prism surface to a vapor saturated with $Si(CH_3)_2Cl_2$. A picture of the contact angle formed with this surface by water is shown in Supporting Information. The hydrophilic silica/cyclohexane data are the same as those shown in the top, right panel of Figure 2.3.

The bulk limits are shown, along with the SHG maxima. For indoline at hydrophobic silica, λ_{max} shifts to 302 ± 3 nm. This result falls between the non-hydrogen bonding and hydrogen bond accepting bulk limits of 300 nm and 307 nm, respectively. In principle, methyl terminated silica can still accept

hydrogen bonds, but the surface's ability to donate hydrogen bonds, however, is largely eliminated.

Table 2.4. Second harmonic data for pNAs and indoline adsorbed to alkane/silica and n-alcohol silica interfaces

Solvent	ε	f(ε)	λ (bulk, nm)		λ (surface, nm)	
			pNAs	indoline	pNAs	indoline
Cyclohexane	2.04	0.41	293	299	321 ± 2	291 ± 2
methyl-cyclohexane	2.03	0.41	294	299	312 ± 3	291 ± 2
1-octanol	10.3	0.82	305	295	297 ± 2	287 ± 2
					320 ± 3	
1-propanol	20.5	0.91	310	293	307 ± 2	290 ± 3
					320 ± 4	
cyclohexane/hydrophobic						302 ± 3

Bulk and surface excitation wavelengths of pNAs and indoline adsorbed to different solid/liquid interfaces. SHG data result from fitting data shown in Figures 2.3, 4 and 6 with Equations 2.2-5 in text.

These results provide deeper insight into studies of surface diffusion studies of single molecules reported by Wirth and coworkers who characterized solute mobility at hydrocarbon terminated, silica surfaces.[35,39,40] Using a variety of

methods including single molecule fluorescence spectroscopy and fluorescence correlation spectroscopy, these investigators found that silica surfaces terminated with long-chain dimethylsilanes still possessed sites capable of strongly binding charged dye molecules from solutions. The strongest of these binding sites were assigned to topographical inhomogeneities resulting from mechanical polishing. The authors proposed that these binding sites were correlated with the isolated or weakly hydrogen-bonded silanol groups reported by Harris and coworkers in the latter's study of pyridine adsorption to silica surfaces.[36,38] Our solvatochromic results contain no direct information about interfacial topography, but the data point clearly to the importance of hydrogen-bond donating properties of silica surfaces in controlling specific solvation interactions compared to the surface's overall polarity and ability to accept hydrogen bonds.

2.5 Conclusions

Data presented above significantly advance our understanding of solvation at polar solid surfaces. The electronic structure of pNAs at weakly and strongly associating interfaces shows that solvent structure and identity play important roles in controlling the local dipolar environment. When a solution of pNAs in a nonpolar (alkane) solvent is brought into contact with hydrophilic silica, the interfacial region assumes a distinctly polar character although the magnitude of the effect depends on solvent structure. This result supports a model where the polar silica surface creates a high-dielectric environment. However, this model begins to break down when a solution having a more polar, protic solvent is

brought into contact with the silica substrate. Alcohol solvents create heterogeneous dipolar environments where one region can be distinctly "alkane-like". The second region remains extremely polar. The nature of this nonpolar region depends on solvent structure and is enhanced with longer-chain alcohol solvents. Solutes sensitive to specific solvation forces do not experience the same solvent-dependent variation in interfacial solvation. Indoline's solvation at the polar silica/liquid interface is homogeneous and appears to be dominated by the hydrogen bond donating properties of the substrate itself and is largely unaffected by the solvent. Only by rendering the silica surface hydrophobic does the nature of the specific solvation at the solid/liquid interface change.

2.6 References

(1) Lynden-Bell, R. M.; Del Popolo, M. G.; Youngs, T. G. A.; Kohanoff, J.; Hanke, C. G.; Harper, J. B.; Pinilla, C. C. *Acc. Chem. Res.* **2007**, *40*, 1138.

(2) Tavana, H.; Neumann, A. W. *Adv. Coll. Int. Sci.* **2007**, *132*, 1.

(3) Li, I.; Bandara, J.; Shultz, M. J. *Langmuir* **2004**, *20*, 10474.

(4) Farrer, R. A.; Fourkas, J. T. *Acc. Chem. Res.* **2003**, *36*, 605.

(5) Lee, S. H.; Rossky, P. J. *J. Chem. Phys.* **1994**, *100*, 3334.

(6) Ribarsky, M. W.; Landman, U. *J. Chem. Phys.* **1992**, *97*, 1937.

(7) Al-Abadleh, H. A.; Mifflin, A. L.; Bertin, P. A.; Nguyen, S. T.; Geiger, F. M. *J. Phys. Chem. B* **2005**, *109*, 9691.

(8) Doerr, A. K.; Tolan, M.; Schlomka, J. P.; Press, W. *Europhys. Lett* **2000**, *52*, 330.

(9) Eisenthal, K. B. *Chem. Rev.* **1996**, *96*, 1343.

(10) Shang, X. M.; Benderskii, A. V.; Eisenthal, K. B. *J. Phys. Chem. B* **2001**, *105*, 11578.

(11) Zhang, X. Y.; Cunningham, M. M.; Walker, R. A. *J. Phys. Chem. B* **2003**, *107*, 3183.

(12) Zhang, X. Y.; Walker, R. A. *Langmuir* **2001**, *17*, 4486.

(13) Catalan, J. *J. Org. Chem.* **1997**, *62*, 8231.

(14) *Quantitative treatments of solute/solvent interactions*; Politzer, P.; Murray, J. S., Eds.; Elsevier: Amsterdam, 1994, pp 368.

(15) Suppan, P. *Journal of Photochemistry and Photobiology A: Chemistry* **1990**, *50*, 293.

(16) Buncel, E.; Rajagopal, S. *Acc. Chem. Res.* **1990**, *23*, 226.

(17) Catalan, J. *J. Org. Chem.* **1995**, *60*, 8315.

(18) Laurence, C.; Nicolet, P.; Dalati, M. T.; Abboud, J. L. M.; Notario, R. *J. Phys. Chem.* **1994**, *98*, 5807.

(19) Matyushov, D. V.; Schmid, R.; Ladanyi, B. M. *J. Phys. Chem. B* **1997**, *101*, 1035.

(20) Bayliss, N. S.; McRae, E. G. *J. Phys. Chem.* **1954**, *58*, 1002.

(21) Esenturk, O.; Walker, R. A. *Phys. Chem. Chem. Phys.* **2003**, *5*, 2020.

(22) Kamlet, M. J.; Abboud, J. L. M.; Abraham, M. H.; Taft, R. W. *J. Org. Chem.* **1983**, *48*, 2877.

(23) Somasundaran, P.; Shrotri, S.; Huang, L. *Pure Appl. Chem.* **1998**, *70*, 621.

(24) Shafir, A.; Andelman, D.; Netz, R. R. *J. Chem. Phys.* **2003**, *119*, 2355.

(25) Hayes, P. L.; Gibbs-Davis, J. M.; Musorrafiti, M. J.; Mifflin, A. L.; Scheidt, K. A.; Geiger, F. M. *J. Phys. Chem. C* **2007**, *111*, 8796.

(26) Hayes, P. L.; Malin, J. N.; Konek, C. T.; Geiger, F. M. *J. Phys. Chem. A* **2008**, *112*, 660.

(27) Lum, K.; Chandler, D.; Weeks, J. D. *J. Phys. Chem. B* **1999**, *103*, 4570.

(28) MacRitchie, F. *Chemistry at Interfaces*; Academic Press: New York, 1990.

(29) Manne, S.; Gaub, H. E. *Science* **1995**, *270*, 1480.

(30) Yu, C. J.; Evmenenko, G.; Richter, A. G.; Datta, A.; Kmetko, J.; Dutta, P. *Appl. Surf. Sci.* **2001**, *182*, 231.

(31) Zhang, X.; Steel, W. H.; Walker, R. A. *J. Phys. Chem. B* **2003**, *107*, 3829.

(32) Israelachvili *Intermolecular and Surface Forces*, 2 ed.; Academic Press: New York, 1992.

(33) Rusling, J. F.; Nassar, A. E. F. *J. Am. Chem. Soc.* **1993**, *115*, 11891.

(34) Iler, R. K. *The Chemistry of Silica*; Wiley: New York, 1979.

(35) Wirth, M. J.; Legg, M. A. *Ann. Rev. Phys. Chem.* **2007**, *58*, 489.

(36) Wong, A. L.; Harris, J. M. *J. Phys. Chem.* **1991**, *95*, 5895.

(37) Gilroy, J. J.; Dolan, J. W.; Snyder, L. R. *J. Chromat. A* **2003**, *1000*, 757.

(38) Hansen, R. L.; Harris, J. M. *Anal. Chem.* **1995**, *67*, 492.

(39) Kovaleski, J. M.; Wirth, M. J. *Anal. Chem.* **1997**, *69*, A600.

(40) Kovaleski, J. M.; Wirth, M. J. *J. Phys. Chem. B* **1997**, *101*, 5545.

(41) Smith, E. A.; Wirth, M. J. *J. Chromat. A* **2004**, *1060*, 127.

(42) Onsager, L. *J. Am. Chem. Soc.* **1936**, *58*, 1486.

(43) Zhuang, X.; Miranda, P. B.; Kim, D.; Shen, Y. R. *Phys. Rev. B* **1999**, *59*, 12632.

(44) Wang, H. F.; Gan, W.; Lu, R.; Rao, Y.; Wu, B. H. *Int. Rev. Phys. Chem.* **2005**, *24*, 191.

(45) Steinhurst, D. A.; Owrutsky, J. C. *J. Phys. Chem. B* **2001**, *105*, 3062.

(46) TamburelloLuca, A. A.; Hebert, P.; Brevet, P. F.; Girault, H. H. *J. Chem. Soc. Faraday Trans.* **1996**, *92*, 3079.

(47) Wang, H. F.; Borguet, E.; Eisenthal, K. B. *J. Phys. Chem. A* **1997**, *101*, 713.

(48) Wang, H. F.; Borguet, E.; Eisenthal, K. B. *J. Phys. Chem. B* **1998**, *102*, 4927.

(49) Steel, W. H.; Beildeck, C. L.; Walker, R. A. *J. Phys. Chem. B* **2004**, *108*, 16107.

(50) Zybill, C. E.; Ang, H. G.; Lan, L.; Choy, W. Y.; Meng, E. F. K. *Journal of Organometallic Chemistry* **1997**, *547*, 167.

(51) Moad, A. J.; Simpson, G. J. *J. Phys. Chem. B* **2004**, *108*, 3548.

(52) Gaussian 03, Revision D.01, Frisch, M. J.; Trucks, G. W.; Schlegel, H. B.; Scuseria, G. E.; Robb, M. A.; Cheeseman, J. R.; Montgomery, Jr., J. A.; Vreven, T.; Kudin, K. N.; Burant, J. C.; Millam, J. M.; Iyengar, S. S.; Tomasi, J.; Barone, V.; Mennucci, B.; Cossi, M.; Scalmani, G.; Rega, N.; Petersson, G. A.; Nakatsuji, H.; Hada, M.; Ehara, M.; Toyota, K.; Fukuda, R.; Hasegawa, J.; Ishida, M.; Nakajima, T.; Honda, Y.; Kitao, O.; Nakai, H.; Klene, M.; Li, X.; Knox, J. E.; Hratchian, H. P.; Cross, J. B.; Bakken, V.; Adamo, C.; Jaramillo, J.; Gomperts, R.; Stratmann, R. E.; Yazyev, O.; Austin, A. J.; Cammi, R.; Pomelli, C.; Ochterski, J. W.; Ayala, P. Y.; Morokuma, K.; Voth, G. A.; Salvador, P.; Dannenberg, J. J.; Zakrzewski, V. G.; Dapprich, S.; Daniels, A. D.; Strain, M. C.; Farkas, O.; Malick, D. K.; Rabuck, A. D.; Raghavachari, K.; Foresman, J. B.; Ortiz, J. V.; Cui, Q.; Baboul, A. G.; Clifford, S.; Cioslowski, J.; Stefanov, B. B.; Liu, G.; Liashenko, A.; Piskorz, P.; Komaromi, I.; Martin, R. L.; Fox, D. J.; Keith, T.; Al-Laham, M. A.; Peng, C. Y.; Nanayakkara, A.; Challacombe, M.; Gill, P. M. W.; Johnson, B.; Chen, W.; Wong, M. W.; Gonzalez, C.; and Pople, J. A.; Gaussian, Inc., Wallingford CT, 2004.

(53) Gilli, G.; Gilli, P. *J. Mol. Struc.* **2000**, *552*, 1.

(54) Zheng, Y. J.; Merz, K. M. *J. Comp. Chem.* **1992**, *13*, 1151.

(55) Markovitch, O.; Agmon, N. *Mol. Phys.* **2008**, *106*, 485.

(56) Allen, M. W.; Bothwell, T. G.; Slaughter, B. D.; Johnson, C. K. *Biophys. J.* **2002**, *82*, 428.

(57) Slaughter, B. D.; Allen, M. W.; Lushington, G. H.; Johnson, C. K. *J. Phys. Chem. A* **2003**, *107*, 5670.

(58) Wirth, M. J.; Piasecki-Coleman, D. A.; Montgomery, M. E. *Langmuir* **1995**, *11*, 990.

(59) Allara, D. L.; Parikh, A. N.; Rondelez, F. *Langmuir* **1995**, *11*, 2357.

(60) Ye, S.; Nihonyanagi, S.; Uosaki, K. *Phys. Chem. Chem. Phys.* **2001**, *3*, 3463.

(61) Benjamin, I. *Chem. Rev.* **2006**, *106*, 1212.

(62) Michael, D.; Benjamin, I. *J. Phys. Chem.* **1995**, *99*, 16810.

(63) Simpson, G. J.; Perry, J. M.; Ashmore-Good, C. L. *Phys. Rev. B* **2002**, *66*.

(64) Zhang, X. Y.; Esenturk, O.; Walker, R. A. *J. Am. Chem. Soc.* **2001**, *123*, 10768.

(65) C. P. Tripp and M. L. Hair *J. Phys. Chem.* **97** (1993) 5693.

(66) M. L. Hair and C. P. Tripp *Colloids and Surfaces A* **105** (1995) 95.

(67) R. W. P. Fairbank, Y. Xiang, and M. J. Wirth *Anal. Chem.* **67** (1995) 3879.

(68) G. Maroulis and C. Pouchan *J. Phys. B: Atomic, Molecular and Optical Phys.* **36** (2003) 201

Chapter 3: Structure of Medium Length Alkanes Adsorbed to Silica/Vapor Interfaces

3.1 Introduction

Understanding hydrocarbon adsorption to solid surfaces has broad impact and application in fields as diverse as tribology, environmental remediation, and catalysis and fuel reforming.[1-8] In many of these areas, silica is the solid surface most often in contact with a hydrocarbon vapor or liquid. Consequently, the origin of observed behavior in these systems arises directly from equilibrium and dynamic properties of the hydrocarbons adsorbed to the polar, dielectric surface. These properties, in turn, will be determined by a balance of asymmetric forces between hydrocarbons and silica, hydrocarbons and the adjacent vapor or liquid phase, as well as lateral interactions amongst the adsorbed hydrocarbons themselves. For example, monolayers comprised of combinations of different alkane molecules between loaded silica and mica surfaces have been shown to minimize stick-slip effects compared to single component liquids due to changes in interfacial film structure and dynamics.[9-15] These surface force apparatus (SFA) experiments illustrate how alkane structure and organization between two solid substrates control friction changes with load, velocity, and lubricant identity.

The importance of hydrocarbon interactions with silica surfaces can be inferred simply from the number and scope of experimental and theoretical studies that have focused on aspects related to hydrocarbon structure and dynamics at interfaces. In addition to the aforementioned SFA measurements, thermogravimetric

analysis and temperature programmed desorption have been used to examine the strength of interaction and free energy of adsorption for hydrocarbons at the silica/vapor interface.[16] Linear adsorption isotherms imply that up to a high percentage of full monolayer coverage, lateral intermolecular interactions between adsorbates remain weak. Infrared spectra show that hydrocarbons adsorb spontaneously onto silica and that adsorption leads to changes in the spectra of surface silanol groups interacting directly with adsorbed species.[17] Hydroxyl groups in zeolite (Si(OH)Al) materials exhibit absorption band shifts that depend on the strength of interaction with adsorbed alkane species. Stronger interactions or hydrogen bonds between silica and short (C_3-C_6) hydrocarbon adsorbates lead to lower hydroxyl group frequencies.[18,19] Atomic force microscopy and ellipsometric measurements of hydrocarbon films on silica have reported film thicknesses of different alkanes and have led investigators to interpret hydrocarbon structure within these films.[20] Measurements suggest that an incomplete monolayer forms from vapor adsorption up to high vapor pressures, and that the thickness of the equilibrium monolayer is consistent with alkane molecules lying flat. While all of these studies show clearly that hydrocarbons interact relatively strongly with silica interfaces, they fail to address directly questions about interfacial hydrocarbon structure and organization.

Supporting experimental results are simulations of alkane adsorption onto the silica surfaces. Calculated heats of adsorption from Monte Carlo simulations show that the adsorption energy increases with chain length, and that interactions are disproportionally enhanced at low coverage. As the alkyl chain lengthens, adsorbing

alkanes show an increasing tendency to layer.[21] Molecular dynamics simulations of alkanes having lengths between 4 and 8 carbons packed in porous silica gel conclude that linear alkanes pack together efficiently in the interfacial monolayer.[22] What is still missing from this characterization of alkane-silica interactions, however, is a clear, experimentally validated picture of how interfacial interactions lead the alkanes in direct contact with the silica to organize at the surface. To clarify how alkanes adsorb to and organize at silica interfaces, experiments described in this chapter use second order nonlinear optical (NLO) spectroscopy to determine the relative orientations and structures of medium length alkane molecules adsorbed to the silica/vapor interface.

Alkane molecules adsorbed to the silica/vapor interface can interact directly with both the polar substrate and adjacent adsorbed alkanes. Previous studies of solvent polarity at solid/liquid interfaces have shown that the interface formed between nonpolar alkane solvents and hydrophilic silica interfaces are surprisingly polar.[23] Depending on the specific alkane, the interface between the silica and an alkane liquid can have effective dielectric constants greater than 80 based on solvatochromic shifts of adsorbed solute excitation energies. These results have led researchers to speculate that silica may enhance solvent density and induce a net polarization in solvents that are in direct contact with the surface. Additional support for this picture comes from x-ray scattering studies that showed certain alkanes to have anomalously high densities adjacent to silica surfaces.[24] In the data presented below, surface specific vibrational spectra of medium length (C_8-C_{11}) alkanes adsorbed directly to the silica/vapor interface provide definitive evidence that alkane

chains lie flat, primarily with extended conformations that direct methylene groups towards and away from the interface. By comparing the spectral features present under different experimental polarization conditions, as well as certain bands' relative intensities, these results provide a clear picture of organization at the solid/vapor interface, from which the dominant interactions can be inferred.

3.2 Theory/Experimental

3.2.1 Vibrational Sum Frequency Generation Spectroscopy

VSFG is an ideal tool to measure the structure and orientation of interfacial solvent molecules. The technique is sensitive only to those molecules subject to interfacial anisotropy, and different polarization conditions described below allow experiments to selectively probe the orientation of specific functional groups.[25-31] The origin of the technique's surface specificity has been described elsewhere, and will only be summarized here. Signal from the surface arises from the spatial and temporal overlap of two photons at the interface, one visible photon, and one infrared. The SF field is proportional to the product of incident fields:

$$E^{(2)}_{\omega 1 + \omega 2} = \chi^{(2)}_{\omega 1 + \omega 2} \; E_{\omega 1} E_{\omega 2} \qquad (3.1)$$

where $\chi^{(2)}$ is the sample's macroscopic second order susceptibility. This third ranked tensor contains all of the information related to the spatially averaged hyperpolarizability of molecules at surfaces, and, under the electric dipole approximation, is zero in isotropic media. The tensor contains both resonant and nonresonant contributions:

$$\chi^{(2)} = \chi^{(2)}_{R} + \chi^{(2)}_{NR} \qquad (3.2)$$

Typically, the resonant portion is much larger than the nonresonant term, and can be expressed as a function of real and virtual excitation energies:

$$\chi_R^{(2)} = \sum_{k,e} \frac{\langle g | \alpha_{lm} | v \rangle \langle v | \mu_n | g \rangle}{(\omega_{ir} - \omega - i\Gamma)} \qquad (3.3)$$

Due to the relation of the surface response from the macroscopic susceptibility to that of the molecular response, defined by the hyperpolarizability, we can determine the orientation of specific functional groups by identifying which vibrational transition dipoles give rise to signals under different experimental polarization combinations. In a typical experiment, we direct a beam of visible and infrared light of known polarizations at the sample, and collect using a spectrometer and CCD the polarization resolved, coherently scattered SF field.

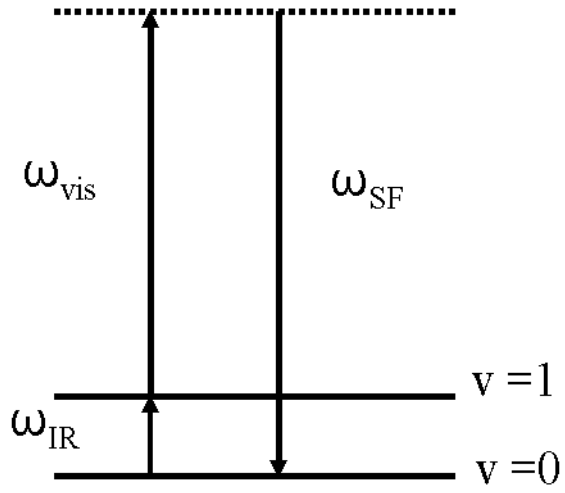

Figure 3.1. Schematic energy diagram of the VSFG experiment. Two incident beams are used, one resonant with an allowed IR transition and one nonresonant (output of the 800 nm amplified Ti:Saph laser).

By changing the polarization of visible, IR, and SF light we use and detect, we can selectively probe different elements of the $\chi^{(2)}$ tensor and deduce the average molecular orientation.

Typically, 3 or 4 unique polarization combinations are used to acquire spectra. These combinations are designated with a three letter sequence where the first letter characterizes the polarization of the SF light, the middle letter describes the polarization of the visible light, and the last letter the IR light. For example $\mathbf{P}_{SF}\mathbf{P}_{VIS}\mathbf{P}_{IR}$ describes a combination where all three fields are polarized in the plane defined by the surface normal and the propagation direction of the incident visible and IR fields. Likewise, in the $\mathbf{S}_{SF}\mathbf{S}_{VIS}\mathbf{P}_{IR}$ spectrum, the IR field remains polarized in the vertical plane, but the SF and visible field polarizations are defined as being parallel to the plane of the interface. The four unique combinations sample different elements of the $\chi^{(2)}$ tensor:[29,31]

$$\begin{aligned}\chi^{(2)}_{ppp} &= -L_{xx}L_{xx}L_{zz}\cos\theta_{SF}\cos\theta_{vis}\sin\theta_{IR}\chi_{xxz} - L_{xx}L_{zz}L_{xx}\cos\theta_{SF}\cos\theta_{vis}\sin\theta_{IR}\chi_{xzx} \\ &+ L_{zz}L_{xx}L_{xx}\sin\theta_{SF}\cos\theta_{vis}\cos\theta_{IR}\chi_{zxx} + L_{zz}L_{zz}L_{zz}\sin\theta_{SF}\sin\theta_{vis}\sin\theta_{IR}\chi_{zzz}\end{aligned} \tag{3.4}$$

$$\chi^{(2)}_{ssp} = L_{xx}L_{xx}L_{zz}\sin\theta_{SF}\chi_{xxz} \tag{3.5}$$

$$\chi^{(2)}_{sps} = L_{xx}L_{zz}L_{xx}\sin\theta_{SF}\chi_{xzx} \tag{3.6}$$

$$\chi^{(2)}_{pss} = L_{zz}L_{xx}L_{xx}\sin\theta_{SF}\chi_{zxx} \tag{3.7}$$

where L_{ii} are diagonal elements of the Fresnel matrix determined by the refractive indices of the two phases, and the angle of the incident and reflected beams. Equation 4 shows that spectra acquired under PPP conditions contain all elements of the surface susceptibility, but SSP and SPS spectra each sample only one unique element. Assuming a symmetric Raman polarizability tensor, the SPS and PSS spectra will contain equivalent information.

The simplest interpretations of VSF spectra often compare data acquired under SSP and SPS polarization conditions. Under SSP conditions, any resonant

bands that appear in the SFG spectrum must correspond to molecular vibrations that have a projection of their IR transition moment along the surface normal. If a feature shows up in the SPS spectrum, we expect that the vibrational transition dipole lies in the plane of the surface. A feature that appears in both spectra means the transition moment lies at an angle such that it has projections both in- and out-of-plane, and by comparing the relative intensities of several features in each spectrum, we can estimate the molecule's average orientation. PPP conditions sample all nonzero $\chi^{(2)}$ elements, each one of which has a well defined phase that can interfere constructively or destructively. Therefore interpretation of this spectrum can become complicated.

3.2.2 Experimental

SFG spectra acquired in this work were collected using a broadband, counter-propagating geometry SFG spectrometer that has been described elsewhere. The solid/vapor data were acquired by putting a drop inside of quartz cells, and letting the system equilibrate at 22±0.5ºC. Typically, we record SF spectra for 1-2 minutes at each central IR wavelength, then tune the laser 50 cm^{-1} and scan again. This procedure results in 8 broadband wavelength scans per spectrum. All spectra were normalized to the instrument response measured by the nonresonant spectrum acquired from the gold/vapor interface, and calibrated by placing a polystyrene card in front of the gold surface along the IR path.[32] Four points corresponding to known adsorption bands from polystyrene were used for a wavelength calibration, leading to an accuracy in reported frequencies on the order of ±2 cm^{-1}. Relative intensities of bands within the same spectrum typically reproduced to within 10 percent. Also, by systematically benchmarking intensities of each silica/alkane vapor interface against a

known standard (DMSO at the silica/vapor interface), absolute intensities could be compared between systems. Given that the instrument response does not vary day-to-day by more than 10 percent (i.e. the nonresonant SF signal from gold, and resonant band intensity from the methylene symmetric stretch frequency at the silica/vapor interface with DMSO adsorbed), spectra taken on subsequent days could be scaled relative to each other. In this way we were able to compare absolute intensities for different silica/alkane interfaces for a given polarization condition.

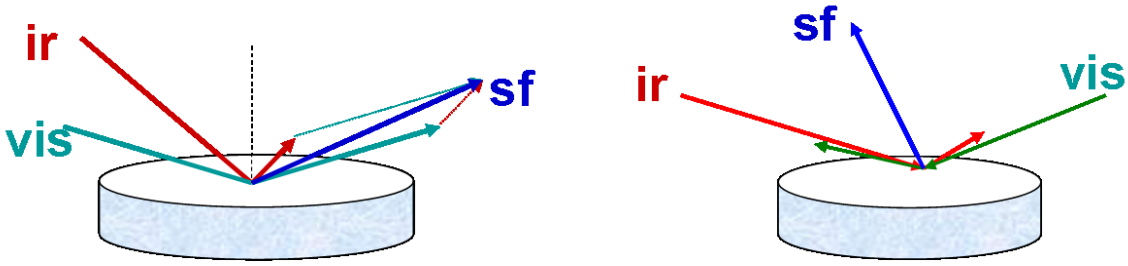

Figure 3.2. Picture of beam geometry at the sample. Typically, most broadband VSFG instruments use a copropagating geometry as shown on the right. Measurements presented in this work were collected on a broadband counter-propagating system, which has advantages such as small scattered background, and ease of changing samples.

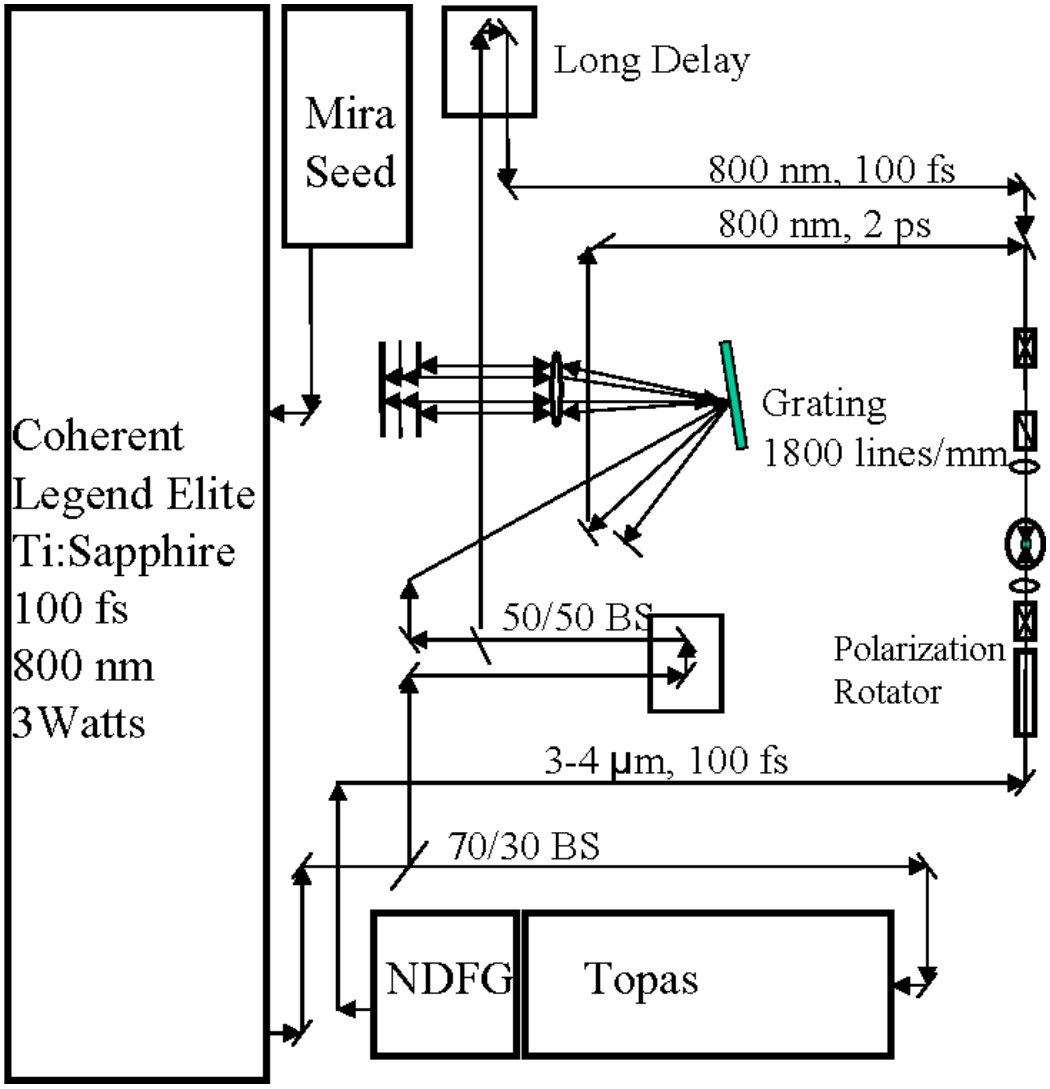

Figure 3.3. Schematic layout of the broadband VSFG system used to acquire VSFG spectra of alkanes adsorbed to the silica/vapor interface. Our static, broadband spectra only required the IR and spectrally narrowed, 2 picosecond pulse duration 800 nm visible light.

3.3 Results and Discussion

Identifying the resonant vibrational bands that appear in VSFG spectra of alkane monolayers adsorbed to the silica/vapor interface is an effective means of

quantifying molecular organization at this boundary. Sampling the different non-zero polarization combinations enables features to be assigned unambiguously and with enough redundancy to inspire confidence in the results of fitting data to Equations 3.1-3. Spectra acquired under the PPP condition sample all nonzero elements of the nonlinear susceptibility and require careful consideration when fitting features to the molecular response, given that different elements of the $\chi^{(2)}$ tensor can have different phases. The SSP and SPS polarization conditions, however, only sample one nonzero element each with SSP spectra probing vibrations having IR transition moments along the surface normal, and SPS spectra sampling those vibrations having in-plane IR transition moments.

Alkanes adsorbed to the silica surface can organize themselves in a variety of ways that will lead to different anticipated VSFG responses under the polarization conditions sampled. First, medium chain alkane molecules could organize as linear amphiphilic molecules do in a Langmuir-like film with the long molecular axis aligned along the surface normal. These adsorbed molecules would interact with the surface through the methyl group at one end. Van der Waals interactions between adjacent chains would enhance intermolecular interactions and lead to greater conformational order. In fact, x-ray scattering and nonlinear optical studies of the alkane liquid/vapor interface show that linear alkanes ($n > 12$) adopt this conformation when they undergo a surface freezing transition at temperatures slightly above bulk freezing.[33,34] Likewise, x-ray scattering studies of long chain alkanes adsorbed in thin films at the silica and silver surface show corresponding degrees of order.[35] With the methylene groups all having their transition moments parallel to the

plane of the surface, and the methyl group on either end directed normal to the surface, SSP and SPS spectra of alkanes in this regime should resemble previous results from well ordered neutral surfactant monolayers adsorbed to aqueous/vapor interfaces. These monolayer structures are characterized by SSP spectra having dominant contributions assigned to the methyl symmetric stretch (r^+) and Fermi resonance(r^+_{FR}), and very little, if any signal from either the methylene symmetric stretch (d^+) or methyl asymmetric stretch (r^-). Typically the only feature present in the SPS spectrum of this monolayer structure is a band assigned to r^-. Because methylene groups are aligned with transition moments in the plane of the surface *and* with local symmetry through the center of each carbon-carbon bond, contributions to $\chi^{(2)}$ from adjacent groups cancel leading to no net surface nonlinear susceptibility.

A second way in which alkane molecules can adsorb to the silica/vapor interface is to lie flat along the surface. In this case, adsorbed alkanes may lay flat with little correlation between adjacent molecules, or lay flat but have long range order due to chain-chain interactions that align adjacent adsorbed molecules relative to each other. These two possibilities would necessarily lead to differences in the VSFG spectral features acquired under different polarization conditions. A monolayer of randomly oriented alkane molecules at the silica/vapor interface would show very little intensity in SFG spectra acquired under any polarization condition. Typically, a lack of polar ordering amongst alkane chains in the monolayer would lead to only small intensities from features regardless of experimental polarization. However, if the adsorbed monolayer both lays flat and is well ordered (i.e. lying with the carbon backbone along the surface in all-trans conformations), then

corresponding spectra should show strong features that will indicate if the C_2 axes of methylene groups are normal or parallel to the interfacial plane. Expected features in the SSP spectra in either case include r^+, d^+, d^-, and possibly r^-. Furthermore, systematic changes in specific bands associated with the methyl stretching vibrations would be anticipated as a function of chain length. For example, fully extended n-octane has two methyl groups pointed in different directions, as defined by the axis of the molecule. Fully extended n-nonane, being one carbon longer, has both methyl groups pointed in the same relative direction.

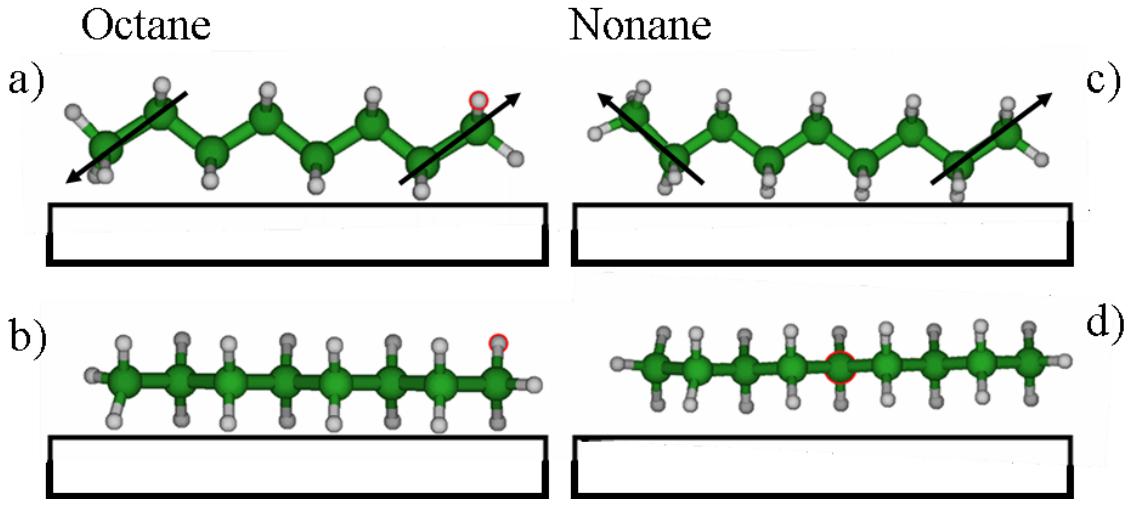

Figure 3.4. Schematic picture detailing possible flat orientations of octane and nonane adsorbed to the silica surface. The panels detail: a) octane lying flat with vertically oriented methyl groups, b) nonane lying flat with vertically oriented methyl groups, c) octane lying flat with C-C-C bonds in the interfacial plane, and d) nonane lying with carbon bonds in the surface plane. Superimposed are the vector directions of the methyl symmetric stretch transition moments.

This difference in methyl group orientation will lead to destructive (octane) or constructive (nonane) interference of the r^+ band. Octane, with its chain in a fully extended conformation, has the transition moments of the methyl symmetric stretch equal in magnitude, but opposite in sign. Therefore, if octane molecules adsorb in either an upright (i.e. the molecular long axis projects along the surface normal), or

flat but with methylene groups projected into/out of the surface (like the upper panel of Figure 3.4), one might expect partial cancellation of SFG signal. In principle, this cancellation could be quantitative, but the methyl group interacting more directly with the silica surface will see a different environment from the methyl group directed away from the surface. Nonane, on the other hand, might have a small signal due to methyl group cancellation if standing upright, but not if the molecule lays flat with both methyl groups preferentially oriented into or out of the silica surface, as seen in Figure 3.4c. Nonane having a significantly larger r^+ intensity than octane in the SSP spectrum could arise either from increased surface coverage – unlikely given nonane's slightly larger size - or from molecules fully extended laying flat along the interface. Comparing the normalized spectral intensities in SSP spectra from octane and nonane adsorbed to the silica/vapor interface shows the r^+ band in the octane spectrum to have only 15 percent of the intensity that appears in the nonane spectrum. Comparing results from films of decane and undecane adsorbed to the silica surface reinforces this interpretation.

Quantitatively comparing signal intensities between different systems of similar molecules adsorbed to the silica/vapor interface is made possible by carefully monitoring the instrument response to a known interfacial standard having an invariant signal for a given experimental conformation. The r^+ signal from DMSO adsorbed to the silica/vapor interface has been well characterized, and used as an internal reference in previous studies.[36] In order to maintain reproducible signal intensity to within 10 percent, the spectrum of DMSO adsorbed to the silica/vapor interface was acquired before and after every new sample. Two PPP spectra taken on

different days of the silica/vapor interface with DMSO adsorbed are shown in Figure 3.5. This level of reproducibility is typical provided that the overall alignment of the entire system remains unchanged.

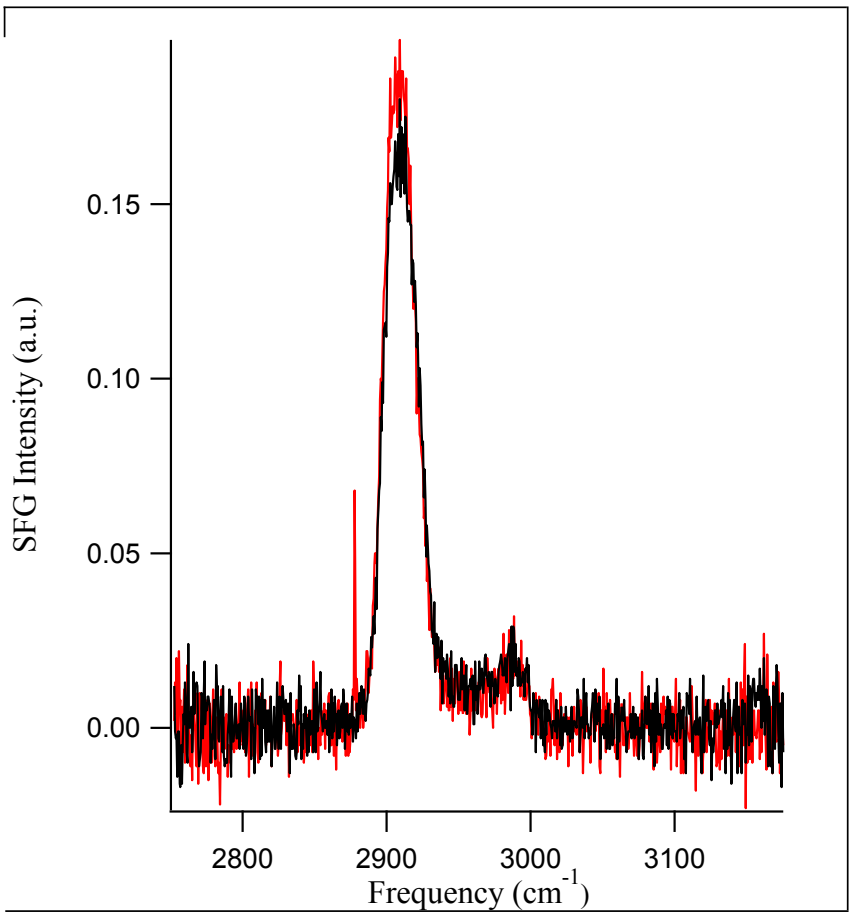

Figure 3.5. PPP spectra of the silica/vapor interface with a monolayer of DMSO adsorbed.

Figure 3.6 shows the PPP, SSP, and SPS spectra of octane, nonane, decane, and undecane adsorbed to the silica/vapor interface. All four spectra for each polarization combination appear qualitatively similar, although several general trends do emerge. First, the integrated intensities of the SSP spectra for both nonane and undecane are much larger than for octane and decane, indicating that the odd length

alkanes have much larger out of plane nonlinear susceptibilities than even length alkanes at the silica/vapor interface. A similar correlation can be made from the SPS spectra of these systems. Both the PPP and SSP spectra are dominated by two bands with approximate center frequencies of 2875 and 2945 cm^{-1}. Additional features appear in SSP spectra of nonane and undecane. SPS spectra are weaker and show a pair of features for octane and decane at 2925 and 2960 cm^{-1}. The SPS spectrum of nonane shows only the higher frequency feature. The SPS spectrum of undecane shows no features. All line positions and peak intensities are summarized in Table 3.1. Despite having similar IR and Raman spectra, these n-alkanes adsorbed to silica surfaces have decidedly different SFG spectra indicating that these molecules are organized differently at the silica/vapor interface.

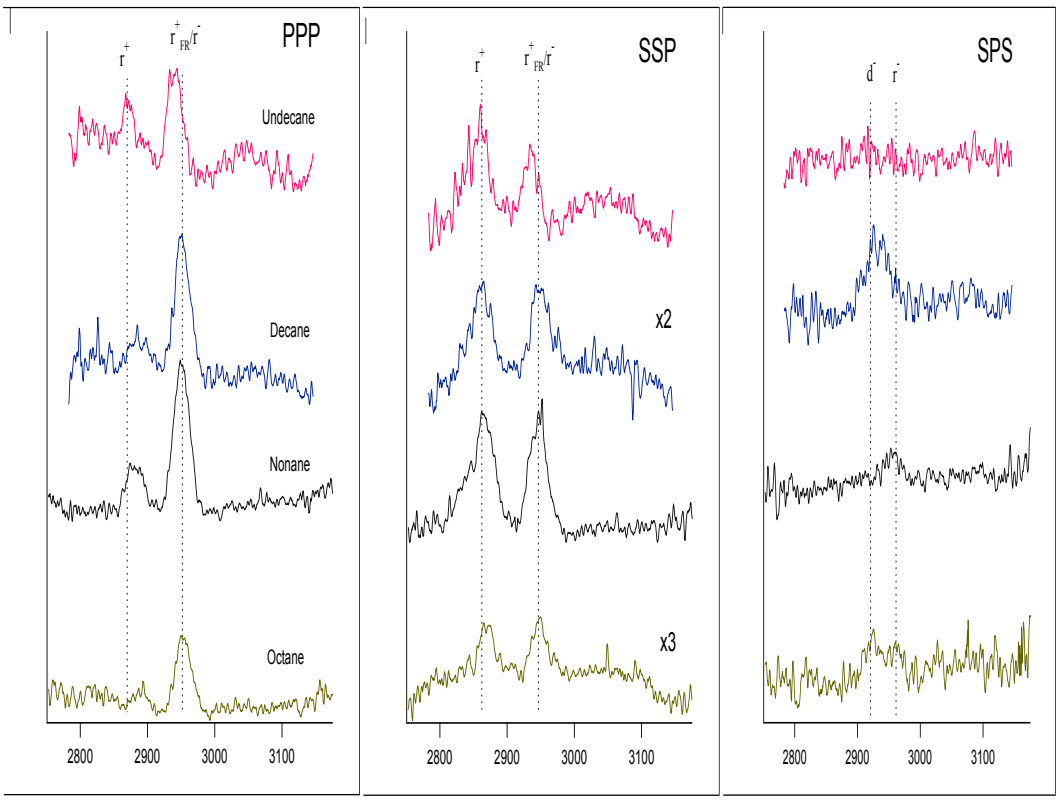

Figure 3.6. VSFG Spectra acquired under PPP, SSP, and SPS polarization conditions of the silica/vapor interface with adsorbed octane, nonane, decane, and undecane.

In general, SSP spectra are generally the simplest to interpret because this polarization combination samples only a single element of the $\chi^{(2)}$ tensor and requires that molecular vibrations at the surface have a net projection of their IR transition moments along the surface normal. Three features appear in SSP spectra, and are assigned to a methylene symmetric stretch (d^+) at 2845 cm^{-1}, a methyl symmetric stretch at 2875 cm^{-1}, and a band centered around 2945 cm^{-1} that could could contain contributions from both a methyl symmetric stretch Fermi resonance (r^+_{FR}), and the methyl asymmetric stretch (r^-).[37] Typically, spectra with this combination of features arise from interfacial methyl groups having some degree of long range order projected along the surface normal.[38,39] The d^+ feature appearing in the SSP spectrum can result either from gauche defects in chains aligned along the surface normal or from chains aligned parallel to the surface with methylene groups pointing alternately up and down. The fact that the r^+ intensity shows a significant even-odd effect supports a model where the molecules adopt an all-trans conformation lying flat along the surface.

Notable in the SPS spectra is a qualitative difference in the spectral features present for systems with an even or odd number of carbons in the alkyl backbone. SPS spectra of octane and decane reproducibly include a broad feature that covers frequencies assigned to both d^- and r^-. Any contribution from r^+_{FR} is discounted because of the absence of a feature at ~2875 cm^{-1}. The spectrum of nonane adsorbed to the silica/vapor interface contains only one narrower peak that can be assigned to r^- exclusively and the SPS spectrum of undecane shows no features at all. Since SPS

spectra probe vibrations having a net projection of IR transition moments in the plane of the surface, and because the r^+ and r^- normal mode transition moments are orthogonal, the r^- band is usually expected in an SPS spectrum when r^+ appears in the corresponding SSP spectrum. Methylene bands appearing in these SPS spectra are also expected, based on the features present under other polarization combinations. Specifically, intensity assigned to d^+ in SSP spectra indicates that the molecules lie flat such that the C-H bonds of the methyl groups point into and out of the surface as in the upper panel of Figure 3.4c. This conformation at the interface also requires that the d^- IR transition moment lie in the plane of the surface. Though these features are not consistent for all systems, and have relatively weak SFG intensities, their presence provides strong evidence in support of the alkanes adsorbed at the silica/vapor interface laying flat with methylene and methyl groups sticking into or out of the surface, rather than parallel to the interface.

Interpreting PPP spectra requires more careful treatment. According to Equation 4, spectra acquired under PPP polarization conditions should reflect contributions from non-zero elements of the surface nonlinear susceptibility. At first glance, one might assume this to mean that all features present under other polarizations must also be in the PPP spectrum, however data here show that while the d^+ band is assigned to features found in several SSP spectra, it is notably absent from *all* spectra acquired under PPP conditions. The presence of d^+ under SSP conditions, and this band's absence in SPS show that the $\chi^{(2)}_{iiz}$ and $\chi^{(2)}_{izi}$ are nonzero and zero, respectively, where i=x or y. $\chi^{(2)}_{zii}$ will also be zero given the assumed symmetry of the Raman polarizability tensor. Thus the cancellation of d^+ observed in

PPP spectra must result from $\chi^{(2)}_{xxz}$ and $\chi^{(2)}_{zzz.}$ Careful inspection of the expression describing intensity observed in a PPP spectrum (Equation 4.4) shows that two separate terms sample vibrational modes having a projection of their IR transition moments along the surface normal: $\chi^{(2)}_{iiz}$ and $\chi^{(2)}_{zzz}$. Scaling these terms are the Fresnel factors and angles of incident and scattered fields. Under the experimental conditions of our assembly, these experimental factors can cause the two $\chi^{(2)}$ terms to interfere constructively. Therefore, the difference in sign must arise from the nonlinear susceptibility elements themselves. More specifically, the factors weighting these $\chi^{(2)}$ elements in Equation 4 are $-L_{xx}L_{xx}L_{zz}\cos\theta_{SF}\cos\theta_{vis}\sin\theta_{IR}$ for χ_{xxz} and $L_{zz}L_{zz}L_{zz}\sin\theta_{SF}\sin\theta_{vis}\sin\theta_{IR}$ for χ_{zzz}. Considering the angles for counterpropagating sample geometry (θ_{SF}= -35º, θ_{vis}= 64º, θ_{IR}= -54º), one can readily see that both pre-factors have a positive sign, and that cancellation is due to opposite signs for the respective nonlinear susceptibility elements. This result agrees with findings from Moad and Simpson, whose detailed analysis of selection rules for nonlinear optical spectroscopy predicted that these two elements of the susceptibility tensor must be opposite in sign.[40]

Data presented here stand in contrast to VSFG results from the neat alkane liquid/vapor interface.[32] Previous results showed that alkanes at liquid/vapor interfaces show more out of plane disorder with increasing chain length, as evidenced by an increasing d^+ to r^+ ratio and the absence of any clear even-odd intensity pattern. In the liquid/vapor studies, the proposed structure that gives rise to such spectra requires that molecules adopt a conformation having (at least) one methyl group directed toward the vapor phase with a net r^+ transition moment projected along the

surface normal. However, the liquid/vapor systems did show evidence of persistent in-plane organization as evidenced by an r^+ to d^+ ratio that scales with statistical limits, and SPS spectra that are consistent with an ordered molecular layer. In contrast, spectra of alkanes adsorbed to the silica/vapor interface show relatively weak SPS spectra that depend more on the number of carbons in the alkyl chain (even-odd) rather than the overall chain length itself. Comparing this previous study with results presented in this work, we see two separate organizational structures, one governed only by intermolecular forces between identical interfacial species, and another the result of interaction with the solid silica surface.

3.4 Conclusion

To summarize, results presented here include VSFG measurements recorded using a broadband counterpropagating beam geometry spectrometer, of linear C_8-C_{11} alkanes adsorbed to the silica/vapor interface. Analysis of the vibrational bands present under different experimental polarization conditions and relative intensities between systems under the same polarization suggests that the molecules lie flat on the surface, with carbon-carbon bonds sampling an orientation that has some net projection along the surface normal.

Table 1. Band assignments, frequencies and relative intensities of features from acquired SFG spectra of octane, nonane, decane and undecane at the silica/vapor interface. Recorded is the frequency in cm^{-1} of the maximum intensity of each feature, and that feature's maximum absolute scaled intensity. The even-odd effect is reflected When the peak intensities for all features in each spectrum are added. Octane, nonane, decane, and undecane have total SSP peak intensities of 0.40, 3.34, 1.12, and 3.17, respectively

Solid/Vapor		d+ (rel. intensity) cm-1	r+	d-	$r+_{FR}$/r-	r-
octane	PPP		2886, 0.30		2950, 0.86	
	SSP		2875, 0.16		2950, 0.24	
	SPS			2927, 0.19		2966, 0.14
nonane	PPP		2875, 0.76		2950, 0.24	
	SSP	2846, 0.78	2866, 1.22		2852, 1.34	
	SPS					2959, 0.14
decane	PPP		2885, 0.28		2949, 1.25	
	SSP	2845, 0.1	2865, 0.54		2951, 0.48	
	SPS			2926, 0.35		2949, 0.25
undecane	PPP		2868, 1.27		2944, 1.44	
	SSP	2943, 1.07	2960, 1.28		2937, 0.82	
	SPS					

3.5 References

(1) Groszek, A. J. *Am. Soc. Lubrication Eng. Trans.* **1962**, *5*, 105-14.

(2) Adhvaryu, A.; Biresaw, G.; Sharma, B. K.; Erhan, S. Z. *Ind. Eng. Chem. Res.* **2006**, *45*, 3735-40.

(3) Schofer, J.; Rehbein, P.; Stolz, U.; Lohe, D.; Zum Gahr, K. H. *Wear* **2001**, *248*, 7-15.

(4) Lin, P. J.; Parcher, J. F. *J. Coll. Int. Sci.* **1983**, *91*, 76-86.

(5) Suri, S. K.; Patel, M. *J. Coll. Int. Sci.* **1981**, *84*, 36-41.

(6) O'Brien, M. J.; Grob, R. L. *J. Chromatogr.* **1978**, *155*, 129-48.

(7) Nikolla, E.; Schwank, J. W.; Linic, S. *Catal. Today* **2008**, *136*, 243-48.

(8) Yang, M.; Somorjai, G. A. *J. Am. Chem. Soc.* **2004**, *126*, 7698-708.

(9) Berman, A. D.; Ducker, W. A.; Israelachvili, J. N. *Langmuir* **1996**, *12*, 4559-63.

(10) Gourdon, D.; Israelachvili, J. N. *Phys. Rev. E: Stat., Nonlinear, Soft Matter Phys.* **2003**, *68*, 021602/1-02/10.

(11) Luan, B.; Robbins Mark, O. *Phys. Rev. Lett.*, *93*.

(12) Ruths, M.; Ohtani, H.; Greenfield, M. L.; Granick, S. *Tribol. Lett.* **1999**, *6*, 207-14.

(13) Somasundaran, P.; Shrotri, S.; Huang, L. *Pure and Appl. Chem.* **1998**, *70*, 621-26.

(14) Thompson, P. A.; Robbins, M. O. *Science* **1990**, *250*, 792-4.

(15) Yoshizawa, H.; Israelachvili, J. *J. Phys. Chem.* **1993**, *97*, 11300-13.

(16) Schlangen, L. J. M.; Koopal, L. K.; Stuart, M. A. C.; Lyklema, J.; Robin, M.; Toulhoat, H. *Langmuir* **1995**, *11*, 1701-10.

(17) Subbotina, I. R.; Shelimov, B. N.; Kazanskii, V. B. *Kinet. Catal.* **2002**, *43*, 412-18.

(18) Gu, Y.; Kar, T.; Scheiner, S. *J. Am. Chem. Soc.* **1999**, *121*, 9411-22.

(19) Scheiner, S. *Advances in Molecular Structure Research* **2000**, *6*, 159-207.

(20) Levinson, P.; Valignat, M. P.; Fraysse, N.; Cazabat, A. M.; Heslot, F. *Thin Solid Films* **1993**, *234*, 482-5.

(21) Gordon, P. A.; Glandt, E. D. *Ind. Eng. Chem. Res.* **1998**, *37*, 3221-29.

(22) Krishna, R.; Smit, B. *Chem. Innovation* **2001**, *31*, 27-33.

(23) Brindza, M. R.; Walker, R. A. *J. Am. Chem. Soc.* **2009**, *131*, 6207-14.

(24) Holzwarth, A.; Leporatti, S.; Riegler, H. *Europhys. Lett.* **2000**, *52*, 653-59.

(25) Conboy, J. C. In *Ph. D. Thesis. Univ. of Oregon,Eugene,OR, 1996*, 1996, p 224 pp.

(26) Eisenthal, K. B. *Chem. Rev.* **1996**, *96*, 1343-60.

(27) Huang, J. Y.; Shen, Y. R. *Adv. Ser. Phys. Chem* **1995**, *5*, 5-53.

(28) Miranda, P. B.; Shen, Y. R. *J. Phys. Chem. B.* **1999**, *103*, 3292-307.

(29) Shen, Y. R. *Nonlinear Spectroscopy for Molecular Structure Determination* **1998**, 249-71.

(30) Shultz, M. J.; Baldelli, S.; Schnitzer, C.; Simonelli, D. *J. Phys. Chem. B.* **2002**, *106*, 5313-24.

(31) Wang, H. F.; Gan, W.; Lu, R.; Rao, Y.; Wu, B. H. *Int. Rev. Phys. Chem.* **2005**, *24*, 191-256.

(32) Esenturk, O.; Walker, R. A. *J. Chem. Phys.* **2006**, *125*, 174701/1-01/12.

(33) Ocko, B. M.; Wu, X. Z.; Sirota, E. B.; Sinha, S. K.; Gang, O.; Deutsch, M. *Phys. Rev. E: Stat. Phys., Plasmas, Fluids, Relat. Interdiscip. Top.* **1997**, *55*, 3164-82.

(34) Sefler, G. A.; Du, Q.; Miranda, P. B.; Shen, Y. R. *Chem. Phys. Lett.* **1995**, *235*, 347-54.

(35) Mo, H.; Trogisch, S.; Taub, H.; Ehrlich, S. N.; Volkmann, U. G.; Hansen, F. Y.; Pino, M. *J. Phys.: Condens. Matter* **2004**, *16*, S2905-S10.

(36) Ding, F.; Zhong, Q.; Brindza, M. R.; Fourkas, J. T.; Walker, R. A. *Optics Express*, *Submitted, May 2009*.

(37) MacPhail, R. A.; Strauss, H. L.; Snyder, R. G.; Elliger, C. A. *J. Phys. Chem.* **1984**, *88*, 334-41.

(38) Ohe, C.; Sasaki, T.; Noi, M.; Goto, Y.; Itoh, K. *Anal. Bioanal. Chem.* **2007**, *388*, 73-79.

(39) Chen, X.; Clarke, M. L.; Wang, J.; Chen, Z. *Int. J. Mod. Phys. B* **2005**, *19*, 691-713.

(40) Moad, A. J.; Simpson, G. J. *J. Phys. Chem. B.* **2004**, *108*, 3548-62.

Chapter 4: Octanol Isomer Structure at Interfaces

4.1 Introduction

Understanding the intermolecular interactions responsible for solvent structure and organization at liquid interfaces has direct impact on many fields including biochemistry, electrochemistry, and separation science. The structure and ordering present at liquid interfaces will depend upon a balance of asymmetric forces between the two bulk phases as well as lateral interactions between the surface species themselves. Numerous techniques have evolved to probe liquid structure at interfaces including x-ray and neutron scattering, as well as nonlinear optical spectroscopies.[1-14] Most of the systems previously studied have been relatively simple, meaning that the liquids themselves are small molecules, and/or films adsorbed to the interface are ordered in Langmuir-like monolayers.[5,7,15] Surprisingly little attention has focused on the organization of asymmetric molecules at interfaces, despite the prevalence of these species in natural product and synthetic surfactant systems. Here the term asymmetric describes any molecule having C_1 point group symmetry. These systems are particularly difficult to model at surfaces because of the subtle and competing forces responsible for interfacial organization. Strong intermolecular interactions between interfacial molecules, as well as with the adjacent phases, can lead to small changes in overall surface energetics and dramatically different organizations. For example, results have shown that self assembled monolayers of alkane thiols on gold exhibit large variations in molecular tilt depending on the length of the molecule.[16] These adsorbates all interact with the substrate through the same thiol linkage,

meaning that changes in interfacial structure arise due to small differences in van der Waals interactions between adjacent adsorbates.

At solid/vapor or liquid/vapor interfaces, the considerations of forces responsible for adsorbate structure and organization are relatively simple. Molecules adsorbed in a single layer or less on a solid substrate can interact only with the rigid solid surface and with other adsorbates. The solid/liquid interface becomes more complicated however, since here the opportunity exists for fast exchange between surface species and the bulk liquid. On solid surfaces, adsorbate organization follows the registry of the underlying substrate. Thus, there have been numerous studies of the interactions of molecules, both chemisorbed and physisorbed onto solid interfaces.[17-20] A large number of studies have sought measure the long range order and structure and orientation of long amphiphilic or surfactant molecules adsorbed to the liquid interface and found that conformational order increases dramatically with chain length.[16,21-24] The structure and organization of liquid surfaces has been investigated by nonlinear optical spectroscopy,[5,11,25] x-ray and neutron scattering experiments,[7,8,10] as well as molecular dynamics simulations.[26-28] Typically, scattering experiments infer the position of molecules through constrast in electron or atomic density measurements, while spectroscopic results show the orientation and local environment of molecules at an interface.[3,6-8,12-14,29] Despite all of the progress in the area of molecular surface science, however, we still lack a general, predictive understanding of what types of interactions dominate surface organization of asymmetric molecules at interfaces.

Such an understanding is essential for predicting the structure and properties of a large number of naturally occurring systems. For example, cell plasma membranes are two-dimensional assemblies that typically contain up to 25 different lipids having different head groups and different degrees of unsaturation in the acyl chains.[30,31] Of these ~25 lipids only 4-5 will be dominant and the identity of these lipids varies from cell type to cell type. Despite this opportunity for highly variable and heterogeneous structures, nature has conspired to bring together well defined, reproducible collections of lipids having specific shapes and interactions in order to confer well defined properties and functionality to different types of cell plasma membranes.[32-37] In addition to the biological questions surrounding molecular structure and organization in two dimensions, many naturally occurring atmospheric processes depend on the surface adsorption of small organic molecules to aerosol or dirt particles in the marine boundary layer.[38-40] Again, these adsorbates are likely to be asymmetric but somehow they must organize to minimize the particle's free energy.

Studies described in this chapter examine the structure and organization of octanol isomers at solid/vapor, solid/liquid, and liquid vapor inerfaces. Motivating these experiments are previous nonlinear spectroscopic results that showed heterogeneous interfacial polarity at the aqueous/n-alcohol and silica/n-octanol interfaces.[41,42] In this prior work, resonance enhanced second harmonic generation was used to examine the interfacial polarity surrounding solvatochromic solutes adsorbed to the liquid/liquid and solid/liquid interfaces. As the distance increased between the hydrophobic, polarity-sensitive end of the molecule and the solvated

charged head group, the solvation environment across liquid/liquid interfaces changed from very polar (aqueous-like), to nonpolar (alkane-like), then back to moderately polar (octanol-like).[42] This result was interpreted in the context of a Langmuir-like monolayer of octanol molecules that formed the first layer of the organic solvent. Interfacial polarity at the silica/octanol solid/liquid interface has also been shown to be heterogeneous, with solvatochromic solutes at that interface having populations that sample both extremely polar and nonpolar environments.[41] These results lead one to predict that a 1-octanol solvent in contact with a silica interface forms a Langmuir-like monolayer film in the first solvent layer with the –OH functional groups of the solvent hydrogen bonded to the surface silanol groups and the long alkyl chains well ordered due to van der Waals interactions. Such an arrangement would create a nonpolar region between a polar surface and a bulk solvent having a medium static dielectric constant ($\varepsilon \sim 10.5$).

Consistent with these inferences are spectroscopic and thermodynamic measurements of 1-octanol *monolayers* formed at the aqueous/vapor interface from solutions saturated with the alcohol. Data from these studies provide clear evidence of a tightly packed, well ordered monolayer with adsorbed molecules adopting an upright orientation with little or no conformational disorder.[43] AFM measurements also show that 1-octanol monolayers adsorbed to the mica solid/vapor interface form close packed monolayers and not bilayers.[44] Both of these experimental studies have been bolstered by findings from molecular dynamics simulations of 1-octanol at different solid/vapor and aqueous/vapor interfaces.[45,46] In contrast, monolayers of 2- and 3-octanol adsorbed to the aqueous/vapor interface show that at terminal

monolayer coverage, these isomers form more expanded monolayers that minimize hydrophobic interactions between the long and short alkyl segments and the aqueous subphase.[43] This finding is consistent with additional studies of solvent polarity at aqueous/3-octanol interfaces that found the nonpolar region to extend a shorter distance than in the case of 1-octanol, and transition abruptly to the bulk 3-octanol limit.[42]

Implicit in the studies of polarity across the silica/octanol and aqueous/octanol buried interfaces was an assumption that the octanol structure at the aqueous/*vapor* and silica/*vapor* interfaces closely resembles the structure of the first layer of solvent at the corresponding buried interfaces. However, resolving questions about interfacial solvent structure requires knowing explicitly how solvent molecules in contact both with the neat liquid and with the adjacent polar, solid phase organize themselves in two dimensions. Scattering methods can examine some aspects of interfacial structure, including solvent density, roughness, and interfacial width;[7,8,10,14,47,48] however these techniques lack the ability to sample directly the interactions between molecules that are responsible for interfacial structure and organization. Using vibrational sum frequency spectroscopy (VSFG), a surface specific, second order nonlinear optical method, experiments described in this chapter measure directly octanol isomer structure and orientation at the solid/vapor, solid/liquid, and liquid/vapor interfaces. Doing so allows us to quantify interfacial solvent organization, as well as extrapolate how the balance of forces between phases and between interfacial species leads to changes in molecular ordering at these different boundaries. By changing the isomer structure of octanol adsorbed to these

three interfaces, we can show that the ability of these solvent molecules to form ordered layers depends on interactions between the substrate and the solvent, interactions between the solvent and neighboring molecules, and the inferred dynamic exchange of solvent molecules between the interfacial and bulk regions of the liquid.

4.2 Experimental

VSFG is an ideal tool to measure the structure and orientation of interfacial solvent molecules. The technique is sensitive only to those molecules subject to interfacial anisotropy, and different polarization conditions described below allow experiments to selectively probe the orientation of specific functional groups. The origin of the technique's surface specificity has been described in Chapter 3, and will be omitted here.

SFG spectra were collected using a broadband, counter-propagating geometry SFG spectrometer that has been described in Chapter 3. This sample geometry allows for easily changing between the solid interfaces and the neat liquid. The solid/vapor and (solid/liquid) spectra were acquired after putting a drop inside (filling) of the quartz cells, and letting the system equilibrate. The neat liquid/vapor spectra were recorded from the open-to-air liquid interface in a clean dish. Typically, we record SFG spectra for 1-4 minutes at each central IR wavelength, then shifted the laser 50 nm and acquired again. This procedure leads to 8 broadband wavelength scans per spectrum. All spectra were normalized to the instrument response measured by the nonresonant spectrum acquired from the gold/vapor interface, and calibrated by placing a polystyrene card in front of the gold surface along the IR path. Four points corresponding to known adsorption bands from polystyrene were used for a

wavelength calibration, leading to an accuracy in reported frequencies on the order of ± 2 cm^{-1}. While absolute intensities of spectra from different systems cannot be compared quantitatively, relative intensities of bands within the same spectrum typically reproduced to within 10 percent.

In addition to spectroscopic measurements of octanol films adsorbed to the silica/vapor interface, thermogravimetric analyses (TGA) of similar systems were also performed. In these experiments, silica gel particles were exposed to a saturated alcohol vapor for several hours. The samples were then loaded into the TGA instrument and the mass loss was measured as a function of temperature and time as the temperature was elevated slowly. Silica gel was used as purchased and allowed to equilibrate with octanol isomer vapor for several hours prior to sample loading. A Thermal Advantage Q500 was used for TGA analysis. Approximately 15-20 mg of the sample was loaded into a platinum weighing boat. In a typical experiment, the samples were allowed to equilibrate at 16º C before the sample was heated at 2ºC/min to 200º C and then held isothermally for 2 hours. Ultra high purity N_2 was used in all experiments.

To compare interfacial free energies of different octanol isomers, surface tension measurements of the neat liquid/vapor interfaces were performed using the Wilhelmy plate method.[49-51]

4.3 Results

Figure 4.1 shows the VSFG spectra of 1-octanol adsorbed to the silica/vapor interface for three different polarization combinations. The spectra show three features assigned to the methyl symmetric stretch (r^+, 2872 cm^{-1}), the r^+_{FR} at

2940 cm^{-1}, and the methyl asymmetric stretch (r^- near 2955 cm^{-1}). Smaller, low intensity peaks at 2840 and 2925 cm^{-1} in the SSP spectrum are assigned to alkyl methylene symmetric stretch (d^+) and asymmetric stretch (d^-), respectively.

Qualitatively, the appearances of the r^+ and r^+_{FR} in the SSP spectrum and r^- in the SPS spectrum are consistent with well ordered monolayers whose alkyl chains stand upright with few, if any, gauche defects. Closer inspection of relative band intensities indicates that the 1-octanol monolayer adsorbed to the silica interface is less well ordered than monolayers formed by comparable length alcohols adsorbed to the aqueous/vapor interface. This conclusion is based on the smaller relative intensity of the r^+ to r^+_{FR} features in the SSP spectrum. For tightly packed n-alcohol monolayers ($n \geq 8$) adsorbed to the aqueous/vapor interface, the r^+/r^+_{FR} ratio is approximately 3-4.[43] Monolayers packed less closely typically show r^+ to r^+_{FR} ratios closer to unity.[43,52] If one considers the area per surface silanol group on hydrophilic silica to be approximately 33-40 $Å^2$/silanol, an estimate based on NMR analysis of deuterium exchanged silica gels, and assume that each site is occupied by a single octanol,[53] then the predicted surface concentration of a 1-octanol monolayer at the silica/vapor interface is ~40% less than terminal monolayer coverage at the aqueous/vapor interface.[54]

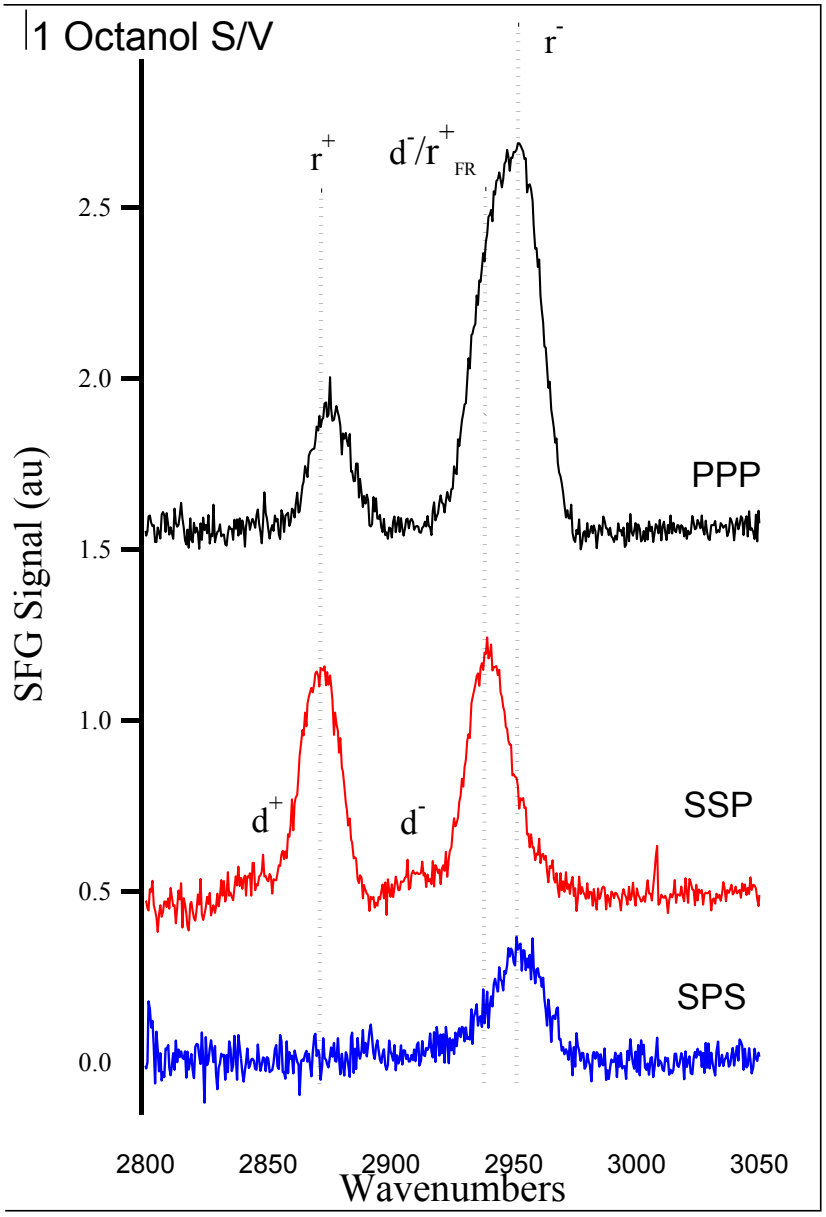

Figure 4.1. VSFG Spectra of 1-octanol adsorbed to the silica/vapor interface. The top spectrum, in black, was acquired under PPP conditions, the red spectrum in the middle, and the blue spectrum at bottom under SSP and SPS conditions, respectively. This order and color scheme is consistent for all spectra shown here. Also shown, and labeled, are dashed lines corresponding to the frequencies reported for the methyl symmetric stretch (r+), methylene asymmetric stretch and methyl Fermi resonance (d-/$r+_{FR}$), and methyl asymmetric stretch (r-). Relative intensities between spectra acquired under different polarization conditions are not directly comparable.

Comparing the spectra of 1-octanol adsorbed to the silica/vapor interface to those of other octanol isomers adsorbed to the same surface (Fig. 4.3) shows few dramatic changes in the spectral features or relative intensities.

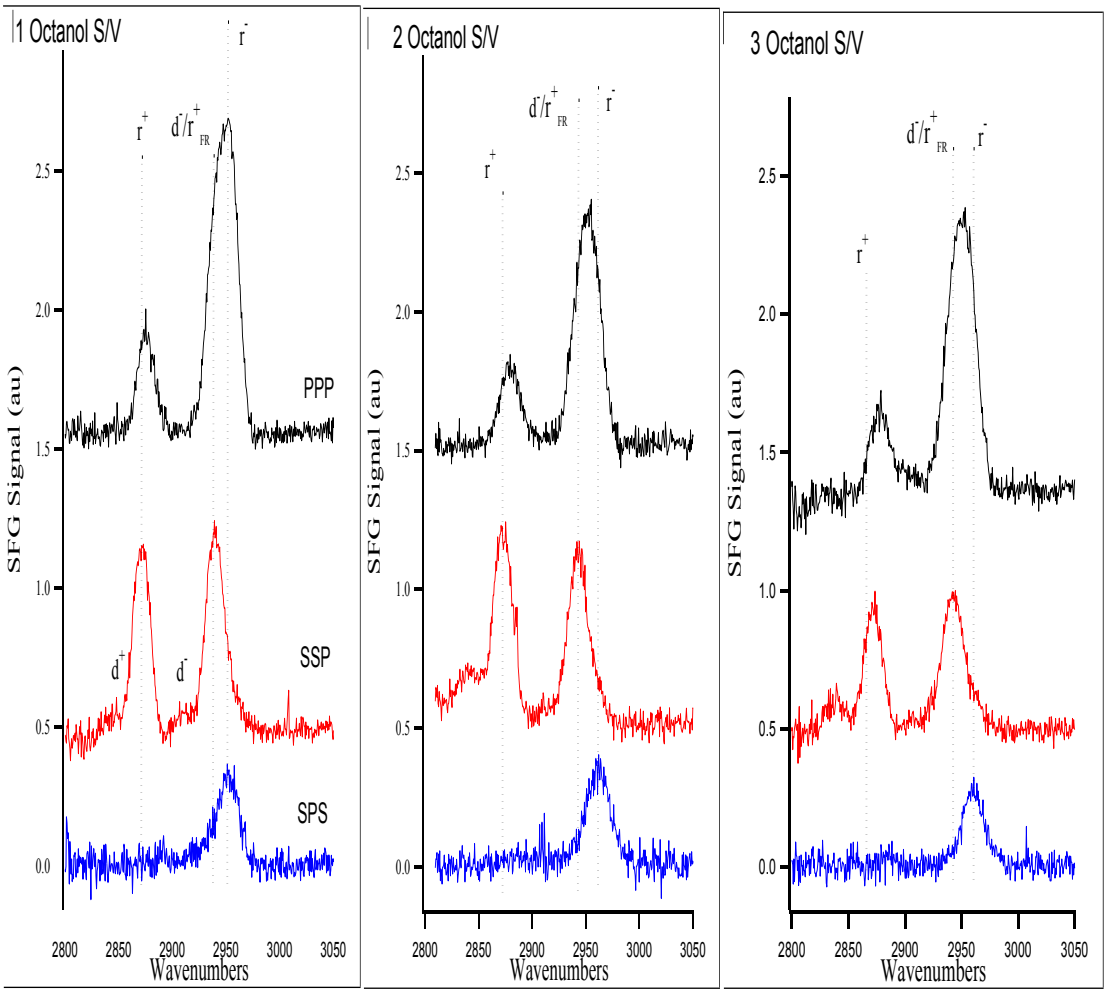

Figure 4.2. VSFG Spectra of 1-,2-, and 3-octanol acquired under PPP, SSP, and SPS polarization conditions. Each spectrum represents the sum of 8 separate one minute acquisitions that have been normalized to the instrument response as measured by the nonresonant SF signal acquired from the neat gold surface.

This result contrasts with spectra recorded of octanol isomer monolayers at the aqueous/vapor interface, in that 2-, and 3-octanol having a higher corresponding surface areas showed changes in relative band intensities consistent with conformational changes and reduced molecular ordering.

One might naively assume alcohol structure at the aqueous/vapor and silica/vapor interfaces to be similar. At both surfaces adsorbed octanol can form a strong hydrogen bond with the adjacent phase. One major difference between the two interfacial systems, however, is that at the aqueous/vapor interface the adsorbed alcohol hydroxyl group is solvated, and branched alcohols must then decide whether or not to solvate the short alkyl segment. Previous results show that 2-hexadecanol adsorbed to the aqueous/vapor interface remains linear and tightly packed (~23 $Å^2$/molecule) with a solvated methyl group. In contrast, 2-octanol adsorbed to the aqueous/vapor interface forms more expanded monolayers at terminal surface coverage (41 $Å^2$/molecule). At silica surfaces, the hydroxyl group is hydrogen bonded to the substrate but cannot be solvated. Conformational defects for 2- and 3-octanol are unavoidable, and the octanol hydroxyl group can only enjoy close contact with the surface, not complete solvation. Despite the differences between 1-, 2-, and 3-octanol adsorbing to the interface, however, the data in Figure 4.2 show no apparent change in the major spectral features other than the small intensity growth of the d+ band.

Several factors will control octanol surface coverage at the aqueous/vapor and silica/vapor interfaces. Not least among them are the number of available hydrogen bonding sites. Hydroxyl group density at the hydrophillic silica surface has been reported as high as 70-80% of all surface Si-O structures, giving an average molecular area per hydroxyl group of approximately 33-40 $Å^2$.[55] Surface tension measurements of aqueous solutions saturated with 1-octanol show that some octanol adsorbs to the aqueous/vapor interface to form tightly packed monolayers with

surface coverages corresponding to 20 $Å^2$/molecule. Assuming that the strongest interaction between adsorbed octanol and the silica surface is hydrogen bond donation from the silica, and assuming a 1:1 silanol to octanol association, the monolayer formed at the solid/vapor interface is expected to be less densely packed, allowing for greater disorder within the self assembled monolayer. In order for 2-, and 3-octanol to interact with surface silanol groups through hydrogen bond formation, and have the long alkyl segments directed along the surface normal, the adsorbed species must disorder. One reason that the spectra of 1-, 2- and 3-octanol films formed at the solid/vapor interface have such similar spectra is that 2- and 3-octanol may actually both adopt conformations having gauche defects and still form monolayers with small enough surface area per monomer to hydrogen bond with all available silanol groups. Previous work has shown that the molecular footprint of 2- and 3-octanol isomers with two gauche defects is on the order of ~40-45 $Å^2$/molecule.[43] These branched isomers adsorbed to the silica/vapor interface can form more expanded layers yet still strongly associate with all available sites on the substrate.

We believe that the disorder induced in adsorbed 2- and 3-octanol monomers results in lower surface coverage than for 1-octanol. This claim is based upon TGA measurements of adsorbed octanol films at the silica/vapor interface, shown in Figure 4.4. These experiments measure the mass (by percent) lost from small silica particles with octanol adsorbed from the saturated vapor. TGA results show that more than twice as much 1-octanol is initially adsorbed to the silica gel particles compared to 2-, or 3-octanol. At the liquid/vapor interface branched alcohols formed monolayers with

approximately half the surface coverage as linear alcohols. The same observations also appear to be true for branched alcohols adsorbed to the solid/vapor interface. Additional similarities between the aqueous/vapor and silica/vapor interfaces come from the VSFG spectra of branched octanols at both boundaries that are characterized by a modest increase in d+ band intensity, much like spectra acquired from the silica/vapor interface. Growth of this feature requires a net polar ordering of solvent methylene groups with C_2 axes projecting along the surface normal.

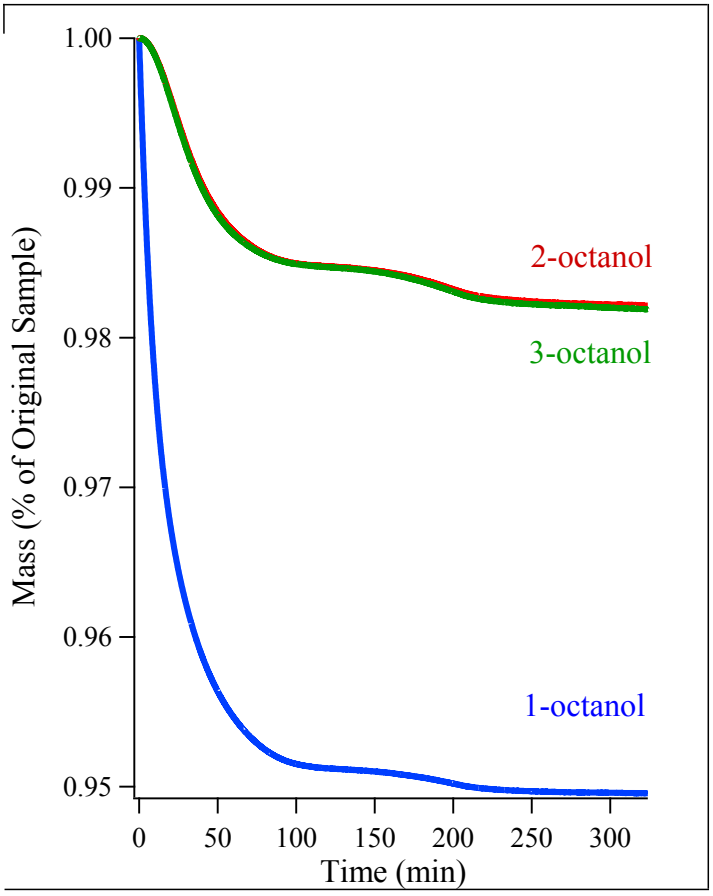

Figure 4.3. TGA data showing mass loss from silica gel particles with adsorbed octanol isomers. Reported value is percent of total mass lost vs. time.

When considering solvent structure at solid/liquid interfaces, one can wonder if the first layer of solvent molecules resembles that of the monolayer adsorbed to the silica/vapor interface. Another way of framing this question is to wonder what role an adjacent, dense, mobile, polar phase has on the structures of interfacial solvent species. Previous studies have shown that the structures of surfactant monolayers chemisorbed to silica/liquid interfaces depends on the identity and packing efficiency of the liquid phase.[56] To address these questions about *solvent* structure at solid/liquid interfaces, we filled the cells so that the liquid was in direct contact with the silica surface and acquired new SFG spectra. Comparing the SFG spectra of 1-octanol from the solid/vapor to those from the solid/liquid interfaces we find that some degree of molecular ordering persists, but that the liquid/solid interface is considerably more disordered than the solid/vapor interface (Figure 4.4). The SSP spectrum still shows some intensity that we attribute to r+, however the methylene SS (d+) and the methylene AS (d-) bands have also begun to make significant contributions to the SFG spectrum. Furthermore, the SPS spectrum still only has one feature, which has shifted and now appears with a frequency corresponding to the d^- band. Collectively these spectra imply that interfacial solvent structure is not as ordered as is suggested by studies of interfacial polarity.

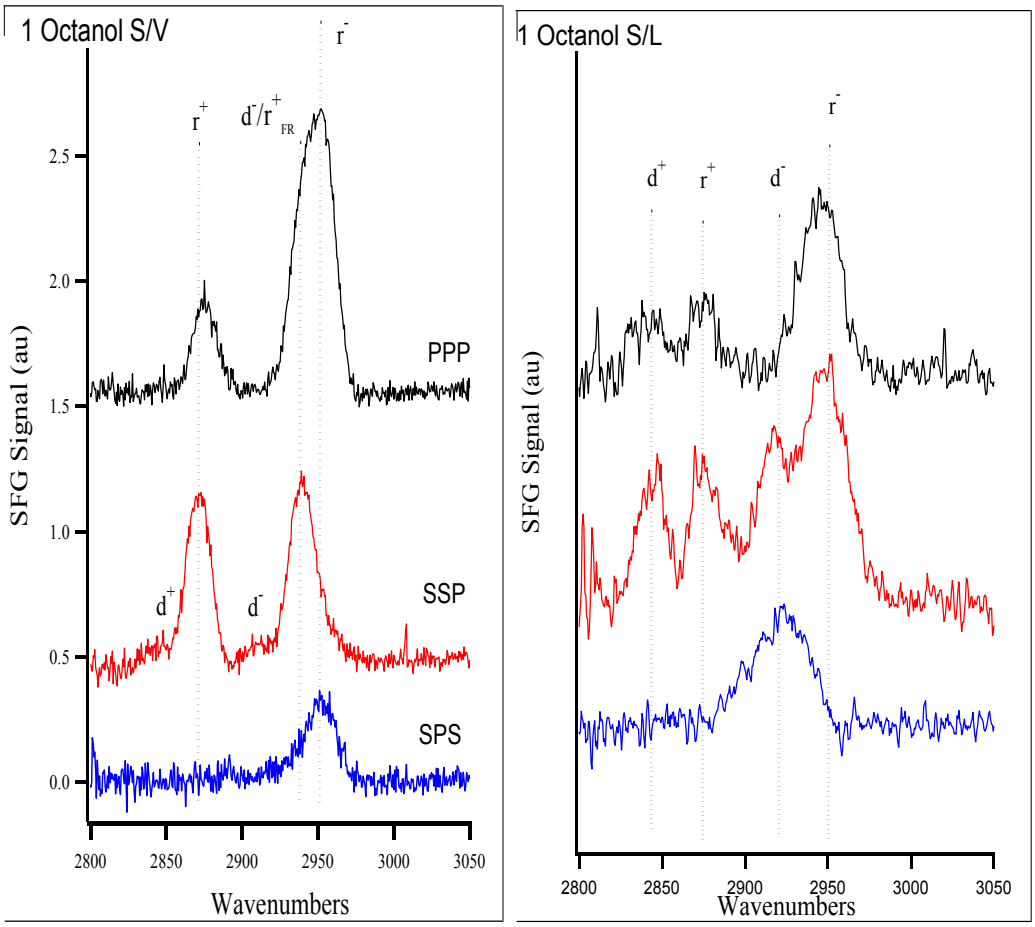

Figure 4.4. Comparison of the VSFG spectra acquired from the silica/vapor interface with 1-octanol adsorbed and the silica/liquid interface formed between the solid and liquid 1-octanol. The silica/vapor spectra are reprinted from Figure 4.1. Acquisition time for the silica/liquid spectra was 4 times longer than the silica/vapor.

At the silica surface, one can reasonably expect interfacial octanol species to have strong hydrogen bonding interactions with the silica substrate and modest van der Waals interactions between the chains. Nevertheless, the SFG spectra show a considerable amount of conformational disorder in the solid/liquid spectra as evidenced by the growth of the d^+ band relative to the r^+ band and the overall loss of signal intensity beyond the ~2 fold reduction attributed to refractive index considerations. Assigning loss of signal intensity to a loss of order is not always a straightforward exercise because signal cancellation can arise from *ordered* bilayer

structure at the interface with opposing layers having opposite orientations. However, this explanation is not supported by polarity measurements across aqueous/octanol interfaces, where polarity converges to the bulk limit on a scale comparable to the length of one interfacial octanol molecule. Furthermore, if the first layer of adsorbed solvent is not packed as closely as tightly packed monolayers, we would expect the second layer to partially penetrate into the first solvent layer, leading to an increase in interfacial disorder. We note that one series of MD simulations has predicted multilayer structure extending further away from the interface,[45] but these simulations stand in contrast to other simulations and related scattering experiments.[57] A second source of low VSFG intensity - rapid dynamic exchange between surface and bulk is considered below and thought to be not important. Thus we conclude that the silica/1-octanol solid/liquid interface possesses some degree of solvent ordering, but the presence of a liquid leads to significant disordering relative to 1-octanol monolayers at the silica/vapor interface.

When we compare the spectra of 1-octanol at the silica/liquid surface to those of 2-, and 3-octanol, we see that the loss of interfacial order and monolayer molecular structure becomes even more pronounced. Spectra from both 2-octanol and 3-octanol at the silica/liquid interface show an almost total absence of long range order within the interfacial region. The silica/3-octanol PPP and SSP spectra show only intensity in the region of the methyl AS (r^-). No signal rises above the baseline in the SPS spectrum. These data are consistent with a very disordered layer at the interface, where the molecules orient their alkyl chains parallel to the surface but with little

correlation between individual monomers. Such a picture predicts very little, if any organization in the solvent adjacent to the solid/liquid interface.

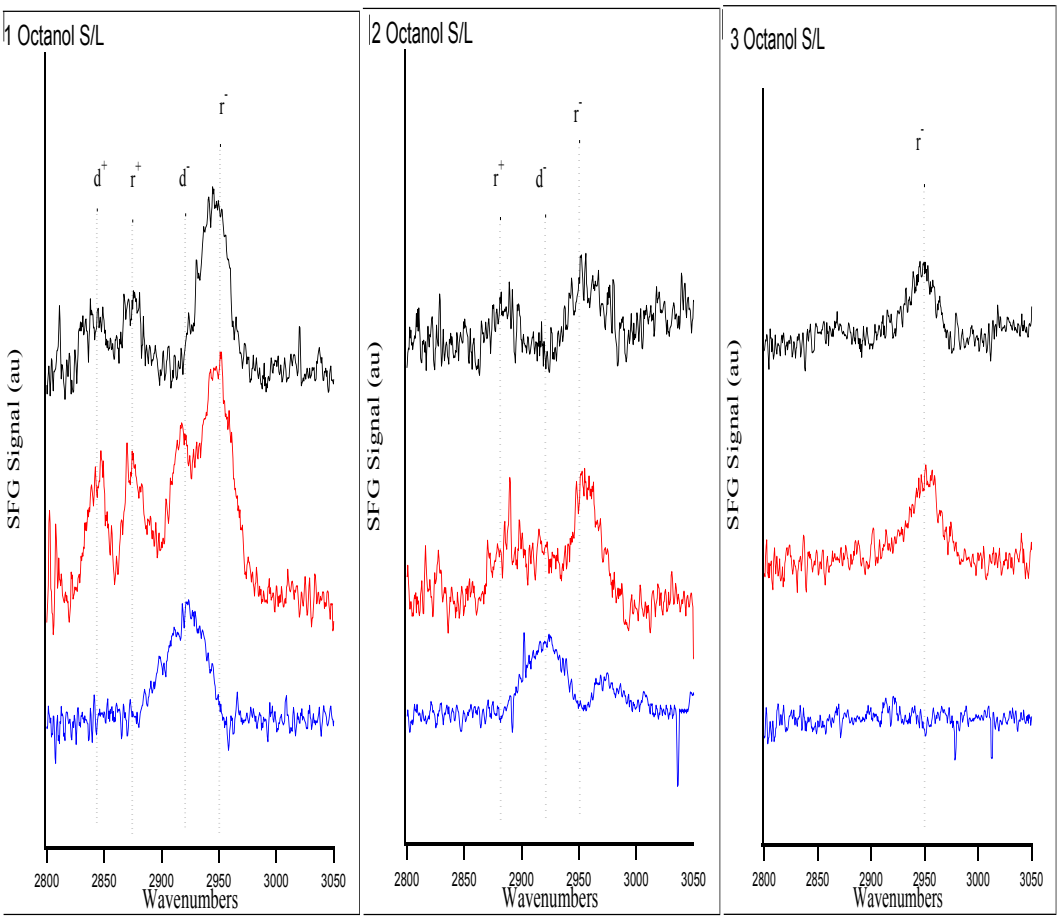

Figure 4.5. VSFG spectra of the silica/liquid interfaces made by bringing 1-,2-, and 3-octanol into contact with hydrophilic silica. Shown on the silica/1-octanol spectrum are the asignments for the d+, r+, d-, and r-, respectively.

A second possible source of interfacial disorder could be dynamic exchange between interfacial solvent and solvent from the bulk phase. Fast exchange necessarily requires weak surface-solvent interactions and would lead to little structural correlation between interfacial solvent species. However, this explanation is not supported by data from the liquid/vapor interface (*vide infra*) or from TGA measurements. TGA data show that much less 2- and 3-octanol are adsorbed to silica

gel particles compared to 1-octanol but the temperature dependence of the mass loss profiles are very similar, indicating that on a per-monomer basis, the substrate-adsorbate interactions are of similar strength for all isomers.

To understand better how dynamic exchange might disrupt interfacial structure, we acquired VSFG spectra from the neat 1-,2-, and 3-octanol/vapor interfaces. (Figure 4.6) Data from all three systems are consistent with an interfacial region having noticibly more order than the solid/liquid interface. Strong intensity in SSP spectra from the r^+ and $r+_{FR}$ implies a net polar ordering with chain ends pointing in a vertical direction, although intensity assigned to the d^+ suggests the 1-, 2-, and 3-octanol/vapor interfaces are less well ordered than the standard benchmarks of upright, long alkyl chain monolayers. The only feature appearing in SPS spectra is assigned to the r^-, again consistent with the interfacial solvent being moderately well ordered with methyl groups directed along the surface normal. In the absence of a strongly associating polar substrate, only surface tension forces are responsible for keeping molecules confined to the interfacial region. Of the three isomers, 1-octanol's measured surface tension is largest (27.5 ± 0.5 mN/m^2), followed by 2- and 3-octanol's measured surface tensions of 26.3 and 25.7 ± 0.5 mN/m^2, respectively. Such similarity leads us to expect similar structure and organization between the isomers at liquid/vapor interfaces. More importantly, one expects exchange between the interface and bulk to be most facile at the liquid/vapor interface, yet these interfaces evince noticeably more polar ordering than the solid/liquid interfaces. Instead of imposing long-range organization on a strongly

associating liquid solvent, the silica surface appears to disrupt the ability of the solvent to order.

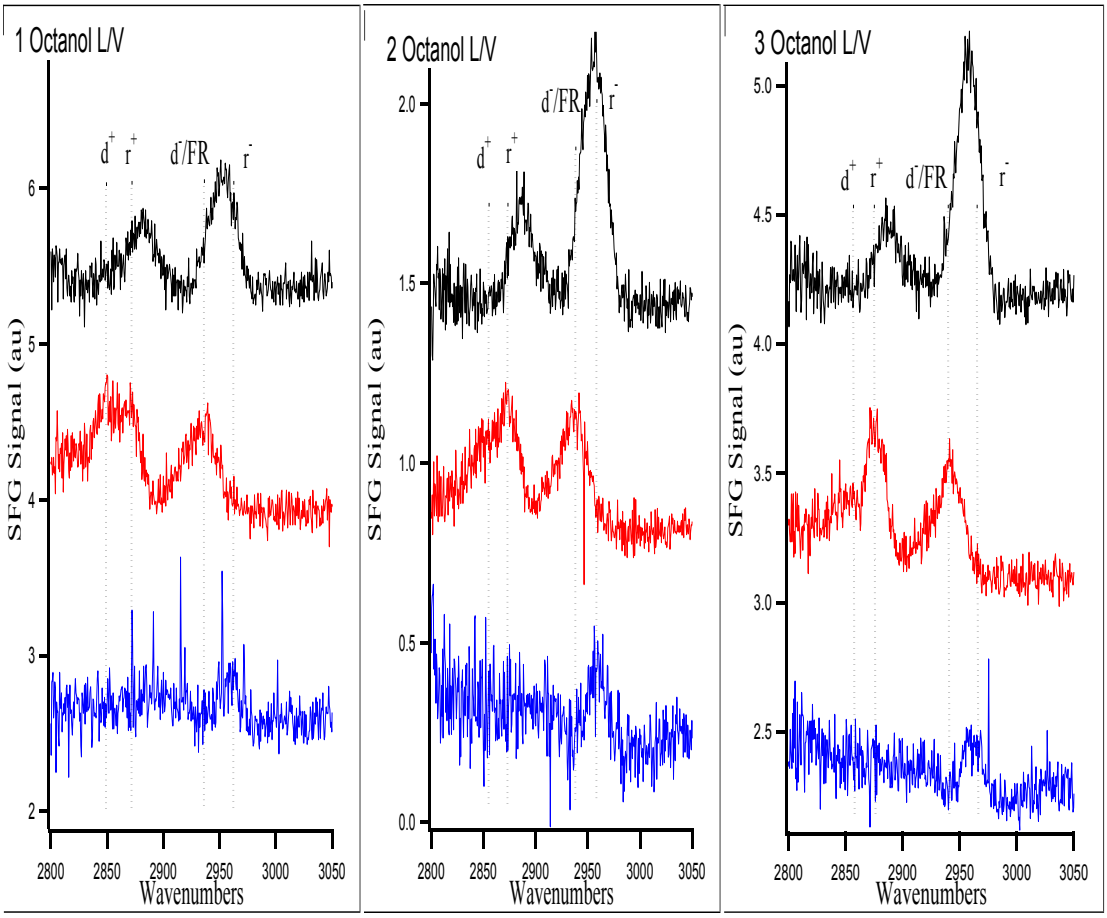

Figure 4.6. VSFG spectra of the liquid/vapor interfaces of 1-,2-, and 3-octanol. Shown on the are the asignments for the d+, r+, d-/FR, and r-, respectively.

Directly comparing these data to solid/liquid measurements, the most striking difference is the increased ordering that occurs when moving from the silica/3-octanol to the 3-octanol/vapor interface. 3-Octanol is the least ordered at the solid/liquid interface, although its liquid/vapor interface is consistent with a moderately high degree of organization. These results are consistent with other spectroscopic studies, and molecular dynamics simulations that show order and organization to persist for multiple molecular layers at the 3-octanol/vapor interface.[45]

4.4 Discussion

Data presented above show that a given isomer can organize in a variety of ways at different interfaces. Furthermore, at a given interface (solid/liquid or solid/vapor or liquid/vapor) different isomers will adopt different structures to minimize interfacial free energy. Molecular structure and organization at interfaces will be determined through a balance of competing forces. For example, a single 1-octanol molecule adsorbed from the gas phase to a silica surface will lie flat in order to maximize both hydrogen bonding opportunities and van der Waals contacts. This phenomenon is evidenced by similar observations that show conformational disorder in low density monolayers of long chain alkanethiols chemisorbed to the silica/vapor interface.[58] However a *monolayer* of 1-octanol molecules will minimize it's free energy by allowing all monomers to hydrogen bond with the surface and take advantage of chain-chain van der Waals interactions resulting in monomers tightly packed with all-trans conformations.

In this instance, the monolayer formed at the silica/vapor interface is expected to be very stable because desorption would require breaking both the hydrogen bonds formed with the surface and losing the attractive chain-chain van der Waals interactions. In contrast, the barrier to 1-octanol desorption from the solid/liquid interface should be much smaller because the penalty paid during desorption can be at least partially recouped through solvation in the 1-octanol bulk liquid. The persistence of some interfacial order at the silica/1-octanol solid/liquid interface means that the energy of desorption into the liquid is at least comparable to the free

energy of solvation. The more pronounced lack of order at the silica/2- and 3-octanol solid/liquid interfaces implies that solvent-solvent interactions in bulk are markedly stronger than interactions between monomers and the surface and between adsorbed monomers themselves.

Determining the free energy of adsorption for an octanol molecule moving from the bulk liquid to the silica/liquid interface is challenging. In principle such information could come from experiments that determine heats of immersion, but such measurements are scarce in the literature and not systematic in the specific solid/liquid combinations sampled.[59-61] Furthermore, studies that *do* exist often compare small molecules not relevant to this work, and results depend on sample choice and preparation,[62] making comparisons between studies unreliable.

The heat of adsorption from the liquid is also difficult to model directly because this quantity reflects the energy required to dissociate from the surface (a positive number), the energy required to break van der Waals contacts with other adsorbates (also a positive number that should depend on chain length), and the heat of solvation in the bulk (a negative value). Modeling these quantities accurately is difficult. Instead, we choose to approximate desorption from the solid/liquid interface by considering the thermodynamic cycle shown in Figure 4.7. Heats of adsorption from the gas phase onto silica surfaces have been measured, and the heat of solvation from the gas phase is simply the negative of the $\Delta H_{vap.}$ What this model does not take into account are the lateral interactions between adsorbed monomers. Heats of adsorption for linear alcohols are reported for propanol and butanol isomers[63] but not for longer branched alcohols. Nevertheless, using reported results

from smaller linear and branched isomers allows us to semi-quantitatively evaluate the likelihood that interfacial order observed at the solid/vapor interface will persist at the solid/liquid interface.

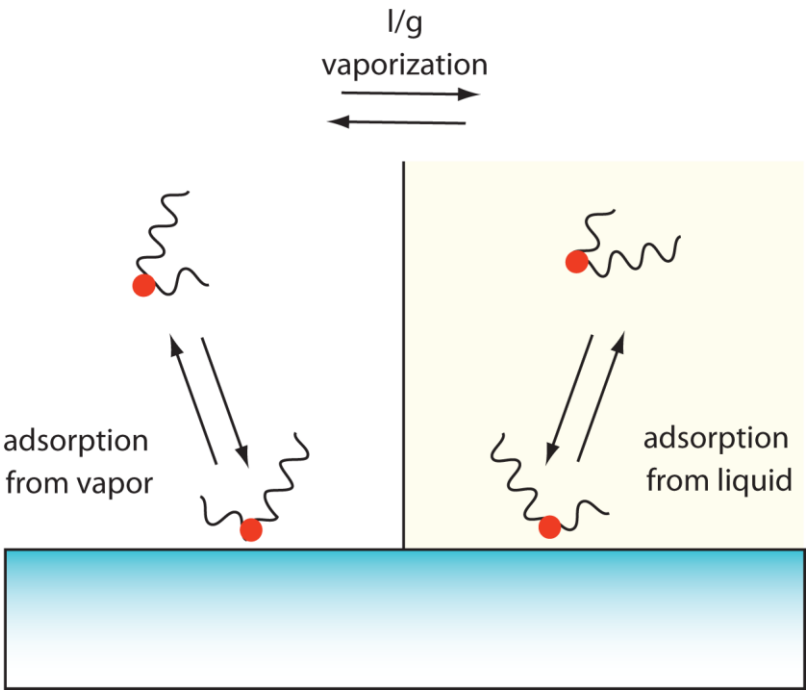

Figure 4.7. Schematic representation of the thermodynamic cycle detailing adsorption to solid/vapor and solid/liquid interfaces. If the difference between the heat of adsorption from the vapor, and the energy of solvation in the bulk is large enough, preserved order is expected at the solid/liquid interface.

For molecules to remain organized at solid/liquid interfaces, ΔH_{ads} must be large and negative and with a greater magnitude than ΔH_{solv}. The most complete data for molecules most closely related to octanol isomers studied in this chapter are thermodynamic quantities for *n*- and t-butanol. The reported heat of adsorption values are ~50 kJ/mol and 40 kJ/mol for *n*- and *t*-butanol, respectively.[63,64] Adding in the heat of vaporization, which is 52.3 kJ/mol, and 46.7 kJ/mol for *n*-and t-butanol,[65] respectively, we see that the difference between these two values is less positive for the linear isomer. We would expect t-butanol to not be as well ordered as n-butanol

at the solid/liquid interface, as these values suggest a higher likelihood for molecules to want to prefer being in the bulk. Furthermore, studies have shown that the heat of immersion for silica gel particles in *n*-butanol is greater in magnitude (and negative in sign) than t-butanol.[66]

4.5 Conclusions

This chapter presents VSFG spectra of 1-,2-, and 3-octanol adsorbed to the silica/vapor, silica/liquid, and neat liquid/vapor interfaces. Comparing the vibrational modes appearing under certain experimental polarization conditions shows that all isomers form ordered monolayers at the silica/vapor interface. When the bulk liquid is brought into contact with that surface, however, a loss of signal intensity at some frequencies coupled with increasing band intensities for other vibrational modes suggest a greater degree of either static or dynamic disorder. Vibrational spectra from the neat liquid/vapor interface are also consistent with a high degree of conformational and organizational order, supporting static disorder over dynamic. The ability of order observed in thin films formed at solid/vapor interfaces to persist at solid/liquid interfaces appears to correlate with thermodynamic quantities that are either reported in the literature or can be determined easily.

Tables 4.1-3. Band assignments, frequencies and relative intensities of features from acquired SFG spectra of 1,2, and 3-octanol at the silica/vapor, silica/liquid, and neat liquid/vapor interfaces. Recorded is the frequency of the maximum intensity of each feature, and the ratio of that intensity to the largest appearing in each respective spectrum.

Solid/Vapor		d+(cm^{-1}, rel.intensity)	r+	d-	$r+_{FR}$	r-
1-octanol	PPP		2873, 0.36		2938, 0.76	2952, 1.00
	SSP	2843, 0.11	2872, 0.87	2917, 0.12	2939, 1.00	
	SPS					2952, 1.00
2-octanol	PPP		2978, 0.38		2939, 0.58	2955, 1.00
	SSP	2842, 0.31	2872, 1.00	2920, 0.17	2943, 0.93	
	SPS					2960, 1.00
3-octanol	PPP		2878, 0.25		2937, 0.51	2953, 1.00
	SSP	2840, 0.26	2871, 0.89	2922, 0.25	2942, 1.00	
	SPS					2960, 1.00

Solid/Liquid		d+(cm^{-1}, rel.intensity)	r+	d-	$r+_{FR}$	r-
1-octanol	PPP	2845, 0.40	2875, 0.49	2923, 0.37	2941, 1.00	2952, 0.93
	SSP	2842, 0.56	2869, 0.65	2918, 0.71	2942, 0.93	2952, 1.00
	SPS			2921, 1.00		
2-octanol	PPP		2882, 0.69			2956, 1.00
	SSP		2890, 0.93			2954, 1.00
	SPS			2922, 1.00		
3-octanol	PPP					2949, 1.00
	SSP					2949, 1.00
	SPS					

Liquid/Vapor		d+(cm^{-1}, rel.intensity)	r+	d-	$r+_{FR}$	r-
1-octanol	PPP	2847, 0.44	2884, 0.73			2951, 1.00
	SSP	2850, 1.00	2872, 0.92		2939, 0.87	
	SPS					2959, 1.00
2-octanol	PPP		2885, 0.41			2957, 1.00
	SSP	2848, 0.80	2873, 1.00		2941, 0.98	
	SPS					2956, 1.00
3-octanol	PPP		2885, 0.47			2958, 1.00
	SSP	2949, 0.64	2874, 1.00	2920, 0.55	2941, 0.89	
	SPS					2960, 1.00

4.6 References

(1) Corn, R. M.; Higgins, D. A. *Chem. Rev.* **1994**, *94*, 107-25.

(2) Brevet, P. F.; Girault, H. H. *Liquid-Liquid Interfaces* **1996**, 103-37.

(3) Butler, P. D.; Hamilton, W. A.; Magid, L. J.; Hayter, J. B.; Slawecki, T. M.; Hammouda, B. *J. Chem. Soc., Faraday Trans.* **1997**, *104*, 65-78.

(4) Conboy, J. C. In *Ph. D. Thesis. Univ. of Oregon,Eugene,OR, 1996*, 1996, p 224 pp.

(5) Eisenthal, K. B. *Chem. Rev.* **1996**, *96*, 1343-60.

(6) Forsman, W. C.; Latshaw, B. E. *Polym. Eng. Sci.* **1996**, *36*, 1114-24.

(7) Li, M.; Schlossman, M. L. *Nucl. Sci. Tech.* **2006**, *17*, 322-33.

(8) Magid, L.; Penfold, J.; Schurtenberger, P.; Wagner, N. *Curr. Opin. Coll. Int. Sci.* **2002**, *7*, 193-95.

(9) Miranda, P. B.; Shen, Y. R. *J. Phys. Chem. B.* **1999**, *103*, 3292-307.

(10) Schlossman, M. L. *Curr. Opin. Coll. Int. Sci.* **2002**, *7*, 235-43.

(11) Shen, Y. R. *IEEE Journal of Selected Topics in Quantum Electronics* **2000**, *6*, 1375-79.

(12) Thomas, R. K. *Surfactant Sci. Ser.* **1999**, *83*, 417-79.

(13) Thomas, R. K. *Annu. Rev. Phys. Chem.* **2004**, *55*, 391-426.

(14) Yu, C. J.; Richter, A. G.; Kmetko, J.; Dugan, S. W.; Datta, A.; Dutta, P. *Phys. Rev. E: Stat., Nonlinear, Soft Matter Phys.* **2001**, *63*, 021205/1-05/8.

(15) Can, S. Z.; Chang, C. F.; Walker, R. A. *Biochim. Biophys. Acta, Biomembr.* **2008**, *1778*, 2368-77.

(16) Nishi, N.; Hobara, D.; Yamamoto, M.; Kakiuchi, T. *J. Chem. Phys.* **2003**, *118*, 1904-11.

(17) Noguchi, H.; Hiroshi, M.; Tominaga, T.; Ping Gong, J.; Osada, Y.; Uosaki, K. *Phys. Chem. Chem. Phys.* **2008**, *10*, 4987-93.

(18) Phillips, D. C.; York, R. L.; Mermut, O.; McCrea, K. R.; Ward, R. S.; Somorjai, G. A. *J. Phys. Chem. C* **2007**, *111*, 255-61.

(19) Kim, J.; Opdahl, A.; Chou, K. C.; Somorjai, G. A. *Langmuir* **2003**, *19*, 9551-53.

(20) Ye, S.; Noda, H.; Morita, S.; Uosaki, K.; Osawa, M. *Langmuir* **2003**, *19*, 2238-42.

(21) Guo, Z.; Zheng, W.; Hamoudi, H.; Dablemont, C.; Esaulov, V. A.; Bourguignon, B. *Surf. Sci.* **2008**, *602*, 3551-59.

(22) Heinz, H.; Vaia, R. A.; Krishnamoorti, R.; Farmer, B. L. *Chem. Mater.* **2007**, *19*, 59-68.

(23) Haehner, G.; Zwahlen, M.; Caseri, W. *Langmuir* **2005**, *21*, 1424-27.

(24) Watry, M. R.; Tarbuck, T. L.; Richmond, G. L. *J. Phys. Chem. B* **2003**, *107*, 512-18.

(25) Wright, J. C.; LaBuda, M. J.; Zilian, A.; Chen, P. C.; Hamilton, J. P. *Journal of Luminescence* **1997**, *72-74*, 799-801.

(26) Bopp, P. A.; Buhn, J. B.; Maier, H. A.; Hampe, M. J. *Chem. Eng. Commun.* **2008**, *195*, 1437-56.

(27) Stevens, M. J.; Grest, G. S. *Biointerphases* **2008**, *3*, FC13-FC22.

(28) Benjamin, I. *Chem. Phys. Lett.* **2004**, *393*, 453-56.

(29) Corn, R. M. *Proceedings of SPIE-The International Society for Optical Engineering* **1992**, *1636*, 117-24.

(30) Stahelin Robert, V. *J Lipid Res 50 Suppl*, S299-304. FIELD Reference Number:44 FIELD Journal Code:0376606 FIELD Call Number:.

(31) Sastry, P. S. *Prog Lipid Res 24*, 69-176. .

(32) Van Meer, G. *EMBO J.* **2005**, *24*, 3159-65.

(33) Stahelin, R. V. *J. Lipid Res.* **2009**, S299-S304.

(34) Ivanova, P. T.; Milne, S. B.; Forrester, J. S.; Brown, H. A. *Mol. Interventions* **2004**, *4*, 86-96.

(35) Quinn, P. J.; Joo, F.; Vigh, L. *Prog. Biophys. Mol. Biol.* **1989**, *53*, 71-103.

(36) Small, D. M. *J. Lipid Res.* **1984**, *25*, 1490-500.

(37) Abrahamsson, S.; Dahlen, B.; Lofgren, H.; Pascher, I.; Sundell, S. *Nobel Symp.* **1977**, *34*, 1-23.

(38) Gilman, J. B.; Tervahattu, H.; Vaida, V. *Atmos. Environ.* **2006**, *40*, 6606-14.

(39) Donaldson, D. J.; Vaida, V. *Chem. Rev.* **2006**, *106*, 1445-61.

(40) Gilman, J. B.; Eliason, T. L.; Fast, A.; Vaida, V. *J. Coll. Int. Sci.* **2004**, *280*, 234-43.

(41) Brindza, M. R.; Walker, R. A. *J. Am. Chem. Soc.* **2009**, *131*, 6207-14.

(42) Steel, W. H.; Beildeck, C. L.; Walker, R. A. *J. Phys. Chem. B* **2004**, *108*, 16107-16.

(43) Can, S. Z.; Mago, D. D.; Esenturk, O.; Walker, R. A. *J. Phys. Chem. C* **2007**, *111*, 8739-48.

(44) Wang, L.; Song, Y.; Zhang, B.; Wang, E. *Thin Solid Films* **2004**, *458*, 197-202.

(45) Napoleon, R. L.; Moore, P. B. *J. Phys. Chem. B* **2006**, *110*, 3666-73.

(46) Jedlovszky, P.; Varga, I.; Gilanyi, T. *J. Chem. Phys.* **2004**, *120*, 11839-51.

(47) Fenter, P.; Sturchio, N. C. *Prog. Surf. Sci.* **2005**, *77*, 171-258.

(48) Fragneto-Cusani, G. *J. Phys.: Condens. Matter* **2001**, *13*, 4973-89.

(49) Richter, L.; Vollhardt, D. *Tenside, Surfactants, Deterg.* **2006**, *43*, 256-61.

(50) Prokhorov, V. A. "Apparatus for measuring the surface tension of liquids," Ussr., 1981.

(51) Burri, J.; Hartland, S. *Coll. Polymer. Sci.* **1977**, *255*, 675-81.

(52) Can, S. Z.; Mago, D. D.; Walker, R. A. *Langmuir* **2006**, *22*, 8043-49.

(53) Cook, W. G.; Ross, R. A. *Can. J. Chem.* **1972**, *50*, 1666-74.

(54) Papirer, E.; Editor *Adsorption on Silica Surfaces.* ; Marcel Dekker, Inc.: New York, 2000.

(55) Mueller, R.; Kammler, H. K.; Wegner, K.; Pratsinis, S. E. *Langmuir* **2003**, *19*, 160-65.

(56) Miranda, P. B.; Pflumio, V.; Saijo, H.; Shen, Y. R. *J. Am. Chem. Soc.* **1998**, *120*, 12092-99.

(57) Rockmann, R.; Kalies, G. *J. Coll. Int. Sci.*, *315*, 1-7. .

(58) Liu, Y.; Wolf, L. K.; Messmer, M. C. *Langmuir* **2001**, *17*, 4329-35.

(59) Arnett, E. M.; Ahsan, T. *J. Am. Chem. Soc.* **1991**, *113*, 6861-4.

(60) Mikhail, R. S.; Nashed, S.; Khalil, A. M. *Surf. Technol.* **1978**, *7*, 45-54.

(61) Whalen, J. W. *J. Phys. Chem.* **1962**, *66*, 511-15.

(62) Santos, A. M. M.; Vasconcelos, W. L. *J. Non-Cryst. Solids* **2000**, *273*, 145-49.

(63) Mazaev, V. V.; Tomchuk, N. N.; Lavrenova, N. A. *Russ. J. Phys. Chem. A* **2007**, *81*, 370-73.

(64) Knoezinger, H.; Staehlin, W. *Prog. Colloid Polym. Sci.* **1980**, *67*, 33-40.

(65) Lide, D. R., Ed. *CRC Handbook of Chemistry and Physics, 83rd Edition*; CRC Press/Taylor and Francis: Boca Raton, FL, 2002.

(66) Kondo, S.; Fujiwara, H.; Ichii, T.; Tsuboi, I. *J. Chem. Soc., Faraday Trans.* **1979**, *75*, 646-51.

Chapter 5: Effect of Functional Group Identity on Interfacial Structure

5.1 Introduction

A quantitative, predictive understanding of the forces that control molecular structure and organization at liquid interfaces is necessary for the development of models that can describe a host of naturally occurring and industrially relevant processes. For example, the mobility of pollutants in ground water depend sensitively on the strength of their interactions with soil particles.[1-5] Also, gas uptake kinetics across the liquid/vapor interface depend on the structure and identity of interfacial species.[6-8] Corrosion processes and kinetics depend on the interfacial structure of water and ions at the metal surface.[9-11] In fact, self assembled monolayers with specifically designed structures are used as surface coatings to prevent corrosion by blocking the transport of water and gases to and from the interface.[12-16]

In each case the structure of a liquid or adsorbate at an interface will depend on a balance of forces between the two phases as well as lateral interactions between the surface species themselves. These interactions can be diverse, ranging from charge-charge to charge-dipole to dispersion forces. The simplest interfacial systems to consider are those between either a solid (having an adsorbed thin film) and vapor or a liquid and vapor because the relevant forces are reduced to only those of the interfacial species with the subphase and between the interfacial species themselves. No long range forces with a dense second phase are present to perturb interfacial structure and organization.

Thermodynamic techniques can provide insight into the interactions at both solid and liquid/vapor interfaces as well as buried interfaces between two condensed phases. From surface tension measurements, one can learn about macroscopic energetics at liquid/vapor interfaces (both neat liquid and with adsorbed monolayers) as well as liquid/liquid interfaces.[17-19] Thermogravimetric analysis and temperature programmed desorption (TPD) provide information about the strength of interactions between the solid surface and adsorbates.[20,21] Measuring the contact angle between a liquid drop and the solid surface can tell us the strength of solid/liquid association.[22,23] Ellipsometry can be used to determine film thickness.[24-27] X-ray and neutron scattering experiments provide data about the absolute position of interfacial molecules (or changes in properties such as electron or proton density).[28-31] Only optical spectroscopy, however, can probe directly the strength and directionality of inter- and intramolecular interactions.

Experiments presented in this chapter use nonlinear optical (NLO) spectroscopy to examine how changes in the strength of solvent-substrate interactions change the structure and organization of different functionalized, alkyl liquids adjacent to a hydrophilic solid silica surface. Of particular interest is how the structure of an adsorbed film (assumed to be one monolayer thick) differs from the structure of the same liquid in contact with silica. Differences tell us about the relative importance of lateral interactions versus interface energetics. Previous results presented in Chapter 3 show that even relatively weak van der Waals interactions between adsorbates and with silica are enough to create a measurable amount of conformational order in alkane monolayers at the silica/vapor interface. Studies

described in Chapter 4 show that the addition of strong directional interactions such as hydrogen bonding increases order in molecular monolayers. Surface specific vibrational spectroscopy measurements presented in this work correlate the degree of interfacial order with the type and strength of interaction between different organic functional groups of adsorbates at the silica/vapor interface and the silica/neat-liquid interface.

5.2 Experimental

Vibrational sum frequency generation spectroscopy (VSFG) is an ideal tool for measuring the structure and orientation of interfacial solvent molecules. The technique is sensitive only to those molecules subject to interfacial anisotropy, and different polarization conditions described below allow experiments to selectively probe the orientation of specific functional groups.[25,32-35] The origin of the technique's surface specificity has been described in Chapter 3, and will be omitted here.

VSFG spectra were collected using a broadband, counter-propagating geometry spectrometer that has been described in Chapter 3. This sample geometry allows for easily changing between both different types of samples (solid/vapor vs. solid/liquid) as well as between different samples (silica/octanol vs. silica/octylamine). The solid/vapor (solid/liquid) spectra were acquired after putting a drop inside (filling) the quartz cells and allowing the system to equilibrate. Typically, we record VSFG spectra for 1-4 minutes at each central IR wavelength, then shift the laser 50 nm and acquire again. This procedure leads to 8 broadband wavelength scans per spectrum. All spectra were normalized to the instrument

response measured by the nonresonant spectrum acquired from the gold/vapor interface, and calibrated by placing a polystyrene card in front of the gold surface along the IR path. Four points corresponding to known adsorption bands from polystyrene were used for a wavelength calibration, leading to accuracy in reported frequencies on the order of ± 2 cm^{-1}. While absolute intensities of spectra from different systems cannot be compared quantitatively, relative intensities of bands within the same spectrum typically reproduced to within 10 percent.

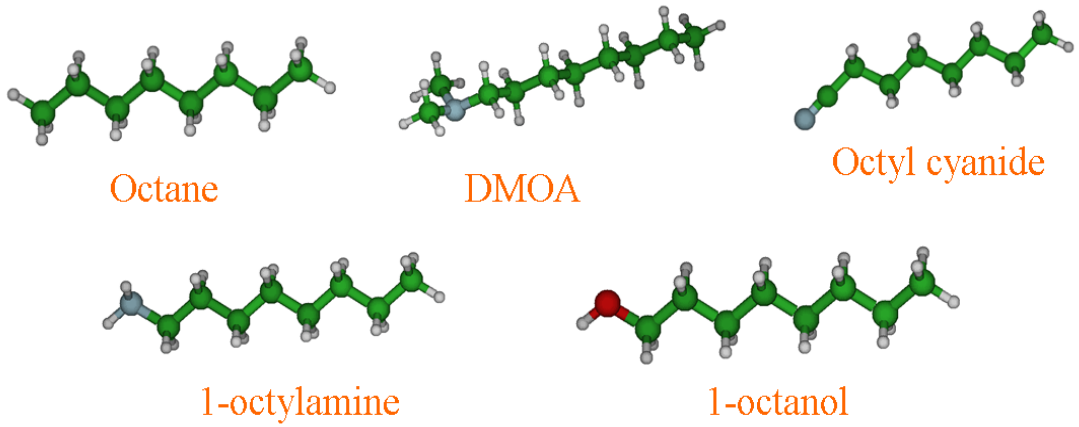

Figure 5.1. Structures of 1-octanol, octyl cyanide, 1-octylamine, N,N-dimethyloctylamine, and octane. Experiments described in this use these molecules to interpret how different types of interactions affect surface organization.

5.3 Results

Figure 5.2 shows the PPP polarization combination VSFG spectra of 1-octanol, octyl cyanide, 1-octylamine, dimethyloctylamine, and octane adsorbed to the silica/vapor interface. The 1-octanol spectrum shows three features assigned to the methyl symmetric stretch (r^+, 2872 cm^{-1}), the r^+_{FR} at 2940 cm^{-1}, and the methyl asymmetric stretch (r^- near 2955 cm^{-1}). PPP spectra of octyl cyanide, 1-octylamine

and octane show two features which can be assigned to the r^+ band (2876, 2885 and 2887 cm^{-1}, respectively) and the r^- band (2955 cm^{-1}, 2950 cm^{-1} for octane).

The spectra of dimethyloctylamine also has two features, but these are centered at 2862 and 2935 cm^{-1}. These bands can not be assigned unambiguously, owing to the more complicated spectroscopy of this molecule. Related molecules with alkyl groups adjacent to amines, such as trimethylamine, and triethylamine have infrared spectra that show spectral shifts toward lower frequencies for the methyl symmetric stretching modes, though the r^- transition remains in approximately the same location as the alkyl limit.[36] The band appearing at 2862 and in the DMOA PPP spectrum can be attributed to possible contributions from the d^+ and r^+ bands, and the feature at 2935 cm^{-1} is assigned to the d^- band.

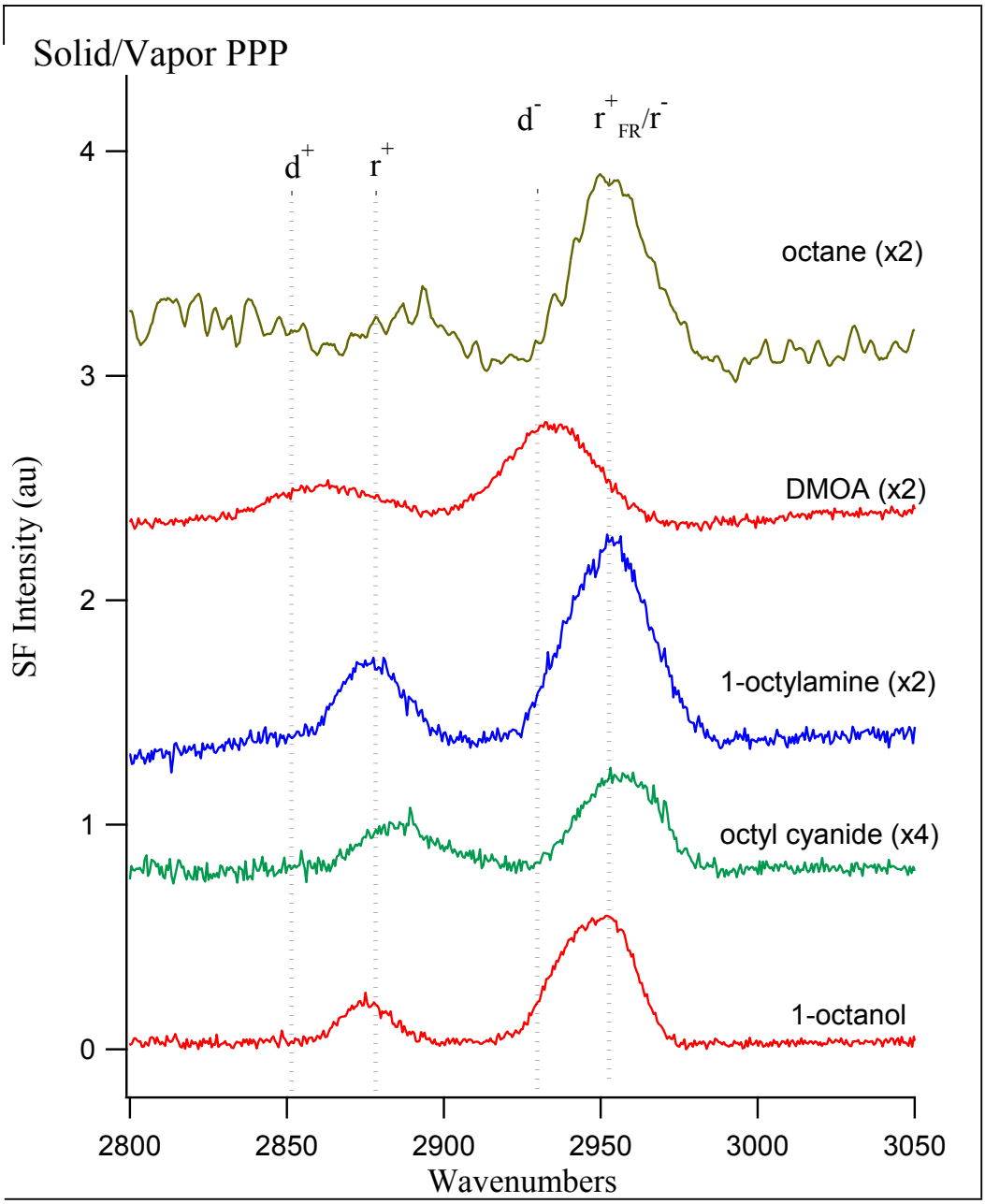

Figure 5.2 PPP Spectra of the silica/vapor interface with adsorbed monolayers of 1-octanol, octane nitrile, 1-octylamine, dimethyloctylamine (DMOA) and octane. The higher frequency peak in the DMOA spectrum can be assigned to either a methyl asymmetric stretch from the methyl groups adjacent the amine, or to the d^-. The broad feature centered around 2862 cm^{-1} is likely a combination of methyl and methylene symmetric stretches. Octane and octanol spectra are reprinted from Chapters 3 and 4, respectively.

SSP spectra of 1-octanol, octane nitrile, 1-octylamine, dimethyloctylamine, and octane adsorbed to the silica/vapor interface are shown in Figure 5.3. The 1-octanol

spectrum shows three features assigned to the methylene symmetric stretch (d^+, 2845 cm^{-1}), r^+ (2872 cm^{-1}), and the r^+_{FR} band at 2940 cm^{-1}. Octyl cyanide, 1-octylamine, and octane spectra also all have three features with appreciable intensity, that can be assigned to the same three vibrational modes, with slightly shifted frequencies (2844, 2874, and 2946 cm^{-1}). Again, the SSP spectrum of DMOA only exhibits two features, at 2840 and 2920 cm^{-1}. Because these features are significantly shifted from the bulk limits of r^+ and r^- bands in triethylamine, they are again assigned to the d^+ and d^- bands, the symmetric and antisymmetric methylene stretches of the alkyl chain.

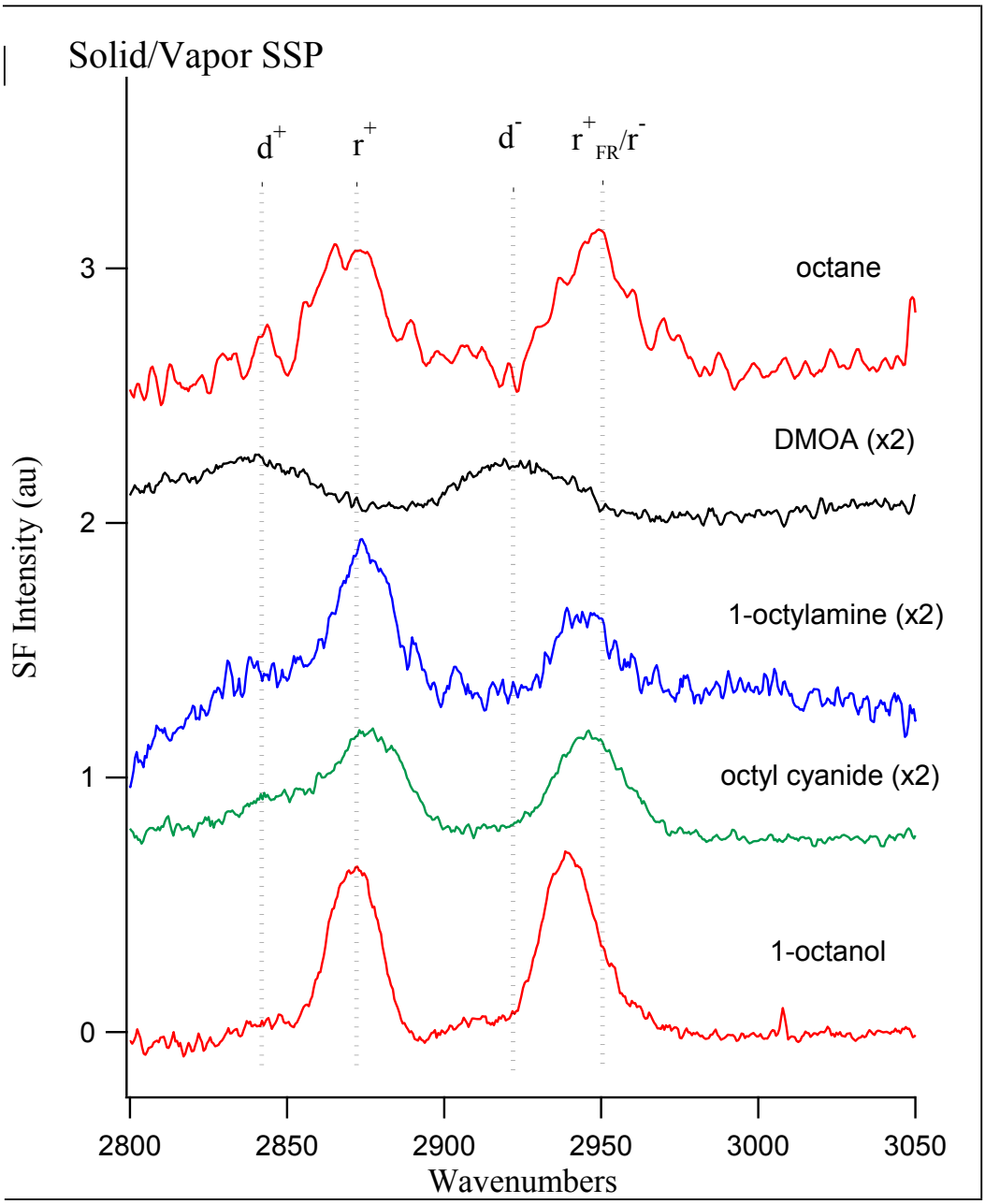

Figure 5.3 SSP Spectra of the silica/vapor interface with adsorbed monolayers of 1-octanol, octane nitrile, 1-octylamine, dimethyloctylamine (DMOA) and octane.

Figure 5.4 shows SPS spectra of 1-octanol, octane nitrile, 1-octylamine, dimethyloctylamine, and octane adsorbed to the silica/vapor interface. The 1-octanol spectrum has only one feature, centered around 2951 cm^{-1}, which is assigned to the r^- band. Both octyl cyanide and 1-octylamine have a small intensity feature that is also

assigned to that same vibrational mode at 2966 and 2961 cm^{-1}, respectively. DMOA's silica/vapor SPS spectrum does not contain any feature with appreciable intensity, and octane has a broad region of spectral intensity which can be assigned to both the methyl and methylene asymmetric stretches. (There cannot be r^{+}_{FR} without r^{+})

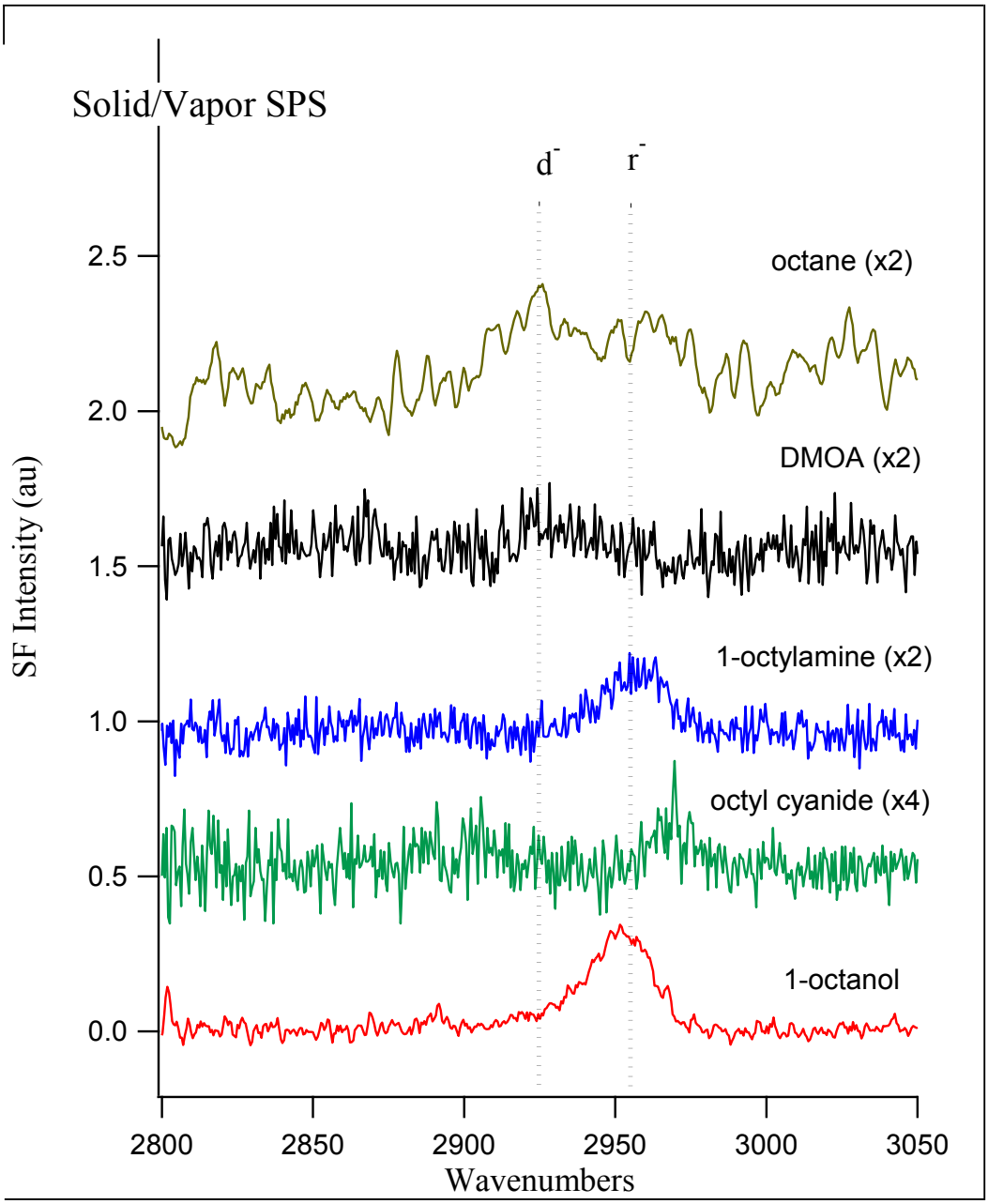

Figure 5.4 SPS Spectra of the silica/vapor interface with adsorbed monolayers of 1-octanol, octane nitrile, 1-octylamine, dimethyloctylamine (DMOA) and octane.

The VSFG spectra in Figures 5.2-5.4 share several common correlations. First, all SSP spectra except for DMOA are dominated by the same two features, namely r^+ and r^+_{FR}/r^- bands. Features appearing in SSP spectra can only arise from molecular vibrational IR transition moments that have a net projection along the surface normal. Therefore, intensity in r^+ implies that the methyl groups at the ends of the adsorbed molecules have a net upright orientation. Additional analysis of spectra acquired under SPS conditions from 1-octanol, octyl cyanide and 1-octylamine leads to a proposed interfacial organization at silica/vapor interfaces that has polar ends interacting with the substrate and alkyl chains standing upright, normal to the surface. As discussed in Chapter 3, the d^- in octane's SPS spectrum is consistent with octane lying parallel to the surface. This result may not be surprising considering that octane lacks a polar functional group to interact preferentially with the silica substrate.

DMOA presents an interesting test of how the balance of forces leads to unique interfacial structure. DMOA can accept hydrogen bonds (like octyl cyanide), but can not donate hydrogen bonds (unlike octylamine). Furthermore, the tertiary amine group is sterically hindered and hydrogen bonds accepted from the silica are expected to be weaker than those accepted by 1-octylamine. The spectra show clearly the consequences of this structural modification. Only methylene bands appear in the SSP spectrum indicating that adsorbed molecules lie flat at the interface. The data are consistent with an ordered monolayer, but one that prefers a horizontal organization of alkyl chains rather than a vertical alignment.

Though it is not possible in this case to compare absolute intensities from one spectrum to another, ratios of relative intensities within each individual spectrum can be used to characterize these systems in terms of increasing interfacial order and organization. Previous results show that SSP spectra of tightly packed *n*-alcohol monolayers ($n \geq 8$) adsorbed to the aqueous/vapor interface have an r^+/r^+_{FR} ratio is approximately 3-4.[37-40] Assuming this number to be an upper limit for extremely well ordered monolayers consisting of upright alkyl chains with virtually no defects, we can compare similar intensity ratios from systems studied here. The three molecules in this study that adopt primarily upright orientations are 1-octanol, octyl cyanide, and 1-octylamine. Data shown in Figure 5.3 show that the r^+/r^+_{FR} ratio for both octanol and octyl cyanide is close to unity, while that ratio for the SSP spectrum of 1-octylamine is approximately 2. Based on these ratios, we propose that of the three species that adopt an overall upright geometry, 1-octylamine forms the most ordered monolayer film adsorbed to the silica/vapor interface. The structures of these monomers in Figure 5.1 provide some insight into the mechanisms responsible for this result.

Octyl cyanide can adsorb to silica both through general dipolar interactions and through accepting hydrogen bonds from surface silanol groups. Octanol and octylamine can both accept *and* donate hydrogen bonds. Octanol can donate a single hydrogen bond, and accept two through the oxygen lone pairs. Octylamine on the other hand, can donate two hydrogen bonds and accept only one through the nitrogen lone pair. An additional consideration is that the hydrophobic silica surface has a coverage of surface silanol groups corresponding to 33-40 $Å^2$/silanol, and these

silanols show a propensity for donating hydrogen bonds.[39-41] Previous results show that the limiting surface area of tightly packed monolayers of *n*-octanol at the aqueous/vapor interface is ~20 $Å^2$/molecule.[37,42] As discussed in Chapter 4, if each silanol hydrogen bonds with a single octanol, octanol monolayers at the silica/vapor interface should have limiting surface coverages that are ~50% less tightly packed than a full monolayer adsorbed to an aqueous/vapor interface.[43] Based on the relative intensities of r^+ and r^+_{FR}, we believe that a monolayer formed from 1-octylamine is more ordered than the monolayer formed by 1-octanol. 1-Octylamine only accepts one hydrogen bond, and therefore has more conformational freedom to optimize both hydrogen bonding with silica *and* hydrogen bonding with adjacent neighbors. In contrast octanol is more constrained by requiring the immobile silica surface to donate two hydrogen bonds in order to satisfy hydrogen bonding opportunities.

Solvation at silica surfaces is dominated by hydrogen bond donating properties of surface silanols. (See Chapter 2) Consequently, n-alkyl amines will be more active partners than equivalent n-alcohols in acid-base chemistry occurring at the interface. SHG measurements from the silica/water interface that show that ~20 percent of surface silanol groups are acidic with a pKa of 4.5, with the remaining 80 percent being weakly basic (pKa of ~8.5).[44] With a pKb of ~3.5-4.5, we expect some fraction of adsorbed amines to be more strongly adsorbed than equivalent length alcohols. This population of strongly bound amines can serve to help organize additional interfacial solvents that might be less weakly bound to the surface silanol groups but can also hydrogen bond to each other. *n*-Alcohols do not have such strongly bound monomers to serve as anchors for the rest of the adsorbed film. These

ideas are born out by heats of adsorption measured in microcalorimetry experiments. For similar sized molecules, amines have the largest adsorption enthalpy, nitriles weakest. For example, results show methylamine's initial heat of adsorption onto silica is ~90 kJ/mol,[43] methanol has the next largest adsorption enthalpy (78 kJ/mol),[45] and acetonitrile binds most weakly (60 kJ/mol).[46]

Spectra presented in Chapter 4 show evidence that the structure and organization at the solid/vapor interface is not always the best indication that order will persist at a solid/liquid interface given the monolayer's ability to interact with an adjacent liquid phase. Octanol isomers at the solid/vapor interface all appear to form moderately well ordered monolayers owing to strong hydrogen bonding interactions with the silica substrate as well as possible lateral van der Waals interactions between monomers. At the solid/liquid interface, however, only 1-octanol has VSFG spectra consistent with some measure of interfacial order. Less ordering persists at the silica/2-octanol solid/liquid interface, and the silica/3-octanol solid/liquid interface shows no evidence of interfacial structure at all. Even the interfacial 1-octanol at silica/liquid interfaces shows less order than does the 1-octanol film at the silica/vapor interface. Given the differences in interfacial organization observed for different alkyl species at solid/vapor interfaces, one can wonder how the presence of a second dense (liquid) phase affects interfacial order.

In order to examine how the strength of interactions between liquid molecules and the silica surface changes interfacial structure and organization between the solid/vapor and solid/liquid interfaces, data presented below include VSFG results of 1-octanol, octyl cyanide, 1-octylamine, and DMOA adsorbed to the silica/liquid interface. All

efforts to acquire spectra from the silica/octane interface led to no measured signal, implying a disordered interface and/or rapid exchange between molecules at the surface and molecules in the bulk. The PPP spectra of 1-octanol and 1-octylamine presented in Figure 5.5 show some similarities, both with each other and with solid/vapor interfaces, but the octyl cyanide spectrum now contains a different combination of features. Specifically, in addition to signal intensity at ~2875 and 2955 cm^{-1}, assigned to r^+ and r^-, both 1-octanol and 1-octylamine PPP spectra include an increase in the intensity at 2840 cm^{-1}, that can be assigned to the d^+ band. Octyl cyanide and DMOA PPP spectra both contain significant contributions to signal intensity at 2875 and 2955 cm^{-1}, consistent with r^+ and r^-.

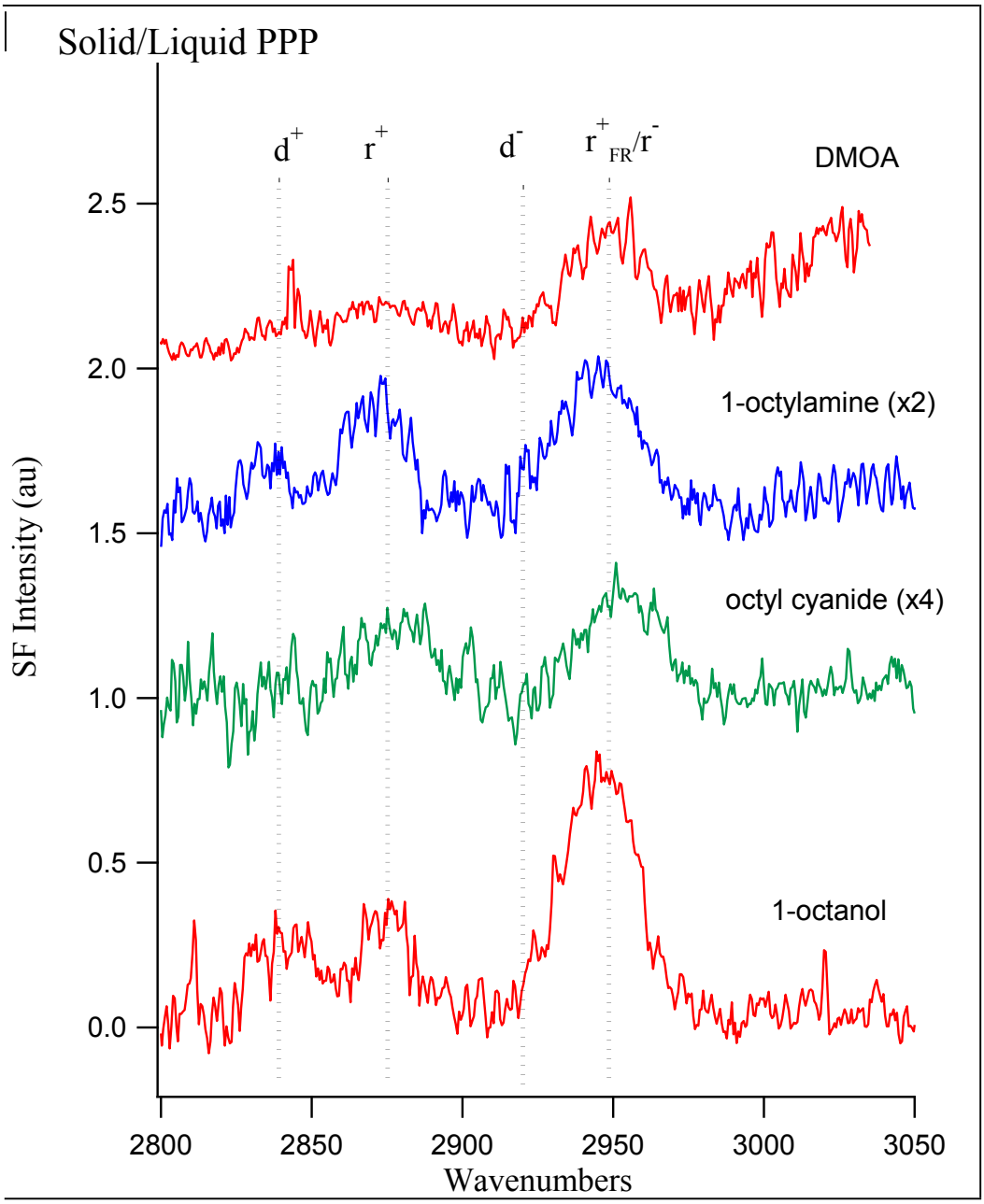

Figure 5.5 PPP Spectra of the silica/liquid interface formed between silica and 1-octanol, octane nitrile, 1-octylamine, and dimethyloctylamine (DMOA). Octanol spectra are reprinted from Chapter 4.

Spectra acquired under SSP conditions, shown in Figure 5.6 again show some similarities and some differences between different functional group-containing liquids at the silica surface. Both 1-octanol and 1-octylamine contain the same three

features, r^+ and r^- at ~2875 and 2955 cm^{-1}, as well as d^+ at 2840 cm^{-1}. The silica/1-octanol spectrum differs from 1-octylamine in that it also includes a d^- peak at 2918 cm^{-1}. SSP spectra of octyl cyanide and DMOA both contain weaker intensity features at 2875 and 2955 cm^{-1}, consistent with the r^+ and r^-.

A few observations can be made about the relative changes between the solid/vapor and solid/liquid SSP spectra. First, the r^+/r^+_{FR} ratio for 1-octanol is now less than unity. This result, combined with the growth in d^+ and d^- intensity, is evidence of decreasing interfacial order. Octylamine's r^+/r^+_{FR} ratio remains similar to that observed from the silica/vapor interface, indicating that interfacial structure in the first solvent layer is preserved.

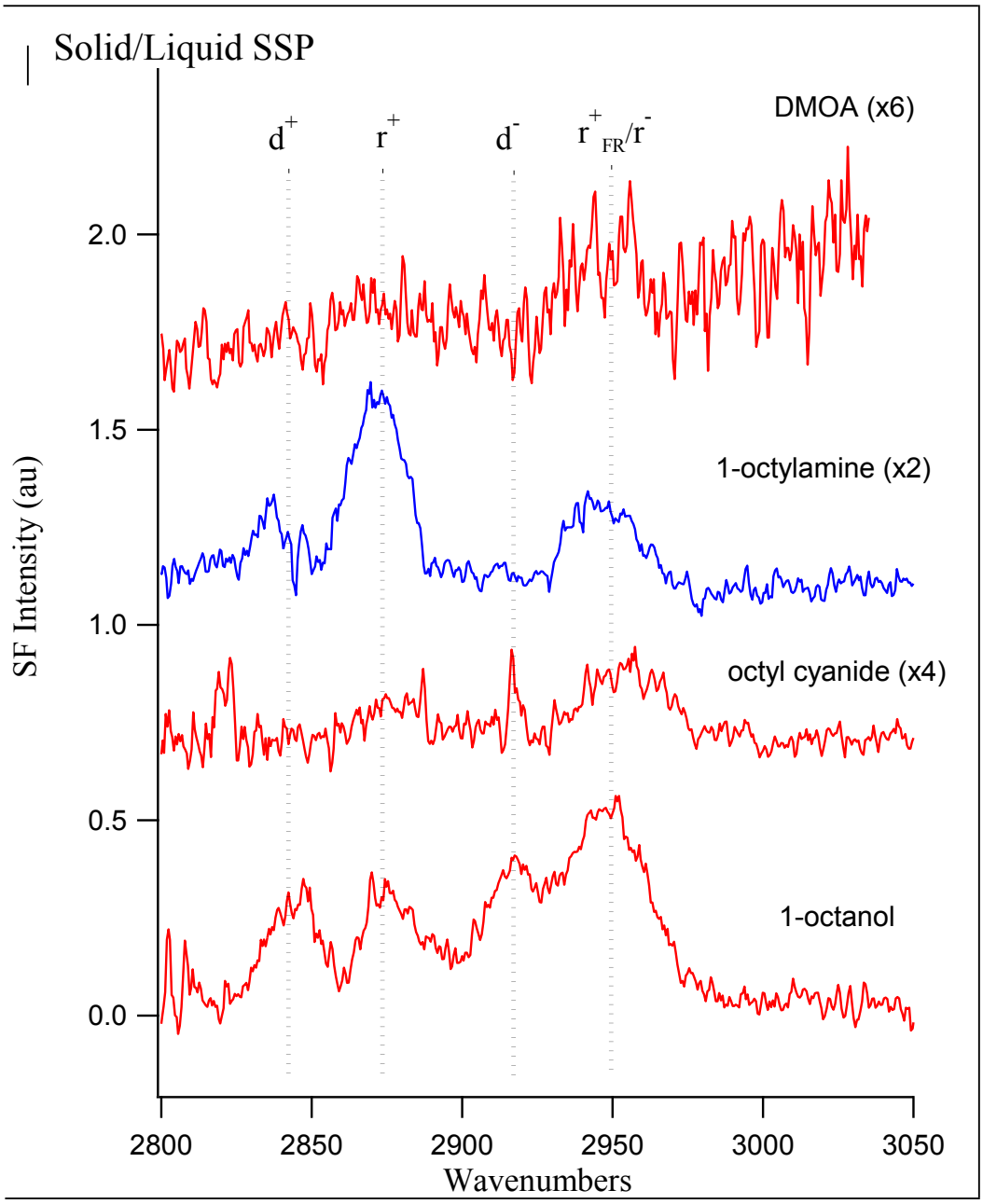

Figure 5.6 SSP Spectra of the silica/liquid interface formed between silica and 1-octanol, octane nitrile, 1-octylamine, and dimethyloctylamine (DMOA).

Comparing of the SSP spectra from Figure 5.3 and 5.6 reveals trends that can be explained by correlating the strength of substrate-adsorbate interaction with the apparent degree of conformational order. First, a high degree of conformational order in monolayers at the solid/vapor interface manifests itself with a strong r^+ band and an

r^+ to the r^+_{FR} ratio greater than unity. Using this criterion, the solid/vapor data show that 1-octylamine films at the silica/vapor interface are the most ordered of the molecules studied here. The next most well ordered solid/vapor systems include 1-octanol and octyl cyanide, which have similar organization. DMOA lies flat on the surface and shows little evidence of extended interfacial order. At the solid/liquid interface, 1-octylamine remains the most ordered of these liquids, with DMOA and octyl cyanide now having similar organization and not showing much evidence of any extended ordering. The silica/1-octanol interface falls between the two extremes.

Silica/liquid SPS spectra of these four molecules, shown in Figure 5.7 support the claims made with regards to interfacial structure. Only 1-octanol, 1-octylamine and DMOA show any appreciable signal intensity above the background. All spectra have features at ~2925 cm^{-1}, assigned to the methylene asymmetric stretch (d^-). As described in Chapter 3, this correlation is consistent with alkyl chains laying down with methylene groups pointing into and out of the surface.

Spectra presented here show that relative strengths of interaction between the solid surface and different adsorbed solvent molecules can predict qualitatively the degree of ordering amongst adsorbates at the solid/vapor interface. Spectra from 1-octylamine and 1-octanol reinforce small molecule adsorption measurements showing these functional groups to have interaction strengths with silica that are similar to each other and larger than nitriles. All three solvents form moderately well ordered monolayers at silica/vapor interfaces, but only 1-octylamine retains the same degree of order at the solid/liquid interface. For VSFG spectra from solid/liquid interfaces to show any appreciable intensity, net polar order must exist across the

interfacial region. As explained in Chapter 4, order observed at solid/vapor interfaces will persist at solid/liquid interfaces only if interfacial species have an energetically favorable mechanism to remain adsorbed. The heat of adsorption onto silica is generally negative, meaning that adsorption from the vapor is thermodynamically favored. The heat of vaporization is, in some limit, a measure of how strongly solvent molecules are solvated. If the difference between these two values is great enough (and negative), we expect molecules adsorbed to the surface to remain at the interface, even when they are free to exchange with a bulk liquid. Again, we can compare these energetic quantities for small, model molecules containing the same functional groups. Methylamine, methanol, and acetonitrile have heats of vaporization of 34.2, 37.5, and 27.0 kJ/mol, respectively.[47] In the high surface coverage limit, heats of adsorption are ~50-70 kJ/mol for methylamine,[43] 60 kJ/mol for methanol,[45] and ~32 kJ/mol for acetonitrile.[46] The differences in these heats of adsorption are much smaller than that between the different heats of adsorption to silica. When we combine the two numbers, however, we see that the different in enthalpies of adsorption and vaporization ($\Delta(\Delta H) = \Delta H_{ads} - \Delta H_{vap}$) of the three solvents is 15-35 kJ/mol for 1-octylamine, 22 kJ/mol for methanol and 5 kJ/mol for acetonitrile. This difference in enthalpies is nothing more than an indicator of whether interfacial solvent molecules will remain adsorbed to the surface or desorb into the bulk solvent. Assuming that these quantities simply scale with alkyl chain length we conclude that the competition between adsorption and solvation interactions for octylamine and octanol are similar and favor adsorption, whereas the small association with the surface shown by acetonitrile is reflected in the complex

reorganization observed at the silica/octyl cyanide solid/liquid interface. We can also use these values to suggest an explanation for the lack of signal at the silica/octane solid/liquid interface. At high coverages, octane's heat of adsorption falls to 44 kJ/mol[48] and very close to it's heat of vaporization (41.5 kJ/mol).[47] The relative difference between these two values is small enough that we expect a very high rate of exchange between molecules at the interface and in the bulk, leading to no order and no VSFG intensity.

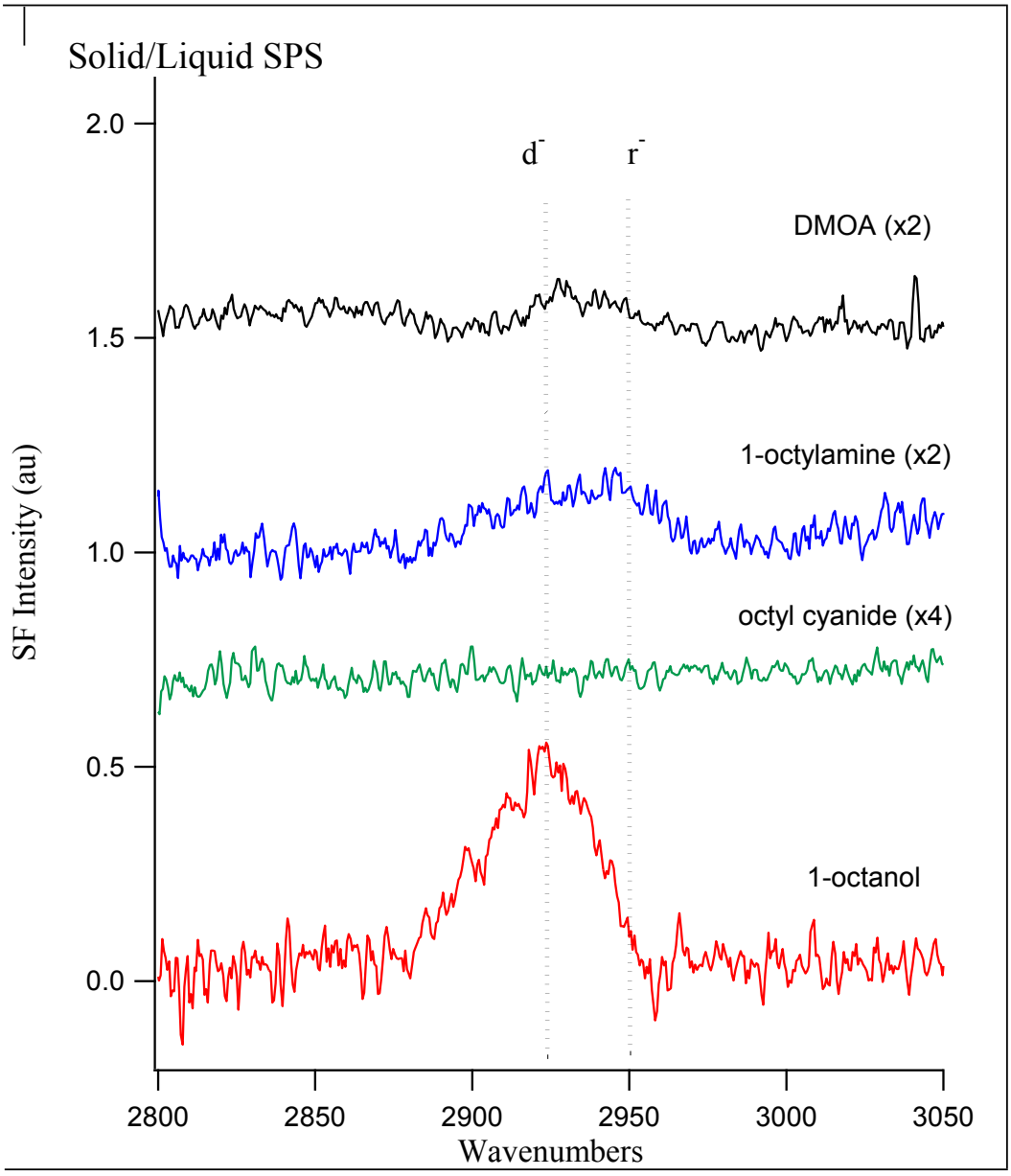

Figure 5.7 SPS Spectra of the silica/liquid interface formed between silica and 1-octanol, octane nitrile, 1-octylamine, and dimethyloctylamine (DMOA).

5.4 Conclusions

Results shown above show that changes in interfacial structure and organization follow trends that track with the nature of solvent-substrate interactions. The data suggest that as both the strength of interaction, and ability of the solvent to sample multiple interactions increases that a monolayer of solvent molecules adsorbed to the

silica/vapor interface will become more ordered. Data presented here also show that more strongly associating monomers, which form more ordered films at the solid/vapor interface, are more likely to maintain that long range order and organization when the surface is brought into contact with the liquid. These findings correlate with thermodynamic properties of adsorption and solvation. The difference between heat of adsorption and heat of vaporization, $\Delta(\Delta H)$, can predict which monolayer at the solid/vapor interface will retain order at the solid/liquid interface.

Tables 5.1-2. Band assignments, frequencies and relative intensities of features from acquired SFG spectra of 1-octanol, octane nitrile, 1-octylamine, dimethyloctylamine, and octane at the silica/vapor and silica/liquid interfaces. Recorded is the frequency of the maximum intensity of each feature, and the ratio of that intensity to the largest appearing in each respective spectrum.

Solid/Vapor		d+ (rel. intensity, cm^{-1}	r+	d-	$r+_{FR}/r^-$	r-
1-octanol	PPP		2873, 0.36		2938, 0.76	2952, 1.00
	SSP	2843, 0.11	2872, 0.87	2917, 0.12	2939, 1.00	
	SPS					2952, 1.00
Octyl cyanide	PPP		2882, 0.51		2955, 1.00	
	SSP		2876, 0.99		2946, 1.00	
	SPS					2966, 1.00
1-octylamine	PPP		2876, 0.28		2953, 1.00	
	SSP		2874, 1.00		2944, 0.53	
	SPS					2961, 1.00
DMOA	PPP	2861, 0.43		2933, 1.00		
	SSP	2841, 1.00		2919, 0.91		
	SPS					
octane	PPP		2886, 0.30		2950, 0.86	
	SSP		2875, 0.16		2950, 0.24	
	SPS			2927, 0.19		2962, 0.14

Solid/Liquid		d+ (rel. intensity, cm^{-1}	r+	d-	$r+_{FR}/r^-$	r-
1-octanol	PPP	2845, 0.40	2875, 0.49	2923, 0.37	2941, 1.00	2952, 0.93
	SSP	2842, 0.56	2869, 0.65	2918, 0.71	2942, 0.93	2952, 1.00
	SPS			2921, 1.00		
Octane nitrile	PPP		2875, 0.66		2951, 1.00	
	SSP		2875, 0.61		2953, 1.00	
	SPS					
1-octylamine	PPP	2838, 0.50	2874, 0.87		2945, 1.00	
	SSP	2837, 0.56	2873, 1.00		2941, 0.56	
	SPS				2942, 1.00	
DMOA	PPP		2875, 0.41		2951, 1.00	
	SSP					2953, 1.00
	SPS					

5.5 References

(1) Musorrafiti, M. J.; Konek, C. T.; Hayes, P. L.; Geiger, F. M. *J. Phys. Chem. C* **2008**, *112*, 2032-39.

(2) Mifflin, A. L.; Konek, C. T.; Geiger, F. M. *J. Phys. Chem. B* **2006**, *110*, 22577-85.

(3) Al-Abadleh, H. A.; Voges, A. B.; Bertin, P. A.; Nguyen, S. T.; Geiger, F. M. *J. Am. Chem. Soc.* **2004**, *126*, 11126-27.

(4) Weng, L.; Fest, E. P. M. J.; Fillius, J.; Temminghoff, E. J. M.; Van Riemsdijk, W. H. *Environ. Sci. Technol.* **2002**, *36*, 1699-704.

(5) Kordel, W.; Dassenakis, M.; Lintelmann, J.; Padberg, S. *Pure Appl. Chem.* **1997**, *69*, 1571-600.

(6) Harper, K.; Minofar, B.; Sierra-Hernandez, M. R.; Casillas-Ituarte, N. N.; Roeselova, M.; Allen, H. C. *J. Phys. Chem. A* **2009**, *113*, 2015-24.

(7) Li, Y.; Demerjian, K. L.; Williams, L. R.; Worsnop, D. R.; Kolb, C. E.; Davidovits, P. *J. Phys. Chem. A* **2006**, *110*, 6814-20.

(8) Vieceli, J.; Ma, O. L.; Tobias, D. J. *J. Phys. Chem. A* **2004**, *108*, 5806-14.

(9) Shultz, M. J.; Schnitzer, C.; Simonelli, D.; Baldelli, S. *Int. Rev. Phys. Chem.* **2000**, *19*, 123-53.

(10) Somorjai, G. A.; Rupprechter, G. *Stud. Surf. Sci. Catal.* **1997**, *109*, 35-59.

(11) Criscenti, L. J.; Cygan, R. T.; Kooser, A. S.; Moffat, H. K. *Chem. Mater.* **2008**, *20*, 4682-93.

(12) Ma, H. Y.; Yang, C.; Chen, S. H.; Jiao, Y. L.; Huang, S. X.; Li, D. G.; Luo, J. L. *Electrochim. Acta* **2003**, *48*, 4277-89.

(13) Srivastava, P.; Chapman, W. G.; Laibinis, P. E. *Langmuir* **2009**, *25*, 2689-95.

(14) Sinapi, F.; Julien, S.; Auguste, D.; Hevesi, L.; Delhalle, J.; Mekhalif, Z. *Electrochim. Acta* **2008**, *53*, 4228-38.

(15) Metikos-Hukovic, M.; Babic, R.; Petrovic, Z.; Posavec, D. *J. Electrochem. Soc.* **2007**, *154*, C138-C43.

(16) Li, D.; Chen, S.; Zhao, S.; Ma, H. *Coll. Surf., A* **2006**, *273*, 16-23.

(17) Guiseppi-Elie, A.; Wnek, G. E.; Wesson, S. P. *Langmuir* **1986**, *2*, 508-13.

(18) Tavana, H.; Neumann, A. W. *Adv. Coll. Int. Sci.* **2007**, *132*, 1-32.

(19) Fowkes, F. M. *J. Phys. Chem.* **1962**, *66*, 382.

(20) Staszczuk, P. *Thermochim. Acta* **1994**, *247*, 169-91.

(21) Czarnecki, J.; Sestak, J. *J. Therm. Anal. Calorim.* **2000**, *60*, 759-78.

(22) Pompe, T.; Herminghaus, S. *Phys. Rev. Lett.* **2000**, *85*, 1930-33.

(23) Janczuk, B.; Bialopiotrowicz, T. *J. Coll. Int. Sci.* **1990**, *140*, 362-72.

(24) Levinson, P.; Valignat, M. P.; Fraysse, N.; Cazabat, A. M.; Heslot, F. *Thin Solid Films* **1993**, *234*, 482-5.

(25) Bain, C. D. *Curr. Opin. Coll. Int. Sci.* **1998**, *3*, 287-92.

(26) Toca-Herrera, J. L.; Muller, H. J.; Krustev, R.; Pfohl, T.; Mohwald, H. *Coll. Surf., A* **1999**, *152*, 357-65.

(27) Hosoda, M.; Kobayashi, H.; Sakamoto, N.; Sakai, K.; Takagi, K. *Rev. Sci. Instrum.* **1996**, *67*, 4224-27.

(28) Fragneto-Cusani, G. *J. Phys.: Condens. Matter* **2001**, *13*, 4973-89.

(29) Inaba, A. *Pure Appl. Chem.* **2006**, *78*, 1025-37.

(30) Magid, L.; Penfold, J.; Schurtenberger, P.; Wagner, N. *Curr. Opin. Coll. Int. Sci.* **2002**, *7*, 193-95.

(31) Schlossman, M. L. *Curr. Opin. Coll. Int. Sci.* **2002**, *7*, 235-43.

(32) Chen, X.; Clarke, M. L.; Wang, J.; Chen, Z. *Int. J. Mod. Phys. B* **2005**, *19*, 691-713.

(33) Miranda, P. B.; Shen, Y. R. *J. Phys. Chem. B.* **1999**, *103*, 3292-307.

(34) Moad, A. J.; Simpson, G. J. *J. Phys. Chem. B.* **2004**, *108*, 3548-62.

(35) Wang, H. F.; Gan, W.; Lu, R.; Rao, Y.; Wu, B. H. *Int. Rev. Phys. Chem.* **2005**, *24*, 191-256.

(36) Pierson, R. H.; Fletcher, A. N.; Gantz, E. S. C. *Anal. Chem.* **1956**, *28*, 1218-39.

(37) Can, S. Z.; Mago, D. D.; Esenturk, O.; Walker, R. A. *J. Phys. Chem. C* **2007**, *111*, 8739-48.

(38) Can, S. Z.; Mago, D. D.; Walker, R. A. *Langmuir* **2006**, *22*, 8043-49.

(39) Edgar, R.; Huang, J. Y.; Popovitz-Biro, R.; Kjaer, K.; Bouwman, W. G.; Howes, P. B.; Als-Nielsen, J.; Shen, Y. R.; Lahav, M.; Leiserowitz, L. *J. Phys. Chem. B* **2000**, *104*, 6843-50.

(40) Casson, B. D.; Braun, R.; Bain, C. D. *J. Chem. Soc., Faraday Trans.* **1997**, *104*, 209-29.

(41) Papirer, E.; Editor *Adsorption on Silica Surfaces.* ; Marcel Dekker, Inc.: New York, 2000.

(42) Rockmann, R.; Kalies, G. *J. Coll. Int. Sci.*, *315*, 1-7. .

(43) Cook, W. G.; Ross, R. A. *Can. J. Chem.* **1972**, *50*, 1666-74.

(44) Ong, S.; Zhao, X.; Eisenthal, K. B. *Chem. Phys. Lett.* **1992**, *191*, 327-35.

(45) Natal-Santiago, M. A.; Dumesic, J. A. *J. Catal.* **1998**, *175*, 252-68.

(46) Curthoys, G.; Davydov, V. Y.; Kiselev, A. V.; Kiselev, S. A.; Kuznetsov, B. V. *J. Coll. Int. Sci.* **1974**, *48*, 58-72.

(47) Lide, D. R., Ed. *CRC Handbook of Chemistry and Physics, 83rd Edition*; CRC Press/Taylor and Francis: Boca Raton, FL, 2002.

(48) Bilinski, B. *J. Coll. Int. Sci.* **2000**, *225*, 105-11.

Chapter 6: Conclusion

6.1 Motivation

This dissertation has presented a series of studies that examine both solute properties and solvent structure and organization at different liquid interfaces. The goal of these studies has been to determine how changes in intermolecular interactions affect properties and structure at different types of interfaces. For more than ten years the Walker Research Group has used nonlinear optical spectroscopy to study how properties change across liquid surfaces, as well as structure of neat liquid interfaces with and without adsorbed monolayers. SHG spectra of "molecular ruler" surfactants have been used to measure interfacial width across liquid/liquid interfaces.[1-4] Other studies have used VSFG spectra of alcohol isomers adsorbed to aqueous/vapor interfaces as evidence for monolayer structure resulting from a balance of forces that occurs when solvating polar and nonpolar functional groups.[5,6]

The work presented in this thesis seeks to combine both of these and provide a complete and quantitative correlation between surface solvation and interfacial solvent structure. SHG experiments systematically examined solute properties in order to suggest possible solvent structures. VSFG then measured directly the solvent structure. Furthermore, we have set up this study to include a systematic approach that enabled us to use spectra from different solvents at similar interfaces in order to present a thermodynamic explanation of how intermolecular interactions give rise to differing interfacial solvent structure.

6.2 Summary of Thesis Experiments

The majority of experiments presented here were conducted using two nonlinear optical spectroscopies, one (SHG) sensitive to changes in solute electronic structure, and the other (VSFG) measuring polarization dependent interfacial vibrational spectra.

In Chapter 2, we presented the results of SHG spectra of two solvatochromic solutes, pNAs and indoline, adsorbed to different solid/liquid interfaces. This work has appeared previously in the literature.[7] A common denominator in all experiments described throughout this thesis is that the solid substrate used was silica. To study different types of solvation at the silica surface we varied the solvent in contact, including two nonpolar alkanes, and two different length alcohols. Spectra of pNAs and indoline adsorbed to the silica/liquid interfaces formed with these liquids show the interfacial polarity (pNAs) and hydrogen bonding opportunities (indoline). Despite having identical bulk polarities, the interfacial polarity at the silica/liquid interfaces formed using cyclohexane and methylcyclohexane were different, and both are more polar than the bulk. The interfaces formed between silica and 1-propanol and 1-octanol both exhibit heterogeneous polarity, with one population of pNAs sampling an environment less polar than bulk, and a second population sampling an environment more polar than bulk. This result is interpreted in terms of the substrate-solvent interaction that induce order in the first solvent monolayer.

In all cases indoline appeared to see a strong hydrogen bonding environment. The only way in which we were able to shift indoline's SHG spectra away from this bulk limit was to modify the silica surface, taking away hydrogen bond donating silanol

groups. This result pointed to strong, directional specific solvation interactions having a large importance at the interface.

Experimental results presented in Chapter 2 make very strong predictions about how inferred solvent structure and interfacial forces affect solvation at solid/liquid interfaces. Additional NLO experiments were performed to explore who solvent structure plays such a strong role in controlling polarity but not interfacial hydrogen bonding. Polarization analysis from VSFG spectra acquired under different conditions but from the same interface make it possible to determine average molecular orientations, as well as estimate the degree of order among solvent molecules in the interfacial region. This technique and the origin of its surface specificity are described in Chapter 3 of this thesis.

The second part of this thesis discusses experiments that probe directly interfacial structure and organization. Studying three different series of molecules adsorbed to different solid and liquid interfaces allowed for a systematic approach to determining those forces most responsible for molecular interfacial organization. In Chapter 3 we present VSFG spectra of linear alkanes (n = 8-11) adsorbed to the silica/vapor interface. Even in these weakly associating systems, where the strongest forces present are induced dipole interactions between the substrate and adsorbates, or van der Waals interactions between adsorbed molecules themselves, results show significant long range order. Furthermore, we were able to use carefully calibrated signal intensities to support an average molecular orientation of adsorbed species. That there was an even-odd effect in feature intensities showed a preferred orientation with methylene groups directed into and out of the surface.

Work presented in Chapter 4 is motivated by indirect solvent organization measurements presented in Chapter 2. That pNAs samples a heterogeneous solvation environment with one population being very nonpolar at the silica/1-octanol interface implies that the solvent molecules organize in an ordered Langmuir-like film with upright orientations. Likewise, previous results of octanol monolayers at the aqueous/vapor interface suggest similar long range order. Because the solid, silanol terminated silica interface is similar in some ways to the aqueous/vapor interface, we measured spectra of octanol isomers adsorbed to the silica/vapor interface. We then brought the neat liquid into contact with the surface, and measured the corresponding order observed at the silica/liquid interface. Results show that all octanol isomers have significant long range order and form upright monolayers at the silica/vapor interface, but that much of that order is lost at the silica/liquid interface. The branched isomers especially lost most or all long range order. This result suggests that lateral interactions play a role in adsorption to the solid/liquid interface, and we found that thermodynamic quantities of adsorption and solvation energetics supported this interpretation.

Finally, to expand our study of how intermolecular interactions affect interfacial organization of solvents, we used VSFG to determine structure and order of equal length, but different functional group containing solvents. These spectra were presented in Chapter 5 and included the silica/vapor and silica/liquid interfaces formed with octane and 1-octanol adsorbed presented earlier as well as with 1-octylamine, dimethyloctylamine, and octyl cyanide. We show again that the energetics of adsorption and solvation balance to determine which monolayers at the

silica/vapor interface will have order persist at the silica/liquid interface. The primary amine has the largest heat of adsorption, which not only leads to the most ordered silica/vapor interface, but since heats of vaporization (and thus condensation) are similar for these different molecules, 1-octylamine has the largest relative difference between the two enthalpies. Therefore, 1-octylamine remains the most ordered at the silica/liquid interface.

Data presented in Chapters 3-5 from this thesis will soon be submitted for publication.

6.3 Future Outlook

Results presented here represent a systematic approach to studying intermolecular forces responsible for interfacial properties and organization, though this is not an exhaustive study. We have chosen model systems that provide valuable insight toward developing predictive theories, but there are still questions that need answered. We present thermodynamic results from similar solvents adsorbed to interfaces as justification for spectral interpretation, assuming similar results for longer carbon chain adsorbates. Whether or not these correlations are universal can be easily tested with another series of experiments examining chain length dependence on the results presented in chapters 4 and 5.

Likewise, results presented in chapter 3 include only a small set of different length molecules. There may exist a transition at some size alkane outside of our sample group toward different interfacial structures. Obviously, these studies can be expanded to a wide variety of surfaces and new classes of solvents. Hopefully results

contained in this thesis provide grist for the mill and advance our understanding of structure and organization at solid/liquid interfaces.

6.4 References

(1) Beildeck, C. L.; Steel, W. H.; Walker, R. A. *Langmuir* **2003**, *19*, 4933-39.

(2) Steel, W. H.; Beildeck, C. L.; Walker, R. A. *J. Phys. Chem. B* **2004**, *108*, 16107-16.

(3) Steel, W. H.; Lau, Y. Y.; Beildeck, C. L.; Walker, R. A. *J. Phys. Chem. B.* **2004**, *108*, 13370-78.

(4) Steel, W. H.; Walker, R. A. *Nature* **2003**, *424*, 296-99.

(5) Can, S. Z.; Mago, D. D.; Esenturk, O.; Walker, R. A. *J. Phys. Chem. C* **2007**, *111*, 8739-48.

(6) Can, S. Z.; Mago, D. D.; Walker, R. A. *Langmuir* **2006**, *22*, 8043-49.

(7) Brindza, M. R.; Walker, R. A. *J. Am. Chem. Soc.* **2009**, *131*, 6207-14.

References

Abrahamsson, S.; Dahlen, B.; Lofgren, H.; Pascher, I.; Sundell, S. *Nobel Symp.* **1977**, *34*, 1.

Adhvaryu, A.; Biresaw, G.; Sharma, B. K.; Erhan, S. Z. *Ind. Eng. Chem. Res.* **2006**, *45*, 3735.

Al-Abadleh, H. A.; Mifflin, A. L.; Bertin, P. A.; Nguyen, S. T.; Geiger, F. M. *J. Phys. Chem. B.* **2005**, *109*, 9691.

Al-Abadleh, H. A.; Voges, A. B.; Bertin, P. A.; Nguyen, S. T.; Geiger, F. M. *J. Am. Chem. Soc.* **2004**, *126*, 11126.

Allara, D. L.; Parikh, A. N.; Rondelez, F. *Langmuir* **1995**, *11*, 2357.

Allen, M. W.; Bothwell, T. G.; Slaughter, B. D.; Johnson, C. K. *Biophysical Journal* **2002**, *82*, 428.

Arnett, E. M.; Ahsan, T. *J. Am. Chem. Soc.* **1991**, *113*, 6861.

Bain, C. D. *Curr. Opin. Coll. Int. Sci.* **1998**, *3*, 287.

Bayliss, N. S.; McRae, E. G. *J. Phys. Chem.* **1954**, *58*, 1002.

Beildeck, C. L.; Steel, W. H.; Walker, R. A. *Langmuir* **2003**, *19*, 4933.

Benderskii, A. V.; Eisenthal, K. B. *J. Phys. Chem. B.* **2000**, *104*, 11723.

Benjamin, I. *Ann. Rev Phys. Chem.* **1997**, *48*, 407.

Benjamin, I. *Chem. Phys. Lett.* **2004**, *393*, 453.

Benjamin, I. *Chem. Rev.* **2006**, *106*, 1212.

Berka, M.; Pla Sandrine, P.; Rice James, A. *Langmuir*, *22*, 687.

Berman, A. D.; Ducker, W. A.; Israelachvili, J. N. *Langmuir* **1996**, *12*, 4559.

Bilinski, B. *J. Coll. Int. Sci.* **2000**, *225*, 105.

Bopp, P. A.; Buhn, J. B.; Maier, H. A.; Hampe, M. J. *Chem. Eng. Commun.* **2008**, *195*, 1437.

Brevet, P. F.; Girault, H. H. *Liquid-Liquid Interfaces* **1996**, 103.

Brindza, M. R.; Walker, R. A. *J. Am. Chem. Soc.* **2009**, *131*, 6207.

Burri, J.; Hartland, S. *Coll. Polymer. Sci.* **1977**, *255*, 675.

Butler, P. D.; Hamilton, W. A.; Magid, L. J.; Hayter, J. B.; Slawecki, T. M.; Hammouda, B. *J. Chem. Soc., Faraday Trans.* **1997**, *104*, 65.

Can, S. Z.; Chang, C. F.; Walker, R. A. *Biochim. Biophys. Acta, Biomembr.* **2008**, *1778*, 2368.

Can, S. Z.; Mago, D. D.; Esenturk, O.; Walker, R. A. *J. Phys. Chem. C* **2007**, *111*, 8739.

Can, S. Z.; Mago, D. D.; Walker, R. A. *Langmuir* **2006**, *22*, 8043.

Casson, B. D.; Braun, R.; Bain, C. D. *J. Chem. Soc., Faraday Trans.* **1997**, *104*, 209.

Catalan, J. *J. Org. Chem.* **1997**, *62*, 8231.

Chanda, J.; Bandyopadhyay, S. *J. Phys. Chem. B* **2006**, *110*, 23443.

Chandross, M.; Lorenz, C. D.; Stevens, M. J.; Grest, G. S. *Langmuir* **2008**, *24*, 1240.

Chandross, M.; Webb, E. B., III; Stevens, M. J.; Grest, G. S.; Garofalini, S. H. *Phys. Rev. Lett.* **2004**, *93*, 166103/1.

Chang, T.-M.; Dang, L. X. *Chem. Rev.* **2006**, *106*, 1305.

Chen, X.; Clarke, M. L.; Wang, J.; Chen, Z. *Int. J. Mod. Phys. B* **2005**, *19*, 691.

Conboy, J. C. Investigation of immiscible liquid/liquid interfaces with second harmonic generation and sum-frequency vibrational spectroscopy (electrolytes, adsorption, surfactants) 1996.

Cook, W. G.; Ross, R. A. *Can. J. Chem.* **1972**, *50*, 1666.

Corn, R. M. *Proceedings of SPIE-The International Society for Optical Engineering* **1992**, *1636*, 117.

Corn, R. M.; Higgins, D. A. *Chem. Rev.* **1994**, *94*, 107.

Cousins, I. T.; Beck, A. J.; Jones, K. C. *Sci. Total Environ.* **1999**, *228*, 5.

Criscenti, L. J.; Cygan, R. T.; Kooser, A. S.; Moffat, H. K. *Chem. Mater.* **2008**, *20*, 4682.

Curthoys, G.; Davydov, V. Y.; Kiselev, A. V.; Kiselev, S. A.; Kuznetsov, B. V. *J. Coll. Int. Sci.* **1974**, *48*, 58.

Czarnecki, J.; Sestak, J. *J. Therm. Anal. Calorim.* **2000**, *60*, 759.

Danielsen, E. M.; Hansen, G. *Mol. Membr. Biol.* **2006**, *23*, 71.

Ding, F.; Zhong, Q.; Brindza, M. R.; Fourkas, J. T.; Walker, R. A. *Optics Express*, *Submitted, May 2009*.

Doerr, A. K.; Tolan, M.; Schlomka, J. P.; Press, W. *Europhys. Lett.* **2000**, *52*, 330.

Donaldson, D. J.; Vaida, V. *Chem. Rev.* **2006**, *106*, 1445.

Edgar, R.; Huang, J. Y.; Popovitz-Biro, R.; Kjaer, K.; Bouwman, W. G.; Howes, P. B.; Als-Nielsen, J.; Shen, Y. R.; Lahav, M.; Leiserowitz, L. *J. Phys. Chem. B* **2000**, *104*, 6843.

Eisenthal, K. B. *Chem. Rev.* **1996**, *96*, 1343.

Esenturk, O.; Walker, R. A. *Phys. Chem. Chem. Phys.* **2003**, *5*, 2020.

Esenturk, O.; Walker, R. A. *J. Chem. Phys.* **2006**, *125*, 174701/1.

Farrer, R. A.; Fourkas, J. T. *Acc. Chem. Res.* **2003**, *36*, 605.

Fenter, P.; Sturchio, N. C. *Prog. Surf. Sci.* **2005**, *77*, 171.

Forsman, W. C.; Latshaw, B. E. *Polym. Eng. Sci.* **1996**, *36*, 1114.

Fowkes, F. M. *J. Phys. Chem.* **1962**, *66*, 382.

Fragneto-Cusani, G. *J. Phys.: Condens. Matter* **2001**, *13*, 4973.

Garfias, F. J. *J. Phys. Chem.* **1980**, *84*, 2297.

Gaussian 03, Revision D.01, Frisch, M. J.; Trucks, G. W.; Schlegel, H. B.; Scuseria, G. E.; Robb, M. A.; Cheeseman, J. R.; Montgomery, Jr., J. A.; Vreven, T.; Kudin, K. N.; Burant, J. C.; Millam, J. M.; Iyengar, S. S.; Tomasi, J.; Barone, V.; Mennucci, B.; Cossi, M.; Scalmani, G.; Rega, N.; Petersson, G. A.; Nakatsuji, H.; Hada, M.; Ehara, M.; Toyota, K.; Fukuda, R.; Hasegawa, J.; Ishida, M.; Nakajima, T.; Honda, Y.; Kitao, O.; Nakai, H.; Klene, M.; Li, X.; Knox, J. E.; Hratchian, H. P.; Cross, J. B.; Bakken, V.; Adamo, C.; Jaramillo, J.; Gomperts, R.; Stratmann, R. E.; Yazyev, O.; Austin, A. J.; Cammi, R.; Pomelli, C.; Ochterski, J. W.; Ayala, P. Y.; Morokuma, K.; Voth, G. A.; Salvador, P.; Dannenberg, J. J.; Zakrzewski, V. G.; Dapprich, S.; Daniels, A. D.; Strain, M. C.; Farkas, O.; Malick, D. K.; Rabuck, A. D.; Raghavachari, K.; Foresman, J. B.; Ortiz, J. V.; Cui, Q.; Baboul, A. G.; Clifford, S.; Cioslowski, J.; Stefanov, B. B.; Liu, G.; Liashenko, A.; Piskorz, P.; Komaromi, I.; Martin, R. L.; Fox, D. J.; Keith, T.; Al-Laham, M. A.; Peng, C. Y.; Nanayakkara, A.; Challacombe, M.; Gill, P. M. W.; Johnson, B.; Chen, W.; Wong, M. W.; Gonzalez, C.; and Pople, J. A.; Gaussian, Inc., Wallingford CT, 2004..

Gilli, G.; Gilli, P. *Journal of Molecular Structure* **2000**, *552*, 1.

Gilman, J. B.; Eliason, T. L.; Fast, A.; Vaida, V. *J. Coll. Int. Sci.* **2004**, *280*, 234.

Gilman, J. B.; Tervahattu, H.; Vaida, V. *Atmos. Environ.* **2006**, *40*, 6606.

Gilroy, J. J.; Dolan, J. W.; Snyder, L. R. *J. Chromatography A* **2003**, *1000*, 757.

Gombos, I.; Kiss, E.; Detre, C.; Laszlo, G.; Matko, J. *Immunol. Lett.* **2006**, *104*, 59.

Gordon, P. A.; Glandt, E. D. *Ind. Eng. Chem. Res.* **1998**, *37*, 3221.

Gourdon, D.; Israelachvili, J. N. *Phys. Rev. E: Stat., Nonlinear, Soft Matter Phys.* **2003**, *68*, 021602/1.

Groszek, A. J. *Am. Soc. Lubrication Eng. Trans.* **1962**, *5*, 105.

Gu, Y.; Kar, T.; Scheiner, S. *J. Am. Chem. Soc.* **1999**, *121*, 9411.

Guiseppi-Elie, A.; Wnek, G. E.; Wesson, S. P. *Langmuir* **1986**, *2*, 508.

Guo, Z.; Zheng, W.; Hamoudi, H.; Dablemont, C.; Esaulov, V. A.; Bourguignon, B. *Surf. Sci.* **2008**, *602*, 3551.

Haehner, G.; Zwahlen, M.; Caseri, W. *Langmuir* **2005**, *21*, 1424.

Hamon, Y.; Bernard, A.-M.; Salles, A.; Hawchar, O.; Marguet, D.; He, H.-T.; Guo, X.-J. *Immunol., Endocr. Metab. Agents Med. Chem.* **2008**, *8*, 358.

Hansen, R. L.; Harris, J. M. *Anal.Chem.* **1995**, *67*, 492.

Harper, K.; Minofar, B.; Sierra-Hernandez, M. R.; Casillas-Ituarte, N. N.; Roeselova, M.; Allen, H. C. *J. Phys. Chem. A* **2009**, *113*, 2015.

Hayes, P. L.; Gibbs-Davis, J. M.; Musorrafiti, M. J.; Mifflin, A. L.; Scheidt, K. A.; Geiger, F. M. *J. Phys. Chem. C.* **2007**, *111*, 8796.

Hayes, P. L.; Malin, J. N.; Konek, C. T.; Geiger, F. M. *J. Phys. Chem. A.* **2008**, *112*, 660.

Heinz, H.; Vaia, R. A.; Krishnamoorti, R.; Farmer, B. L. *Chem. Mater.* **2007**, *19*, 59.

Henn, A. R. *Biophys. Chem.* **2003**, *105*, 533.

Hey, M. J.; Kippax, P. G. *Coll. Surf., A* **2005**, *262*, 198.

Holzwarth, A.; Leporatti, S.; Riegler, H. *Europhys. Lett.* **2000**, *52*, 653.

Honerkamp-Smith, A. R.; Veatch, S. L.; Keller, S. L. *Biochim. Biophys. Acta, Biomembr.* **2009**, *1788*, 53.

Hosoda, M.; Kobayashi, H.; Sakamoto, N.; Sakai, K.; Takagi, K. *Rev. Sci. Instrum.* **1996**, *67*, 4224.

Huang, J. Y.; Shen, Y. R. *Adv. Ser. Phys. Chem* **1995**, *5*, 5.

Ikegami, T.; Tomomatsu, K.; Takubo, H.; Horie, K.; Tanaka, N. *J. Chromatogr., A* **2008**, *1184*, 474.

Iler, R. K. *The Chemistry of Silica*; Wiley: New York, 1979.

Inaba, A. *Pure Appl. Chem.* **2006**, *78*, 1025.

Ishiyama, T.; Morita, A. *J. Phys. Chem. A* **2007**, *111*, 9277.

Israelachvili *Intermolecular and Surface Forces*, 2 ed.; Academic Press: New York, 1992.

Ivanova, P. T.; Milne, S. B.; Forrester, J. S.; Brown, H. A. *Mol. Interventions* **2004**, *4*, 86.

Janczuk, B.; Bialopiotrowicz, T. *J. Coll. Int. Sci.* **1990**, *140*, 362.

Jedlovszky, P.; Varga, I.; Gilanyi, T. *J. Chem. Phys.* **2004**, *120*, 11839.

Kalipatnapu, S.; Chattopadhyay, A. *Cell. Mol. Neurobiol.* **2007**, *27*, 1097.

Kamlet, M. J.; Abboud, J. L. M.; Abraham, M. H.; Taft, R. W. *J. Org. Chem.* **1983**, *48*, 2877.

Kanti Sen, T.; Khilar Kartic, C. *Adv. Coll. Int. Sci.* , *119*, 71.

Kawasaki, M.; Imazeki, S.; Oh-e, M.; Ando, M. *Jpn. J. Appl. Phys.* **2008**, *47*, 6247.

Kim, J.; Opdahl, A.; Chou, K. C.; Somorjai, G. A. *Langmuir* **2003**, *19*, 9551.

Knoezinger, H.; Staehlin, W. *Prog. Colloid Polym. Sci.* **1980**, *67*, 33.

Kondo, S.; Fujiwara, H.; Ichii, T.; Tsuboi, I. *J. Chem. Soc., Faraday Trans.* **1979**, *75*, 646.

Kordel, W.; Dassenakis, M.; Lintelmann, J.; Padberg, S. *Pure Appl. Chem.* **1997**, *69*, 1571.

Kovaleski, J. M.; Wirth, M. J. *Analytical Chemistry* **1997**, *69*, A600.

Kovaleski, J. M.; Wirth, M. J. *J. Phys. Chem. B.* **1997**, *101*, 5545.

Krishna, R.; Smit, B. *Chem. Innovation* **2001**, *31*, 27.

Laha, S.; Tansel, B.; Ussawarujikulchai, A. *J. Environ. Manage.* **2008**, *90*, 95.

Langevin, D. *Adv. Coll. Int. Sci.* **2001**, *89-90*, 467.

Laurence, C.; Nicolet, P.; Dalati, M. T.; Abboud, J. L. M.; Notario, R. *J. Phys. Chem.* **1994**, *98*, 5807.

Lee, S. H.; Rossky, P. J. *J. Chem. Phys.* **1994**, *100*, 3334.

Levi, V.; Villamil Giraldo, A. M.; Castello, P. R.; Rossi, J. P. F. C.; Gonzalez Flecha, F. L. *Biochem. J.* **2008**, *416*, 145.

Levinson, P.; Valignat, M. P.; Fraysse, N.; Cazabat, A. M.; Heslot, F. *Thin Solid Films* **1993**, *234*, 482.

Li, D.; Chen, S.; Zhao, S.; Ma, H. *Coll. Surf., A* **2006**, *273*, 16.

Li, I.; Bandara, J.; Shultz, M. J. *Langmuir* **2004**, *20*, 10474.

Li, M.; Schlossman, M. L. *Nucl. Sci. Tech.* **2006**, *17*, 322.

Li, Y.; Demerjian, K. L.; Williams, L. R.; Worsnop, D. R.; Kolb, C. E.; Davidovits, P. *J. Phys. Chem. A* **2006**, *110*, 6814.

CRC Handbook of Chemistry and Physics, 83rd Edition; Lide, D. R., Ed.; CRC Press/Taylor and Francis: Boca Raton, FL, 2002, pp 2664 pp.

Lin, P. J.; Parcher, J. F. *J. Coll. Int. Sci.* **1983**, *91*, 76.

Liu, Y.; Wolf, L. K.; Messmer, M. C. *Langmuir* **2001**, *17*, 4329.

Lu, J. R.; Thomas, R. K. *Appl. Neutron Scattering Soft Condens. Matter* **2000**, 205.

Lu, J. R.; Thomas, R. K.; Penfold, J. *Adv. Coll. Int. Sci.* **2000**, *84*, 143.

Luan, B.; Robbins Mark, O. *Phys. Rev. Lett.*, *93*.

Lum, K.; Chandler, D.; Weeks, J. D. *J. Phys. Chem. B.* **1999**, *103*, 4570.

Lynden-Bell, R. M.; Del Popolo, M. G.; Youngs, T. G. A.; Kohanoff, J.; Hanke, C. G.; Harper, J. B.; Pinilla, C. C. *Acc. Chem. Res.* **2007**, *40*, 1138.

Ma, H. Y.; Yang, C.; Chen, S. H.; Jiao, Y. L.; Huang, S. X.; Li, D. G.; Luo, J. L. *Electrochim. Acta* **2003**, *48*, 4277.

MacPhail, R. A.; Strauss, H. L.; Snyder, R. G.; Elliger, C. A. *J. Phys. Chem.* **1984**, *88*, 334.

MacRitchie, F. *Chemistry at Interfaces*; Academic Press: New York, 1990.

Magid, L.; Penfold, J.; Schurtenberger, P.; Wagner, N. *Curr. Opin. Coll. Int. Sci.* **2002**, *7*, 193.

Manne, S.; Gaub, H. E. *Science* **1995**, *270*, 1480.

Markovitch, O.; Agmon, N. *Molecular Physics* **2008**, *106*, 485.

Matyushov, D. V.; Schmid, R.; Ladanyi, B. M. *J. Phys. Chem. B.* **1997**, *101*, 1035.

Mazaev, V. V.; Tomchuk, N. N.; Lavrenova, N. A. *Russ. J. Phys. Chem. A* **2007**, *81*, 370.

McHale, J. M.; Auroux, A.; Perrotta, A. J.; Navrotsky, A. *Science* **1997**, *277*, 788.

Metikos-Hukovic, M.; Babic, R.; Petrovic, Z.; Posavec, D. *J. Electrochem. Soc.* **2007**, *154*, C138.

Michael, D.; Benjamin, I. *J. Phys. Chem.* **1995**, *99*, 16810.

Mifflin, A. L.; Konek, C. T.; Geiger, F. M. *J. Phys. Chem. B* **2006**, *110*, 22577.

Mikhail, R. S.; Nashed, S.; Khalil, A. M. *Surf. Technol.* **1978**, *7*, 45.

Miranda, P. B.; Pflumio, V.; Saijo, H.; Shen, Y. R. *J. Am. Chem. Soc.* **1998**, *120*, 12092.

Miranda, P. B.; Shen, Y. R. *J. Phys. Chem. B.* **1999**, *103*, 3292.

Mo, H.; Trogisch, S.; Taub, H.; Ehrlich, S. N.; Volkmann, U. G.; Hansen, F. Y.; Pino, M. *J. Phys.: Condens. Matter* **2004**, *16*, S2905.

Moad, A. J.; Simpson, G. J. *J. Phys. Chem. B.* **2004**, *108*, 3548.

Mueller, R.; Kammler, H. K.; Wegner, K.; Pratsinis, S. E. *Langmuir* **2003**, *19*, 160.

Musorrafiti, M. J.; Konek, C. T.; Hayes, P. L.; Geiger, F. M. *J. Phys. Chem. C* **2008**, *112*, 2032.

Napoleon, R. L.; Moore, P. B. *J. Phys. Chem. B* **2006**, *110*, 3666.

Natal-Santiago, M. A.; Dumesic, J. A. *J. Catal.* **1998**, *175*, 252.

Nath, S. *J. Coll. Int. Sci.* **1999**, *209*, 116.

Nikolla, E.; Schwank, J. W.; Linic, S. *Catal. Today* **2008**, *136*, 243.

Nishi, N.; Hobara, D.; Yamamoto, M.; Kakiuchi, T. *J. Chem. Phys.* **2003**, *118*, 1904.

Noguchi, H.; Hiroshi, M.; Tominaga, T.; Ping Gong, J.; Osada, Y.; Uosaki, K. *Phys. Chem. Chem. Phys.* **2008**, *10*, 4987.

O'Brien, M. J.; Grob, R. L. *J. Chromatogr.* **1978**, *155*, 129.

Ocko, B. M.; Wu, X. Z.; Sirota, E. B.; Sinha, S. K.; Gang, O.; Deutsch, M. *Phys. Rev. E: Stat. Phys., Plasmas, Fluids, Relat. Interdiscip. Top.* **1997**, *55*, 3164.

Ohe, C.; Sasaki, T.; Noi, M.; Goto, Y.; Itoh, K. *Anal. Bioanal. Chem.* **2007**, *388*, 73.

Ong, S.; Zhao, X.; Eisenthal, K. B. *Chem. Phys. Lett.* **1992**, *191*, 327.

Onsager, L. *J. Am. Chem. Soc.* **1936**, *58*, 1486.

Papirer, E.; Editor *Adsorption on Silica Surfaces.* ; Marcel Dekker, Inc.: New York, 2000.

Parikh, S. J.; Lafferty, B. J.; Sparks, D. L. *J. Coll. Int. Sci.*, *320*, 177.

Perry, A.; Ahlborn, H.; Space, B.; Moore, P. B. *J. Chem. Phys.* **2003**, *118*, 8411.

Phillips, D. C.; York, R. L.; Mermut, O.; McCrea, K. R.; Ward, R. S.; Somorjai, G. A. *J. Phys. Chem. C* **2007**, *111*, 255.

Pierson, R. H.; Fletcher, A. N.; Gantz, E. S. C. *Anal. Chem.* **1956**, *28*, 1218.

Pompe, T.; Herminghaus, S. *Phys. Rev. Lett.* **2000**, *85*, 1930.

Prokhorov, V. A. "Apparatus for measuring the surface tension of liquids," Ussr., 1981.

Quinn, P. J.; Joo, F.; Vigh, L. *Prog. Biophys. Mol. Biol.* **1989**, *53*, 71.

Reiter, R.; Motschmann, H.; Orendi, H.; Nemetz, A.; Knoll, W. *Langmuir* **1992**, *8*, 1784.

Ribarsky, M. W.; Landman, U. *J. Chem. Phys.* **1992**, *97*, 1937.

Richter, L.; Vollhardt, D. *Tenside, Surfactants, Deterg.* **2006**, *43*, 256.

Rockmann, R.; Kalies, G. *J. Coll. Int. Sci.*, *315*, 1.

Rusling, J. F.; Nassar, A. E. F. *J. Am. Chem. Soc.* **1993**, *115*, 11891.

Ruths, M.; Ohtani, H.; Greenfield, M. L.; Granick, S. *Tribol. Lett.* **1999**, *6*, 207.

Santos, A. M. M.; Vasconcelos, W. L. *J. Non-Cryst. Solids* **2000**, *273*, 145.

Sastry, P. S. *Prog Lipid Res 24*, 69.

Scheidegger, A. M.; Sparks, D. L. *Soil Sci.* **1996**, *161*, 813.

Scheiner, S. *Advances in Molecular Structure Research* **2000**, *6*, 159.

Schlangen, L. J. M.; Koopal, L. K.; Stuart, M. A. C.; Lyklema, J.; Robin, M.; Toulhoat, H. *Langmuir* **1995**, *11*, 1701.

Schlossman, M. L. *Curr. Opin. Coll. Int. Sci.* **2002**, *7*, 235.

Schmitt, J.; Danner, B.; Bayerl, T. M. *Langmuir* **2001**, *17*, 244.

Schofer, J.; Rehbein, P.; Stolz, U.; Lohe, D.; Zum Gahr, K. H. *Wear* **2001**, *248*, 7.

Scott, R. P. W. *Adv. Chromatogr.* **1982**, *20*, 167.

Searcy, A. W.; Beruto, D. T.; Barberis, F. *J. Chem. Phys.* **2009**, *130*, 184713/1.

Sefler, G. A.; Du, Q.; Miranda, P. B.; Shen, Y. R. *Chem. Phys. Lett.* **1995**, *235*, 347.

Seidl, W. *Atmos. Environ.* **2000**, *34*, 4917.

Sengupta, P.; Hammond, A.; Holowka, D.; Baird, B. *Biochim. Biophys. Acta, Biomembr.* **2008**, *1778*, 20.

Shafir, A.; Andelman, D.; Netz, R. R. *J. Chem. Phys.* **2003**, *119*, 2355.

Shang, X. M.; Benderskii, A. V.; Eisenthal, K. B. *J. Phys. Chem. B.* **2001**, *105*, 11578.

Shen, Y. R. *Nature.* **1989**, *337*, 519.

Shen, Y. R. *Solid State Communications* **1992**, *84*, 171.

Shen, Y. R. *Nonlinear Spectroscopy for Molecular Structure Determination* **1998**, 249.

Shen, Y. R. *IEEE Journal of Selected Topics in Quantum Electronics* **2000**, *6*, 1375.

Shultz, M. J.; Baldelli, S.; Schnitzer, C.; Simonelli, D. *J. Phys. Chem. B.* **2002**, *106*, 5313.

Shultz, M. J.; Schnitzer, C.; Simonelli, D.; Baldelli, S. *Int. Rev. Phys. Chem.* **2000**, *19*, 123.

Simpson, G. J.; Perry, J. M.; Ashmore-Good, C. L. *Phys. Rev. B: Condensed Matter and Materials Physics* **2002**, *66*.

Sinapi, F.; Julien, S.; Auguste, D.; Hevesi, L.; Delhalle, J.; Mekhalif, Z. *Electrochim. Acta* **2008**, *53*, 4228.

Slaughter, B. D.; Allen, M. W.; Lushington, G. H.; Johnson, C. K. *J. Phys. Chem. A* **2003**, *107*, 5670.

Small, D. M. *J. Lipid Res.* **1984**, *25*, 1490.

Smith, E. A.; Wirth, M. J. *J. Chromatography A* **2004**, *1060*, 127.

Somasundaran, P.; Shrotri, S.; Huang, L. *Pure and Appl. Chem.* **1998**, *70*, 621.

Somorjai, G. A.; Rupprechter, G. *Stud. Surf. Sci. Catal.* **1997**, *109*, 35.

Srivastava, P.; Chapman, W. G.; Laibinis, P. E. *Langmuir* **2009**, *25*, 2689.

Stahelin, R. V. *J. Lipid Res.* **2009**, S299.

Staszczuk, P. *Thermochim. Acta* **1994**, *247*, 169.

Steel, W. H.; Beildeck, C. L.; Walker, R. A. *J. Phys. Chem. B* **2004**, *108*, 16107.

Steel, W. H.; Lau, Y. Y.; Beildeck, C. L.; Walker, R. A. *J. Phys. Chem. B.* **2004**, *108*, 13370.

Steel, W. H.; Walker, R. A. *Nature* **2003**, *424*, 296.

Steinhurst, D. A.; Owrutsky, J. C. *J. Phys. Chem. B.* **2001**, *105*, 3062.

Stevens, M. J.; Grest, G. S. *Biointerphases* **2008**, *3*, FC13.

Subbotina, I. R.; Shelimov, B. N.; Kazanskii, V. B. *Kinet. Catal.* **2002**, *43*, 412.

Sun, X.; Dang, L. X. *J. Chem. Phys.* **2009**, *130*, 124709/1.

Suri, S. K.; Patel, M. *J. Coll. Int. Sci.* **1981**, *84*, 36.

Tahery, R.; Modarress, H.; Satherley, J. *Chem. Eng. Sci.* **2005**, *60*, 4935.

Tamburello Luca, A. A.; Hebert, P.; Brevet, P. F.; Girault, H. H. *J. Chem. Soc., Faraday Trans.* **1995**, *91*, 1763.

TamburelloLuca, A. A.; Hebert, P.; Brevet, P. F.; Girault, H. H. *J. Chem. Soc., Faraday Trans.* **1996**, *92*, 3079.

Tavana, H.; Neumann, A. W. *Adv. Coll. Int. Sci.* **2007**, *132*, 1.

Thomas, R. K. *Surfactant Sci. Ser.* **1999**, *83*, 417.

Thomas, R. K. *Annu. Rev. Phys. Chem.* **2004**, *55*, 391.

Thompson, P. A.; Robbins, M. O. *Science* **1990**, *250*, 792.

Toca-Herrera, J. L.; Muller, H. J.; Krustev, R.; Pfohl, T.; Mohwald, H. *Coll. Surf., A* **1999**, *152*, 357.

van Meer, G.; Voelker, D. R.; Feigenson, G. W. *Nat. Rev. Mol. Cell Biol.* **2008**, *9*, 112.

Van Oss, C. J.; Good, R. J.; Chaudhury, M. K. *Langmuir* **1988**, *4*, 884.

Vieceli, J.; Ma, O. L.; Tobias, D. J. *J. Phys. Chem. A* **2004**, *108*, 5806.

Wang, H.; Borguet, E.; Eisenthal, K. B. *J. Phys. Chem. A.* **1997**, *101*, 713.

Wang, H.; Borguet, E.; Eisenthal, K. B. *J. Phys. Chem. B.* **1998**, *102*, 4927.

Wang, H. F.; Gan, W.; Lu, R.; Rao, Y.; Wu, B. H. *Int. Rev. Phys. Chem.* **2005**, *24*, 191.

Wang, L.; Song, Y.; Zhang, B.; Wang, E. *Thin Solid Films* **2004**, *458*, 197.

Watry, M. R.; Tarbuck, T. L.; Richmond, G. L. *J. Phys. Chem. B* **2003**, *107*, 512.

Weng, L.; Fest, E. P. M. J.; Fillius, J.; Temminghoff, E. J. M.; Van Riemsdijk, W. H. *Environ. Sci. Technol.* **2002**, *36*, 1699.

Whalen, J. W. *J. Phys. Chem.* **1962**, *66*, 511.

Wirth, M. J.; Legg, M. A. *Ann. Rev Phys. Chem.* **2007**, *58*, 489.

Wirth, M. J.; Piasecki-Coleman, D. A.; Montgomery, M. E. *Langmuir* **1995**, *11*, 990.

Wolf, C.; Quinn, P. J. *Prog. Lipid Res.* **2008**, *47*, 15.

Wong, A. L.; Harris, J. M. *J. Phys. Chem.* **1991**, *95*, 5895.

Wright, J. C.; LaBuda, M. J.; Zilian, A.; Chen, P. C.; Hamilton, J. P. *Journal of Luminescence* **1997**, *72-74*, 799.

Yang, M.; Somorjai, G. A. *J. Am. Chem. Soc.* **2004**, *126*, 7698.

Ye, S.; Nihonyanagi, S.; Uosaki, K. *Phys. Chem. Chem. Phys.* **2001**, *3*, 3463.

Ye, S.; Noda, H.; Morita, S.; Uosaki, K.; Osawa, M. *Langmuir* **2003**, *19*, 2238.

Yoshizawa, H.; Israelachvili, J. *J. Phys. Chem.* **1993**, *97*, 11300.

Yu, C. J.; Evmenenko, G.; Richter, A. G.; Datta, A.; Kmetko, J.; Dutta, P. *Appl. Surf. Sci.* **2001**, *182*, 231.

Yu, C. J.; Richter, A. G.; Kmetko, J.; Dugan, S. W.; Datta, A.; Dutta, P. *Phys. Rev. E: Stat., Nonlinear, Soft Matter Phys.* **2001**, *63*, 021205/1.

Zhang, X.; Cunningham, M. M.; Walker, R. A. *J. Phys. Chem. B.* **2003**, *107*, 3183.

Zhang, X.; Steel, W. H.; Walker, R. A. *J. Phys. Chem. B*. **2003**, *107*, 3829.

Zhang, X.; Walker, R. A. *Langmuir* **2001**, *17*, 4486.

Zhang, X. Y.; Esenturk, O.; Walker, R. A. *J. Am. Chem. Soc.* **2001**, *123*, 10768.

Zheng, Y. J.; Merz, K. M. *J. Comp. Chem.* **1992**, *13*, 1151.

Zhu, X. D.; Suhr, H.; Shen, Y. R. *Phys. Rev. B: Condensed Matter and Materials Physics* **1987**, *35*, 3047.

Zhuang, X.; Miranda, P. B.; Kim, D.; Shen, Y. R. *Phys. Rev. B: Condensed Matter and Materials Physics* **1999**, *59*, 12632.

Zybill, C. E.; Ang, H. G.; Lan, L.; Choy, W. Y.; Meng, E. F. K. *J. Organometallic Chem.* **1997**, *547*, 167.